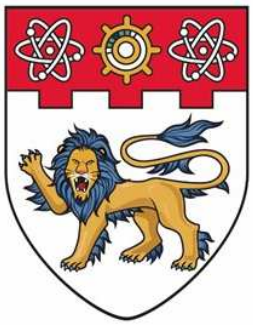

NANYANG TECHNOLOGICAL UNIVERSITY
SINGAPORE

ACTUATION DESIGN AND ASSISTIVE CONTROL FOR A SOFT WEARABLE EXOSUIT

Binh Khanh DINH

Nanyang Technological University, Singapore
School of Mechanical and Aerospace Engineering

Supervisor:

Assistant Professor **Lorenzo MASIA**

A thesis submitted to the Nanyang Technological University
in partial fulfilment of the requirement for the degree of
Doctor of Philosophy

To my Le UYEN, my wife, my forever love...
Brought to me by God's beautiful grace.
Partner with me on a vibrant journey, full of my life.
Thanks for her advices, her endless supports, her patience, and her faith,
Because she always understood.

To my parents and my sister...
Thanks for their unconditional supporting and encouraging me to believe in myself,
Mom and Dad, finally I could make you be proud.

To my VIT, my son...
I love you very much my son,
I found my motivation and inspiration from seeing you.

Acknowledgements

Writing this thesis would not have been possible without the help and support of many friends around me.

First of all, I would like to express my great gratitude for my professor, Asst. Prof. Lorenzo MASIA for not only giving me the opportunity to pursue my study, but also his enormous support, inspiring guidances, encouragements and insightful advices throughout my four-year research. It is my great honour and privilege working with him as a Ph.D. student.

Also, I am very grateful for the friendship of all members in ARIES and SYNERGY Lab: Assoc. Prof. Domenico CAMPOLO, Michele Xiloyannis, Leonardo Cappello, Chris Wilson Antuvan, Sara Contu, Paolo Tommasino, Phan Gia Hoang. I would like to convey my special thanks to them for their generous discussions and assistance during my works.

Special thanks to my senior, Dr. Do Thanh Nho, for his valuable advices and recommendations to my research.

In recognition of all the help and supports I would like to remind all the staffs in Robotic Research Center 1 & 2 in the School of Mechanical and Aerospace Engineering.

Finally, my gratitude is also extended to Nanyang Technological University for the financial support granted me under SINGA research scholarship for my postgraduate studies in Singapore.

Singapore, 2017
(Toughest but most beautiful years of my life) Binh Khanh DINH

Abstract

The development of a portable assistive device to aid patients affected by neuromuscular disorders has been the ultimate goal of assistive robots since the late 1960s. Traditional robotic devices have been engineered to assist the users' limbs in both activities of daily living (ADLs) and physical therapy, mostly consisting of load-bearing exoskeletons made of rigid links that operate in parallel to the human skeleton. These devices can be extremely accurate and are able to deliver high forces/torques to their users, making them optimal solutions for improving physical therapy in clinical environments. However, their structural complexity cause them to be poor candidates for daily at-home use, where portability, lightweight, compliance, and low profile are preferable.

A new frontier of assistive devices aims at designing exoskeletons based on fabric and flexible materials for applications where kinematic transparency is the primary requirement. Bowden-cable transmission is the widely employed solution in most of the aforementioned applications due to advantages in durability, lightweight, safety, and flexibility. The major advantages of soft assistive exoskeletons driven by Bowden-cable transmission can be identified in the superior ergonomics and wearability, allowing users to freely move and allocating the actuation stages far away from the end-effector. Despite of having many advantages in assistive technology, this actuation strategy presents several intrinsic limitations caused by the presence of nonlinearities, such as friction and backlash of the cables, which make it difficult to predict and control the kinematics and dynamics between the device and the user.

In this thesis, I present the design and control implementation of a soft, textile-based exosuit driven by Bowden-cable transmission for assisting human upper limb movements, especially elbow flexion/extension. I describe a model-based design, characterisation and testing of an actuation stage, driving a set of artificial tendons to apply torques to the human elbow joint. I also propose a novel hierarchical control paradigm for the actuation unit, considering all the aspects ranging from human motion intention detection for assistance, to adaptive compensation for the detrimental effects arising from the presence of nonlinear behaviours in the exosuit, i.e. friction

and backlash. The resulting system is a low profile, lightweight, wearable exosuit with high accuracy, designed to intuitively assist the wearer in activities of daily living.

Key words: Assistive technology, wearable exoskeletons, soft exosuits, actuators design, impedance/admittance control, robust nonlinear adaptive control

Contents

List of Figures

List of Tables

1 Introduction

1.1 Background

Disorders of the nervous system are important causes of the death and disability around the world, with a dangerously increasing impact in developing countries, where they are estimated to responsible for over 27% of all years of life lived with disability. A broad range of neuromuscular disorders, including those induced by age, stroke, brachial plexus injury, spinal cord injury, multiple sclerosis, traumatic brain injury and cerebral palsy can result in long-term muscle weakness or neuromuscular damage. These chronic conditions have a significant impact on the quality of the patient's life, hampering the accomplishment of fundamental activities of daily living (ADLs). Consequently, there is a great need to develop intelligent assistive robots that can aid the patients in daily activities.

A wealth of robotic devices has been designed and developed to assist the users' limbs in both ADLs and physical therapy, mostly made of rigid components that operate in parallel to the human skeleton. The design of robotic hardware and the controllers is generally based on the use of rigid links and transmissions, because they help avoiding undesirable dynamic behaviour that may arise from elastic and non-rigid deformations, limiting the number of variables to model and monitor. Especially these rigid devices can be modelled and controlled accurately, and are able to deliver high forces/torques to their users, making them optimal solutions for improving and quantifying physical therapy in clinical environments. For all of the above mentioned reasons, the robotic precept "stiffer is better" has long played a decisive role. Despite significant advances in recent decades, traditional rigid exoskeletons are constrained by limited portability, safety, ergonomics, autonomy and, most of all, cost. One of the common limitations of such devices is posed by the kinematic constrains imposed on the wearer's joints by the rigid frames. Misalignment between the robot's joints

and the biological ones results in hyperstaticity, that is the application of uncontrolled interaction forces, which upsets the natural kinematics of human movements. Most important difficulty is the high cost of such solutions, which partly explains why the rigid exoskeletons are still only available in hospitals and specialised clinics.

Various methods have been proposed to avoid the use of rigid links. The introduction of compliant elements in robotics revolutionised the path to the design of applications with human in the loop: Series Elastic Actuation was the ignition to this new approach which has been widely accepted by a large part of the robotic community.

Compliant actuation opened a new scenario, alternative to the classic robotics precept "stiffer is better"; a new control approach was adopted with the purpose of transforming the force problem into a position problem where the deformation of the compliant element was the main indicator of the interaction forces between the human being and robotic device. Despite the large diffusion there are still several drawbacks which are far from being solved, especially in assistive technology. The aforementioned improvements in actuation and control solutions did not prevent the majority of exoskeletons from employing rigid components in parallel with the human biomechanics, resulting in ergonomics and usability which are still far from being optimal. Furthermore the weight of most of the rigid devices requires unacceptable metabolic costs from the wearer, resulting from movement restrictions and unwanted torques on the human joints [1].

Soft wearable exoskeletons (or referred as exosuits) are the successive step to the introduction of compliant actuation, where not only the actuators but also the structure of the exoskeleton itself is designed to be compliant. Whilst not being suitable for applications requiring large forces and torques where rigid exoskeletons still show higher performance, exosuits' intrinsic compliance, portability and low-power consumption make them ideal for augmenting muscular strength or providing additional support in ADLs such as walking [2, 3] and hand grasping [4, 5]. Exosuits allow to overcome the limitations introduced by conventional exoskeletons where the lack of mechanical compliance in the kinematic structure represents their major limiting factor. As an alternative to the stiff links of conventional exoskeletons, the exosuit design comprises fabrics and meta-materials to connect the human limb to the actuation stage, while the support is provided by the human musculoskeletal system. These systems have a number of substantial benefits: with their fabric construction, exosuits eliminate problems of aligning the rigid frames precisely with the biological joints and their inertia can be extremely low. These two features eliminate resistance to human motion, thus permitting close to natural kinematics. Furthermore, exosuits can be lightweight and sleek, making them to be worn constantly, thus helping patients in

ALDs for longer periods of time throughout the day. Last but not least, using fabric allows a significant reduction of the overall cost of the device, bridging the current gap between the low purchasing power of the majority of the population in need of assistive technology and unbearable cost of state-of-the-art exoskeletons. However, while exosuits do offer potential benefits over traditional rigid exoskeletons, there are several limitations related to controllability and maximum applied forces/torques and thus research remains to characterize and then understand their capabilities.

1.2 Motivation

Typically, soft exosuits combine the use of fabric-based frams and a Bowden cable-driven actuation for motion transmission to directly apply forces/torques at the joints level. Being flexible and compliant, this kind of systems can bring the actuation stage away from human articulations (i.e. in a backpack), and the assistive torques can be transmitted via cables from the actuators to the end-effector. The studies of Bowden-cable transmission exosuits performed so far has shown encouraging results in healthy subjects and cases of mild impairment: Asbeck *et al.* [2] have demonstrated that applying forces with the right timing during the walking cycle can reduce the metabolic cost of walking, and In *et al.* [6] have experimented with a soft glove driven by tendons for restoring up to a 50 N hand grasp.

However, assistance of upper limbs, especially elbow and shoulder, is a challenging task since multiple actions might correspond to multiple controller layers that must account for the dynamic nature of human tasks, ranging from fine manipulation to weight/force compensation, to general interaction with the external environment and unpredictable dynamics. Moreover, the complexity of the upper limb biomechanics is not confined to one plane [7], as for the walking gesture, but may involve multiple joints across multiple task dimensions. Since the upper-limb motions are crucial for patients to perform daily activities, thus effectively assisting such motions for physically disable people brings a huge benefit to ease their daily lives and makes them more productive.

While for rigid exoskeletons the most used control approach is based on torque control with actuation at the joint, for exosuits this approach fails. A model-based controller on individual skeletal muscles is considered more appropriate and descriptive of the dynamic interaction between the exosuit and the human biomechanics. One of the most significant examples of upper-limb exosuit, which employed a fine model-based controller implementation, was from Ueda *et al.* [8]. The novelty of the design was in the integrated human-exoskeleton model used to compute the interaction

between the human muscle forces and torques generated by the exosuit. Assistance was evaluated by an embedded musculoskeletal model which calculated moment-arms from each of the muscles attached to the bones considering a total 51 muscles, while a kinematic model of the exoskeleton that consists of pneumatic actuators and supporting frames was integrated with the human model.

Despite the potentials and the demonstrated efficacy of the proposed computational approach via physiology-based criterion functions, the use of this method on impaired subjects showing a non stereotypical muscular activity is still under debate. That's why other examples of upper limb exosuits are extremely focused on helping subjects in replicating specific motor functions, involving only a limited number of joints and relying on controllers which, in order to preserve robustness, are highly task-specialized. Common strategies for intention detection are the use of biosignals (i.e. electromyography EMG), force trigger detection and proportional control to drive the devices and providing assistance. An example of exosuit triggering assistance by EMG detection is from Delph *et al.* [9] for a cable-driven exosuit for hand and elbow assistance, where the fingers and the arm could be independently actuated using position of force control via surface EMG feedback. Other examples of wearable textile-garment based exosuits for hand rehabilitation come from Lee *et al.* [10] and In *et al.* [6], where an exo-tendon device and exo-glove respectively, used cable actuation to promote the recovery of fingers coordination and restoring functional hand movement after stroke or spinal chord injury. The two devices used different approaches: the exo-tendon was designed to be a rehabilitation device for clinical therapy, where the geometry and the disposition of the tendons, driven by seven motors, aimed at finely replicating different hand gestures (i.e. grasping, lateral grip, pinching etc.) by passive motion paradigm; the exo-glove relied on a more compact design, employing an underactuated mechanism and focusing its strength on the portability and versatility, where assistance was triggered by wrist motion.

The global scenario depicts two main approaches for high-level controlling upper-limb exosuits: the first on EMG-driven criteria functions with the intent of interpreting as accurately as possible the user's motion intention and a second approach which is focused on control robustness and thus simplifies the number of functions that can be accomplished. If on one side the former approach is limited by the accuracy of the EMG signals and highly sensitive to subject specificity, the latter allows the user to replicate only predetermined specific actions.

Furthermore, the presence of nonlinearities, especially friction [11, 12] and backlash [13, 14, 15] occurring between the cable and the outer Bowden sheath, challenges the system control and limits its performances. Inherent friction and backlash in the

Bowden cable-driven system impact on control robustness, introducing a delay in the transmission and inaccuracies in force and position tracking. These nonlinearities introduce significant tension losses across the cable and give rise to motion backlash, cable slack, and input-dependent stability of the servo system [16, 17]. In the absence of a transmission model that accounts for these nonlinear behaviours [18, 19], control performances are extremely poor. Physical design measures have been shown to help: a PTFE lining on the cables and/or housing can reduce friction phenomena, pre-tensioning of the inner cables has shown to significantly reduce slacking [16] and a high-stiffness or slightly pre-tensioned outer housing reduces backlash-related issues [19]. Nevertheless, these choices can only improve the system performance to a certain degree. To obtain higher accuracy one must rely on effective control algorithms [20].

1.3 Contributions of the Thesis

The research work presented in this thesis describes and improves the design and control implementation of an upper-limb soft exosuit for human arm assistance. The major contributions of this thesis are outlined as follows:

- Presenting the preliminary design of a cable-driven soft exosuit for assisting elbow flexion/extension during ADLs, aiming to design a low profile and functional device that a patient with muscle weakness in the upper limbs can use to regain independence in tasks performed on a daily basis, such as eating and drinking. The proposed exosuit comprises a proximally located actuation stage that transmits assistive forces/torques to a custom-designed sleeve through a set of Bowden cables.

- Proposing a novel hierarchical control paradigm which allows to operate the soft arm exosuit providing assistance to the user's elbow movements. The proposed control architecture is referred to be "hierarchical" because it consists of three separate layers in cascade. Differently from previous control schemes proposed in the literature, in this thesis I aim at considering all the aspects ranging from human motion intention detection, to adaptive compensations of unwanted effects arising from the presence of nonlinear behaviour in the exosuit, i.e. friction and backlash occurring when the cable slides along the Bowden sheath.

- Inspiring the concept of active impedance control from Ollinger *et al.* applied in rigid exoskeletons, I propose a high-level controller of the hierarchical control scheme as the human motion intention detection by means of admittance

control. The high-level controller, moreover, is able to evaluate the amount of assistive forces/torques requested by the user, meaning that the level of assistance is strictly dependent on the user's residual motor capacity.

- Introducing a dynamic model to capture the hysteresis phenomena caused by the backlash effect in Bowden-cable transmission. Based on the modelled hysteresis, since the backlash varies, depending on the configurations of the Bowden cables, I propose and implement a nonlinear adaptive controller for time-varying backlash compensation during motions of human arm. This backlash compensation controller also plays a role as a transmission stage or mid level, defining the reference motion for the actuation stage from the human motion intention obtained from high level.

- Developing another nonlinear adaptive controller as low level for compensating the friction effect and computing the control signal sending to the actuation unit. Due to the sliding of the cable along the outer housing, the friction makes the torques generated by the actuator lost during operation. Thus low-level controller eliminates the detrimental effect of friction, improves the position tracking performance and provides required assistive torques to the user.

1.4 Thesis Overview

This thesis consists of six chapters. The contents of each chapter are stipulated as below:

Chapter 1: Introduction

This chapter introduces the background in robotic exoskeleton developments for rehabilitation and assistive technology from traditional rigid devices, series elastic actuators to the new trend using soft actuators and soft materials. The motivation of the research comes from the limitations of current approaches of exosuits in both design and control implementation. The objectives as well as significance of the research are also mentioned along with the thesis organization.

Chapter 2: Literature Review

This chapter provides a literature review of the research, consisting of several main parts: background information of human upper limb anatomy and exoskeleton robots, then focusing on modern approaches of soft exoskeleton devices using a Bowden-cable transmission, and finally introducing associated control strategies.

Chapter 3: Soft Arm Exoskeleton and Actuation Stage Design

A cable-driven soft exoskeleton (or soft exosuit) for human arm assistance is proposed in this chapter. Mainly the development of the suit as well as the mechanical design of the actuation stage for driving Bowden-cable transmission are described in details. In addition, the evaluation of the actuator's bandwidth is tested to verify that the design meets the requirement to assist the user's movements in activities of daily living.

Chapter 4: High-level Assist-as-needed Control Strategy using Admittance Control

This chapter briefly introduces the hierarchical control architecture for the proposed soft exosuit. As the high-level controller, the concept and design of admittance control is explained in details, aiming to decrease the intrinsic mechanical impedance of the human arm and generate a smooth reference trajectory which the actuator must deliver to the human joint. Furthermore the proposed admittance control is able to tune the level of assistance depending on the voluntary motion capacity of the user, this strategy resembles the assist-as-needed paradigm. Finally, the experimental protocols and results are represented at the end of the chapter.

Chapter 5: Mid-level Nonlinear Backlash Compensation Control

After the reference motion for the human elbow joint is defined from Chapter 4, mid-level control described in this chapter transfers that motion into desired trajectory for the actuation stage and compensates the backlash effect occurring in the Bowden-cable transmission. A dynamic model based on the normalized Bouc-Wen model is also presented and employed to capture the associated hysteresis of the backlash phenomenon. Since the backlash is strictly dependent on the curvature angle of the Bowden sheath, which is time-varying and cannot be precisely determined, a nonlinear adaptive control scheme is then proposed for backlash compensation to deal with the uncertainties in the model's parameters and the changes in Bowden cable configurations during motion of the human arm.

Chapter 6: Low-level Nonlinear Friction Compensation Control

The low-level control method driving the actuation stage is presented in this chapter. Beside the inherent backlash, nonlinear friction, which arises when the cable slides along the outer sheath, significantly causes major losses in motion transmission of Bowden-cable mechanism. Thus in order to achieve high precision motion control, friction must be appropriately modelled and compensated. This chapter proposes a dynamic friction model using LuGre approach and then suggests a model-based adaptive control technique to compensate for nonlinear friction, improving the motion tracking performance for the actuator.

Chapter 7: Discussion and Conclusion

The final chapter summarizes the contributions of the thesis, discusses them, and provides suggestions for the future work.

2 Literature Review

The exoskeleton robots were studied for the purposes of industrial or medical applications in the 1960s and 1970s [21, 22, 23, 24, 25, 26]. Hardiman in [23], which was the first whole body exoskeleton robot, was actuated by hydraulic actuators and was supposed to be driven by a human operator from the inside of exoskeleton. In addition, some exoskeleton robots were proposed to extend the strength of the human force [26, 27] in early 1990s. With the advances in recent technology in the fields of mechanical engineering, electronic engineering, biomedical engineering, and artificial intelligence the exoskeleton robot technology has seen a rapid development in recent years. As a result, many upper-limb exoskeleton robot systems and lower-limb exoskeleton robot systems have been proposed for rehabilitation, haptic interaction, human augmentation and power-assist of physically weak individuals.

This chapter presents the literature review for the thesis, ranging from the overview on of human upper limb anatomy towards the development of an upper limb exoskeleton robots. Furthermore the current approaches of soft exoskeleton driven by Bowden cables are focused and discussed in details. Finally a review on the associated control strategies for assistive technology is reported and compared.

2.1 Overview on Biomechanics of Human Upper Limb

This section briefly explains the anatomy of human upper limb which mainly consists of shoulder complex, elbow complex, wrist joint and fingers [28] (Figure 2.1).

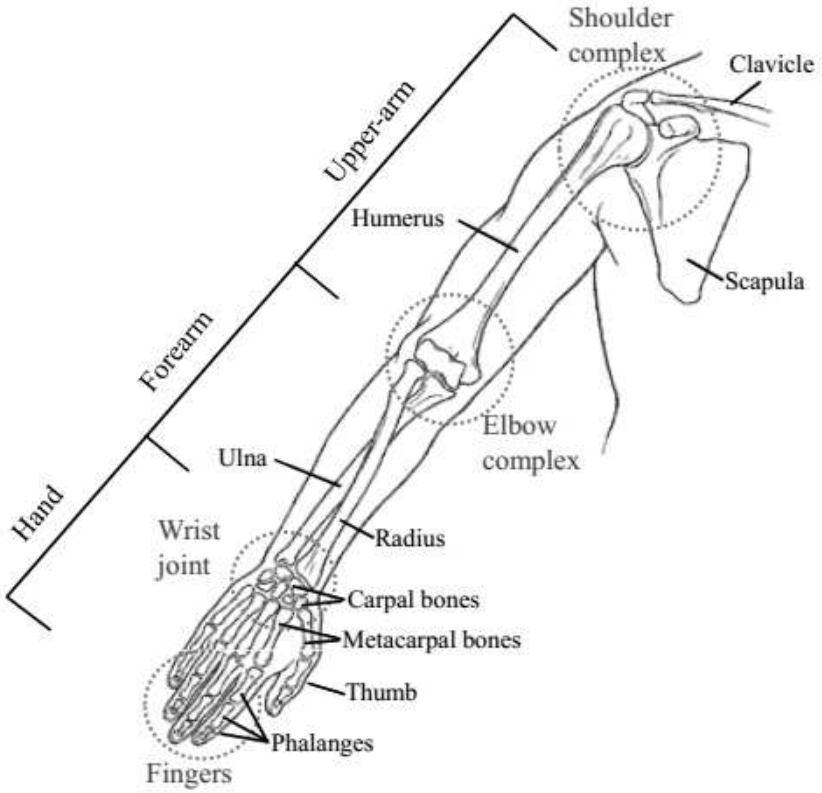

Figure 2.1: Biomechanics of human upper limb, consisting of shoulder complex, elbow complex, wrist joint, and fingers.

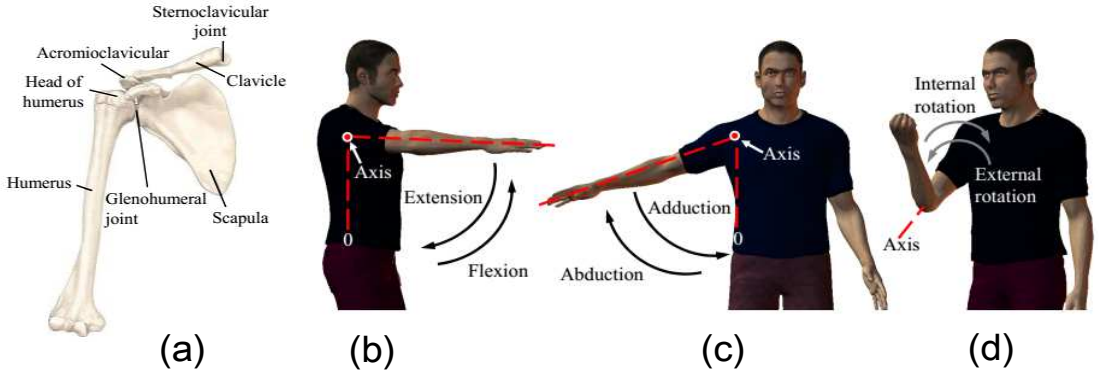

Figure 2.2: Shoulder complex and shoulder motions. (a): Shoulder anatomy. (b): Shoulder flexion/extension motions. (c): Shoulder abduction/adduction motions. (d): Shoulder internal/external rotation.

2.1.1 Shoulder Complex

Shoulder complex shown in Figure 2.2 consists of three bones: the clavicle, scapula, and humerus; and three articulations: the glenohumeral, acromioclavicular, and ster-

noclavicular [29, 30, 31]. The glenohumeral joint is commonly referred as the shoulder joint. The acromioclavicular joint is formed by the lateral end of the clavicle and the acromion of the scapula. The sternoclavicular joint is the joint connecting the shoulder complex to the axial skeleton. Basically, the shoulder complex can be modeled as a ball-and-socket joint. The position of the instantaneous center of rotation (ICR) of the shoulder joint is dynamic and it changes with the position of the upper arm. The shoulder complex possesses three main degrees of freedom (DOFs): shoulder flexion/extension, shoulder abduction/adduction, and shoulder internal/external rotation. Average range of motion of human shoulder are reported in, i.e. shoulder flexion: $0° \rightarrow 180°$, shoulder extension: $0° \rightarrow 60°$, shoulder abduction/adduction: $0° \rightarrow 150°$, internal rotation: $0° \rightarrow 70°$, and external rotation: $0° \rightarrow 90°$ [32, 33].

2.1.2 Elbow Complex

Figure 2.3 illustrates the elbow complex and its motions. The elbow complex includes the elbow joint and the radioulnar joints [29, 34]. The elbow joint is a compound joint consisting of two joints: the humeroradial, between the capitulum and the radial head; and the humeroulnar, between the trochlea and the trochlea notch of the ulnar. In general the elbow complex allows two DOFs: elbow flexion/extension, and forearm supination/pronation. Normal range of motion of the human elbow is $0° \rightarrow 5°$ for extension, and $0° \rightarrow 145°$ for flexion. In addition average range of motion for forearm pronation is reported as $0° \rightarrow 70°$, whilst $0° \rightarrow 85°$ for forearm supination [35, 36, 37].

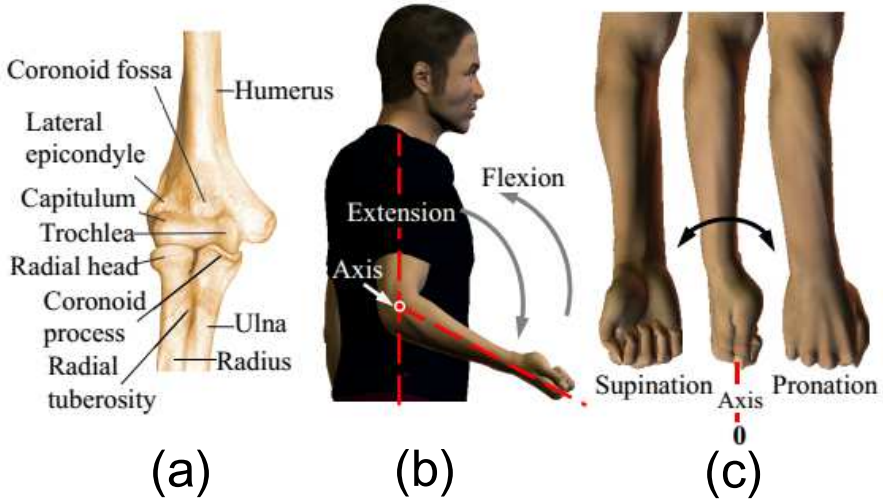

Figure 2.3: Elbow complex and elbow motions. (a): Elbow anatomy. (b): Elbow flexion/extension motions. (c): Forearm supination/pronation motions.

2.1.3 Wrist Joint

The wrist, or carpus, shown in Figure 2.4 is a deformable anatomic entity that connects the hand to the forearm. This is a collection of eight carpal bones and the surrounding soft tissue structure. The wrist joint possess two DOFs: wrist flexion/extension, and wrist radial/ulnar deviation. The wrist motions are generated about four different axes, i.e. the wrist flexion axis is different from the extension axis, similarly the radial deviation axis and the ulnar deviation axis are also different [38]. Although wrist flexion and wrist extension have different axes, they intersect at a point in the capitate. Similarly radial and ulnar deviation axes also intersect. Therefore it can be considered that flexion and extension share one axis, and ulnar and radial deviation share another axis, the slight offset of the rotational axes of the wrist flexion/extension motions and the radial/ulnar deviation is approximately 5mm. Normal range of motion of the wrist joint is recorded as $0° \rightarrow 75°$ for flexion, $0° \rightarrow 70°$ for extension, $0° \rightarrow 20°$ for radial deviation, and $0° \rightarrow 35°$ for ulnar [38, 39, 40].

2.1.4 Fingers

The joints of the human fingers are shown in Figure 2.5 . They are the metacarpophalangeal (MCP), proximal interphalangeal (PIP), and distal interphalangeal (DIP) joints [41, 42]. The MCP joint allows two DOFs, and the center of rotation of the MCP joint changes according to the motion of the joint. While the interphalangeal joints are one DOF with the fixed centers of rotation. The thumb is different in anatomically from

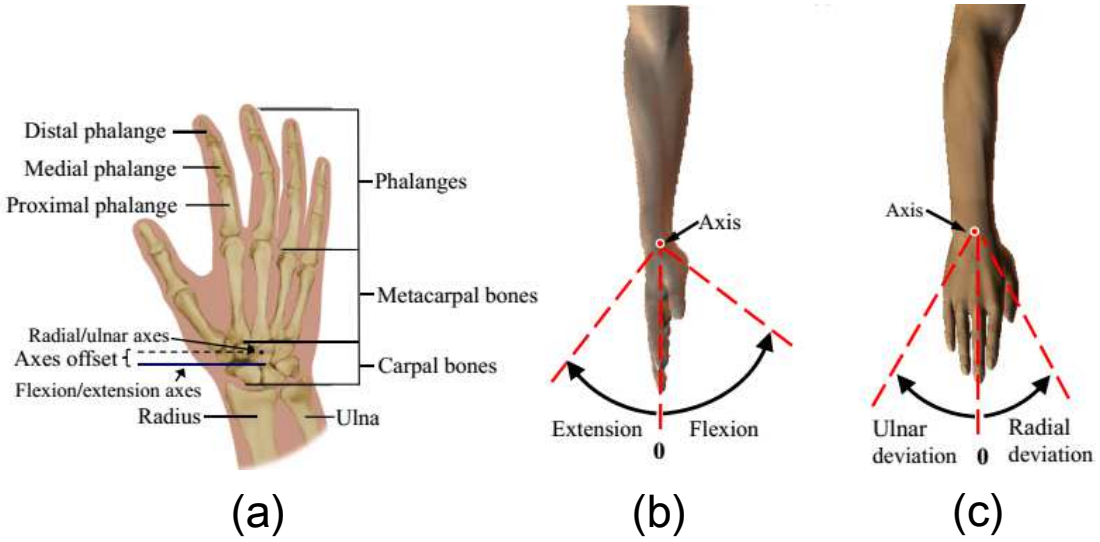

Figure 2.4: Hand and wrist joint motions. (a): Hand anatomy. (b): Wrist flexion/extension motions. (c): Wrist radial/ulnar deviations.

Figure 2.5: Finger anatomy. A finger has metacarpophalangeal (MCP), proximal interphalangeal (PIP), and distal interphalangeal (DIP) joint.

the other fingers, i.e. it contains three joints: the carpometacarpal (CMC), metacarpophalangeal (MCP), and interphalangeal (IP) [43, 44]. Finally the average range of motion of human upper limb, i.e. shoulder, elbow, wrist, and fingers, is summarized in Table 2.1.

Shoulder complex	Flexion	0° → 180°
	Extension	0° → 60°
	Abduction/Adduction	0° → 150°
	Internal rotation	0° → 70°
	External rotation	0° → 90°
Elbow complex	Flexion	0° → 145°
	Extension	0° → 5°
	Forearm pronation	0° → 70°
	Forearm supination	0° → 85°
Wrist joint	Flexion	0° → 75°
	Extension	0° → 70°
	Radial deviation	0° → 20°
	Ulnar deviation	0° → 35°
Finger	MCP joint flexion	0° → 90°
	PIP joint flexion	0° → 90°
	DIP joint flexion	0° → 90°

Table 2.1: Upper limb average range of motion

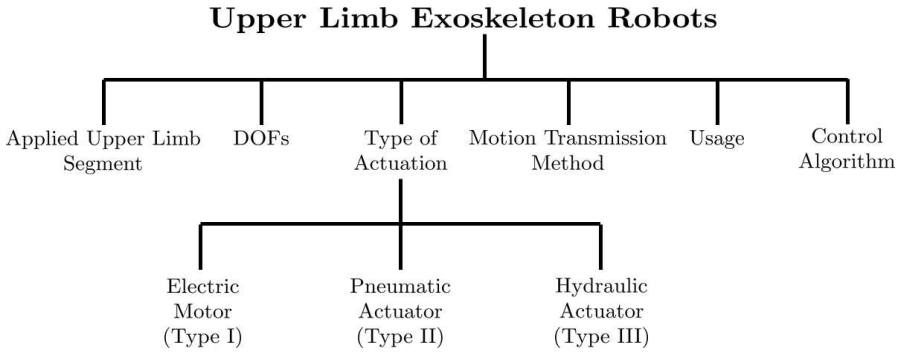

Figure 2.6: Classification of the upper limb exoskeletons.

2.2 Classification of Upper Limb Wearable Exoskeletons

2.2.1 Classification Methods

Upper limb exoskeleton robots can be classified in several ways [45] as shown in Figure 2.6, considering characteristics of the hardware mechanical designs and the control algorithms. In the literature review, the upper limb wearable devices are organized according to:

- **The applied segment of the upper limb:**
  Under this category, the upper limb exoskeletons are divided as hand exoskeleton robot, forearm exoskeleton robot, shoulder exoskeleton robot, full upper limb or combined segments exoskeleton robot.
- **Degree of freedom:**
  The category can be based on the number of active joints, such as 1 DOF, 2 DOF, etc.
- **The methods of actuation:**
  The classification is according to the types of actuation used in the device, such as electric motor, pneumatic, hydraulic, etc.
- **The methods of motion transmission:**
  The classification is according to the motion transmission methods from the actuation to the joint, such as direct drive, gear drive, rigid linkage mechanism, belt drive, ball screw drive, soft Bowden cable drive, etc.
- **The applications:**
  The upper limb wearable exoskeletons can be classified in accordance with

the intended applications, such as rehabilitation, assistive technology, human augmentation, haptic interface, etc.

- **The control methods:**
  This category is based on the control algorithms used to drive the device, such as position control, force control, hybrid force/position control, impedance/admittance control, etc.

In this chapter, the upper limb wearable exoskeletons are classified according to the actuator used in the hardware design. In general there are three main types of actuation:

- **Type I:** Actuation by electric motor
- **Type II:** Pneumatic actuation
- **Type III:** Hydraulic actuation

Reference	**Applied Segments**	**Active DOFs**	**Actuator**	**Motion Transmission**	**Application**
Kiguchi *et al.* [33]	Shoulder, elbow, and forearm	4	DC motors	Cable and gear drive	Assistance
Papadopulus *et al.* [46]	Shoulder	2	DC motors	Geneva and four-bar mechanism	Rehabilitation
Mulas *et al.* [47]	Hand	2	DC motors	Tendon sheath mechanism	Rehabilitation
Rosen *et al.* [48]	Shoulder and elbow	2	DC motors	Cable and gear drive	Assistance
Perry *et al.* [49]	Shoulder, elbow, forearm and wrist	7	DC motors	Cable drive	Rehabilitation Assistance
Kawasaki *et al.* [50]	Forearm, wrist, and fingers	18	DC motors	Linkage and gear drive	Rehabilitation
Gupta *et al.* [51]	Forearm, elbow, and wrist	5	DC motors	Direct drive	Rehabilitation
Frisoli *et al.* [52, 53]	Shoulder and elbow	4	DC motors	Cable drive	Haptics Rehabilitation

Nef *et al.* [54, 55]	Shoulder and elbow	4	DC motors	Cable, gear and linkage drive	Rehabilitation
Mihelj *et al.* [56]	Shoulder, elbow, forearm and wrist	4	DC motors	Cable, gear and linkage drive	Rehabilitation
Ruiz *et al.* [57]	Elbow, forearm and wrist	3	DC motors	Gear drive	Rehabilitation
Johnson *et al.* [58]	Shoulder, elbow and forearm	3	DC motors	Cable drive	Assistance Rehabilitation
Sarakoglou *et al.* [59]	Fingers	7	DC motors	Tendon sheath mechanism	Rehabilitation
Wege *et al.* [60]	Fingers	4	DC motors	Cable and gear drive	Rehabilitation
Carignan *et al.* [61]	Shoulder, elbow and forearm	5	DC motors	Gear drive	Rehabilitation
Ball *et al.* [62]	Shoulder, elbow and wrist	3	DC motors	Cable drive	Rehabilitation
Ball *et al.* [63]	Shoulder and elbow	5	DC motors	Cable drive	Rehabilitation
Chou *et al.* [64]	Shoulder, elbow, forearm and wrist	7	DC motors	Cable drive	Haptics
Delph *et al.* [9]	Hand	10	DC motors	Cable drive	Assistance
Lee *et al.* [10]	Hand	22	DC motors	Tendon sheath mechanism	Rehabilitation
In *et al.* [4]	Hand	9	DC motors	Tendon sheath mechanism	Assistance Rehabilitation
Xiloyannis *et al.* [5]	Hand	8	DC motors	Tendon sheath mechanism	Assistance Rehabilitation

Table 2.2: Upper limb exoskeleton robots actuated by electric motor (**Type I**).

Reference	**Applied Segments**	**Active DOFs**	**Actuator**	**Motion Transmission**	**Application**
Lucas *et al.* [65]	Hand	3	Pneumatic actuators	Cable drive and linkage mechanism	Assistance
Sasaki *et al.* [66]	Wrist	1	Pneumatic muscles	Pneumatics	Assistance

Noritsugu *et al.* [67]	Hand	15	Pneumatic muscles	Pneumatics	Assistance
Tsagarakis *et al.* [68]	Shoulder, elbow, forearm and wrist	7	Pneumatic muscles	Pneumatics	Rehabilitation
Lee *et al.* [69]	Shoulder, elbow, forearm, wrist, and hand	13	Pneumatic actuators	Pneumatics and linkage mechanism	Tele-operation
Takahashi *et al.* [70]	Wrist and hand	3	Pneumatic actuators	Pneumatics	Rehabilitation
Sugar *et al.* [71]	Shoulder, elbow and wrist	4	Pneumatic muscles	Pneumatics	Rehabilitation
Kobayashi *et al.* [72]	Shoulder, elbow and wrist	6	Pneumatic actuators	Pneumatics	Assistance
Polygerinos *et al.* [73]	Hand	10	Pneumatic actuators	Pneumatics and soft materials	Rehabilitation
HK Yap *et al.* [74]	Hand	10	Pneumatic actuators	Pneumatics and soft materials	Assistance Rehabilitation

Table 2.3: Upper limb exoskeleton robots actuated by pneumatic actuator (**Type II**).

Reference	**Applied Segments**	**Active DOFs**	**Actuator**	**Motion Transmission**	**Application**
Mistry *et al.* [75]	Shoulder, elbow, forearm and wrist	7	Hydraulic actuators	Hydraulics	Rehabilitation
Lenzi *et al.* [76]	Elbow	1	Hydraulic actuators	Cable drive	Rehabilitation
Pylatiuk *et al.* [77]	Elbow	1	Hydraulic actuators	Hydraulics	Rehabilitation
Ohnishi *et al.* [78]	Shoulder, elbow, forearm and wrist	7	Hydraulic actuators	Cable drive	Assistance

Table 2.4: Upper limb exoskeleton robots actuated by hydraulic actuator (**Type III**).

2.2.2 Actuation Technologies for the Upper Limb Exoskeletons

Several actuation techniques have been developed for driving the upper limb exoskeleton devices, including electric motor, pneumatic actuator, hydraulic actuator, series elastic actuator, shape memory alloy actuator, etc. However, some of them are not suitable for the applications due to their complicated structure and less torque generation. In existing exoskeleton robots, direct current DC motor, pneumatic actuator, and hydraulic actuator are mostly used. The main advantages and disadvantages of each actuation method are outlined as follow.

Among the comparisons shown in Table 2.2, 2.3, and 2.4, majority of the exoskeleton devices use the electric DC motor for actuation purpose (more than 72%), achieving high speed and high precision in motion control. However, a gear-driven mechanism is also required coupling to the motor, aiming to generate the high torque required for the upper limb's motions. In some cases pneumatic actuators have also been used, providing a high power/weight ratio for the exoskeletons and guaranteeing the compliance in human-robot interaction. However, pneumatic actuator is more difficult to be precisely controlled because air is compressible and responds in a nonlinear behaviour. Furthermore efficiency of the pneumatic actuators is rather low. Therefore about 20% of the upper limb exoskeleton robots have been actuated pneumatically. Finally although hydraulic actuator is able to produce the high torque with adequate accuracy and fast response, it still has several main drawbacks such as fluid leakage and necessity of a wide space for fluid lines. Therefore, hydraulic actuator has rarely been used in the upper-limb exoskeletons (only about 5%).

2.2.3 Motion Transmission Technologies

The motion transmission used in the wearable exoskeletons depends on the actuation method. For example pneumatic or hydraulic actuators use the compressed air or fluid respectively to transmit the motion via piston and cylinder or soft materials. Using an electric motor, the motion can be transmitted by using direct drive, gear/belt drive, rigid linkage mechanism, ball screw, or flexible Bowden cable system. However one of the most common limitations of traditional exoskeletons using rigid frames (i.e. gear, linkage mechanism, ball screw) are the kinematic constrains imposed on the user's joints. Using stiff motion transmissions may also cause the misalignment between the robot's joints and the biological ones, resulting in unnatural articular stress. Moreover it makes the exoskeleton robots bulky and complicated, causing them to be inappropriate for daily at-home use. Thus a new wearable exoskeleton using the Bowden-cable motion transmission combined with fabric structure opened a new

scenario, alternative to the classic exoskeleton robots using rigid frames. The use of flexible Bowden cable-driven system allows the user to freely move and reallocate the actuation unit far from the end-effector. In addition it provides the advantages in activities daily living (ADLs) where portability, light weight, and compliance are preferable.

In the following section I focus on upper limb exoskeleton robots actuated by electric DC motor, and the hardware systems are reviewed in details. They can be classified into two categories: (i) The exoskeletons are designed based on the rigid frames and linkages and (ii) The wearable devices use the soft fabric structure, i.e. clothing-like frames.

2.3 Review on Upper Limb Exoskeleton Robots Actuated by Electric Motor

The electric motor is the most commonly used actuator for the upper limb exoskeleton robots due to its advantages such as fast operations, high precision in motion control, higher controllability using advanced control algorithms, generating high torque, etc. Thus in this section electric motor actuated upper-limb exoskeleton robots are briefly reviewed, taking state-of-the-art robots as examples.

2.3.1 Upper Limb Exoskeletons based on Rigid Frames

Cable-driven Arm Exoskeleton: CAREX

Mao *et al.* [79] demonstrated via experiments with cable-driven arm exoskeleton (CAREX) that it was possible to achieve desired forces on the hand, i.e., both pull and push, in any direction as required in neural training. In the research, an anthropomorphic arm was used to bench test the design and control concepts proposed in CAREX. CAREX was attached to the limb segments of a five DOFs anthropomorphic arm instrumented with joint sensors. The cuffs of CAREX were designed to have adjustable cable routing points to optimize the “tensioned” workspace of the anthropomorphic arm. Simulation results of force field for training and rehabilitation of the arm were first presented. Experiments were conducted to show the performance of a CAREX force field controller when human subjects pull the end-effector of the anthropomorphic arm to travel on prescribed paths. The human-exoskeleton interface was also presented to demonstrate the feasibility of CAREX on human arm.

Upper Limb Exoskeleton Robot from Saga University Japan

Kiguchi *et al.* [32] developed exoskeletal robots to assist the motion of physically weak persons such as elderly persons or handicapped persons. Authors proposed an effective fuzzy-neuro controller, a moving mechanism of the center of rotation (CR) of the shoulder joint of the exoskeletal robot, and an intelligent interface in order to realize a practical and effective exoskeletal robot for shoulder joint motion assist. The fuzzy-neuro controller enabled the robot to assist a person's shoulder motion. The moving mechanism of the CR of the robot shoulder joint was used to fit the CR of the robot shoulder joint to that of the physiological human shoulder joint during the shoulder motion. The intelligent interface was realized by applying a neural network and used to cancel out the effect the human subject's arm posture change.

Anthropometric 7 DOFs Exoskeleton Robot: CADEN-7

A pilot database defining the kinematics and dynamics of the upper limb during daily living activities was one among several factors guiding the development of an anthropomorphic 7 DOFs powered arm exoskeleton by Perry *et al.* [49] . Additional design inputs included anatomical and physiological considerations, workspace analyses,

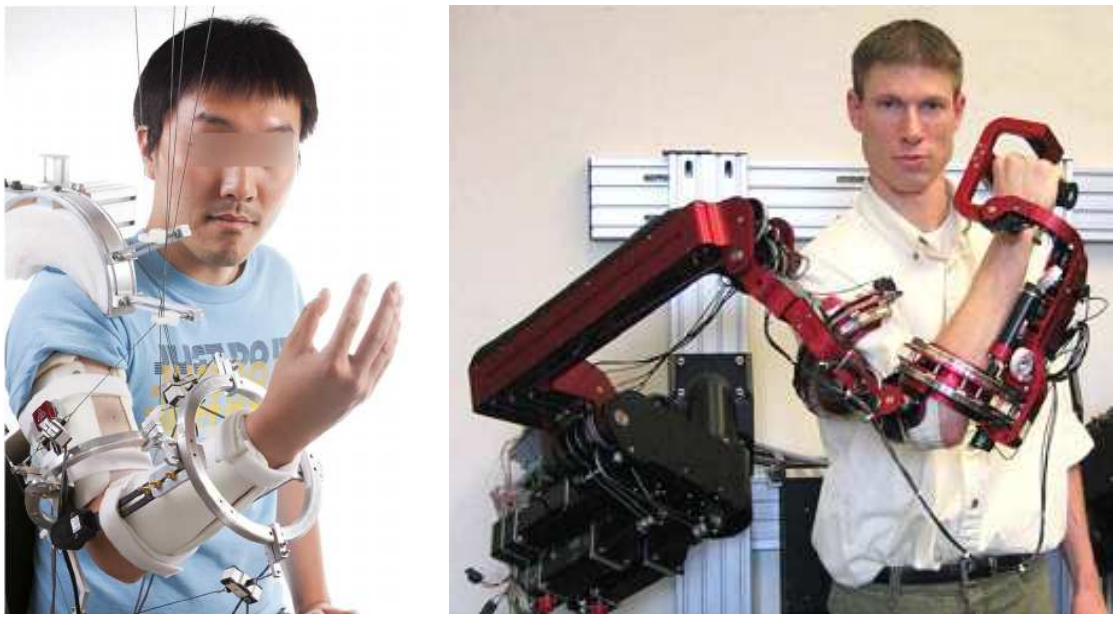

Figure 2.7: (A): Cable-driven Arm Exoskeleton: CAREX. (B): Anthropometric 7 DOFs Exoskeleton Robot: CADEN-7

Figure 2.8: (A): Arm Therapy Exoskeleton with an Ergonomic Shoulder Actuation: ARMin III robot. (B): 4 DOFs Force-feedback Arm Exoskeleton for Haptic Interaction : L-EXOS. (C): High-Performance Ergonomic Exoskeleton for Space Robotics Telepresence: X-Arm-2

and upper limb joint ranges of motion. The database was compiled from 19 arm activities of daily living. The cable-actuated dexterous exoskeleton for neurorehabilitation (CADEN)-7 offered remarkable opportunities as a versatile human-machine interface and as a new generation of assistive technology. Proximal placement of motors and distal placement of cable-pulley reductions were incorporated into the design, leading to low inertia, high-stiffness links, and backdrivable transmissions with zero backlash. The design enabled full glenohumeral, elbow, and wrist joint functionality. Potential applications of the exoskeleton as a wearable robot include: 1) a therapeutic and diagnostics device for physiotherapy, 2) an assistive (orthotic) device for human power amplifications, 3) a haptic device in virtual reality simulation, and 4) a master device for teleoperation.

Arm Therapy Exoskeleton with an Ergonomic Shoulder Actuation: ARMin III robot

Nef *et al.* [80] described a simplified model of the human shoulder. On the basis of that model, a new ergonomic shoulder actuation principle that provides motion of the humerus head was proposed, and its implementation in the ARMin III arm therapy robot was described. The focus lied on the mechanics and actuation principle. The ARMin III robot provided three actuated DOFs for the shoulder and one for the elbow joint. An additional module provides actuated lower arm pronation/supination and wrist flexion/extension. Five ARMin III devices have been manufactured and they are currently undergoing clinical evaluation in hospitals in Switzerland and in the United States.

4 DOFs Force-feedback Arm Exoskeleton for Haptic Interaction : L-EXOS

Frisoli *et al.* [52] presented the mechanical design of the L-EXOS, a new exoskeleton for the human arm. The exoskeleton was a tendon-driven wearable haptic interface with 5 DOFs 4 actuated ones, and was characterized by a workspace very close to the one of the human arm. The design was optimized to obtain a solution with reduced mass and high stiffness, by employing special mechanical components and carbon fiber structural parts. The devised exoskeleton was very effective for simulating the touch by hand of large objects or the manipulation within the whole workspace of the arm. The main features of the first prototype that was developed at PERCRO were presented, together with an indication of the achieved and tested performance.

Other Rigid Exoskeleton Robots

Kawasaki *et al.* [50] designed an exoskeleton with 18 DOFs for rehabilitation therapy. The robot was designed to support the flexion/extension and abduction/adduction motions of fingers and thumb independently as well as the opposability of the thumb. The novelty of the system lies within its finger motion assist mechanism and thumb opposability mechanism.

Sarakoglou *et al.* [59] proposed an exoskeleton hand exerciser. It was combined dexterity with a good range of motion by eliminating inadequacy to combine different modalities such as hand parameter diagnosis and exercise assortment with qualities such as finger dexterity and satisfactory finger range of motion. The system enabled the execution of finger therapy regimes. It could also be used as a motion analysis and lost finger mobility diagnosis tool.

Hand Wrist Assisting Robotic Device (HWARD) was developed by Takahashi *et al.* [81]. It is a 3 DOFs device that exercises flexion and extension of the hand as well as some wrist movement. The aim was to retrain hand grasping and releasing movements using real objects during therapy. This was achieved by providing an unobstructed palm area where various objects could be offered for interaction during exercise. The HWARD is a pneumatic actuated desk mounted exoskeleton robot that supports the patients arm and is attached on the thumb and fingers. It could flex or extend all 4 fingers together at the metacarpophalangeal (MCP) joint, the thumb at the MCP joint and the wrist. Joint angle sensors in the structure were used to measure the movement of the exoskeletons joints, and hence, movement of the limbs of the patient.

A “muscle suit” was proposed by Kobayashi and Hiramatsu in [72] to provide muscular support for the paralyzed or those who are unable to move by them selves. The muscle suit was a garment without using rigid frame and used McKibben actuators driven by

compressed air. Since the actuators were sewn into the garment, metal frames have not been used, the muscle suit was helpful for both muscular and emotional support.

2.3.2 Soft Wearable Upper Limb Exoskeletons based on Fabric Structures

Soft wearable exoskeletons (or referred as soft exosuits) have been demonstrated as a valid means of assisting human movement. Whilst not being suitable for the application of large forces, their intrinsic compliance, portability and low-power consumption make them ideal for reducing human muscle effort in activities of daily living (ADLs) such as walking and grasping. Such kind of solutions allow to overcome the limitations caused by the rigid linkages in conventional exoskeleton devices: these include large output mechanical impedance, misalignment with the user's joints and unnatural articular stress.

One way to overcome the limitations of a rigid wearable robotic device is to rely on the human biomechanics which should provide the "hard" support to bear the loads transmitted by the suit: in such way the function of the rigid structure of a conventional robot is performed by bones and tendons/cables which create the constraints and the degree of mobility to allow human motion.

Typically, soft exoskeletons combine the use of clothing-like frames and a Bowden cable-driven actuation for motion transmission to directly apply forces/torques at the joints level. Being flexible and compliant, this kind of systems allow to relocate the actuation unit away from human articulations, and the assistive torque can be transmitted via cables from the actuators to the end-effector. In the following subsection, several examples of the upper limb soft exoskeletons are provided and discussed.

Soft Robotic Exomusculature Glove for Hand Rehabilitation from Worcester Polytechnic Institute

A cable drive soft glove for post-stroke neurorehabilitation was developed by Worcester Polytechnic Institute, USA (Figure 2.9(A)) [9]. The glove could independently actuate all five fingers in flexion/extension movements (10 DOFs), using position or force control. The actuation stage and electronic circuit system were battery powered and fully self contained in a portable light-weight backpack. The glove could be activated in two modes: switch mode and surface electromyography (sEMG). In the switch mode the glove was controlled by a mechanical switch, performing hand open and close. This mode would be ideal for hand rehabilitation. The sEMG mode allowed the

Figure 2.9: (A): Soft Robotic Exomusculature Glove for Hand Rehabilitation from Worcester Polytechnic Institute. (B): BiomHED: Biomimetic Hand Exotendon Device

user to drive the glove based on the classification of the myoelectric signals. Within this mode, the system was able to provide active assistance to the user in ADLs. Despite the presented soft glove has several advantages, analyses on the hardware mechanical design of the actuation stage and the control algorithm were still missing. Thus the performance of the glove was extremely poor and needed to be improved.

BiomHED: Biomimetic Hand Exotendon Device

Lee *et al.* [10] developed and tested a soft exoskeleton device shown in Figure 2.9(B) for hand rehabilitation (22 DOFs) by adopting a "biomimetic" design approach, i.e. mimic the geometry of the major tendons of the human hand. With BiomHED the complex hand movements could be generated with a limited number of actuators, which were located on a forearm brace designed to be worn by the user. The overall system was designed to be wearable, as the entire forearm apparatus including motors and the brace weighs less than 1kg. This design allowed practice of functional hand movements to be incorporated with various proximal arm movements and allowed users to perform functional upper extremity movements such as *reach-and-grasp* tasks.

Three experimental protocols were implemented to test the performance of the device. In the first session, the dynamic function of each exotendon (i.e., mapping of each exotendon force to multi-joint movements) was evaluated. In the second session, the capacity of the BiomHED to restore finger kinematics was examined. Specifically, the restoration of the functional workspace of the fingertip and multi-joint coordination patterns of the finger were evaluated. Finally, the device efficacy in reproduction of the kinematics of a representative functional manual task was tested. The obtained results demonstrated a significant increase in the kinematic workspace of the fingers

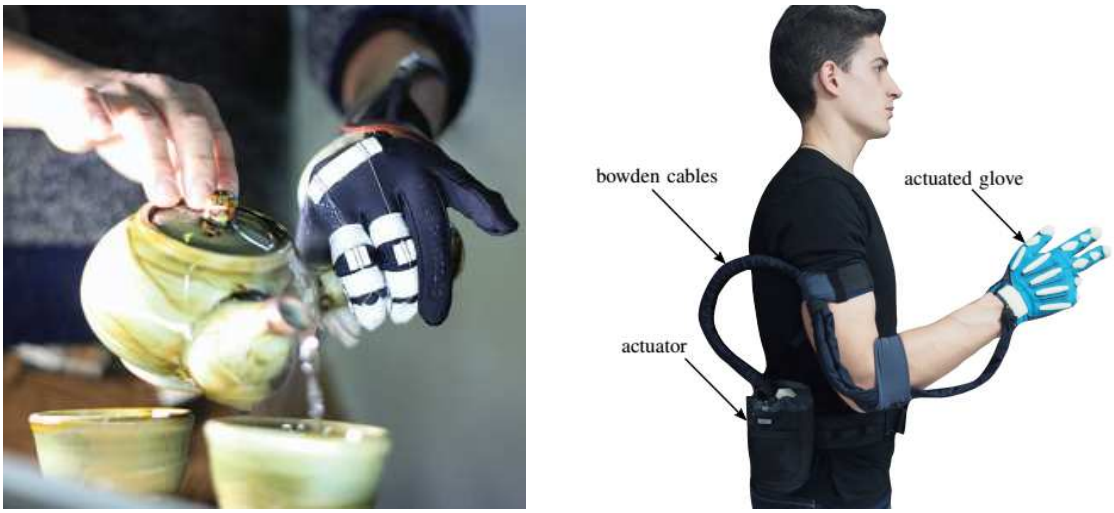

Figure 2.10: (A): Exo-Glove: Soft Wearable Robot for Hand with a Tendon Routing System. (B): Soft Robotic Tendon-driven Glove with Synergy-based Actuator.

in stroke patients, as well as the improvement in the kinematics of functional task performances. However authors used seven brushed DC motors with gear-heads, making the system complicated. Since some of the hand muscles were not involved in the design of the BiomHED glove, limiting the capacity of the device to accurately reproduce kinematics of certain manual tasks, and the total finger flexion angles could not be reached by the presented device. Furthermore the sensory systems and control scheme for the exotenton soft glove were not well explained, reducing the precision in the control of hand movements.

Exo-Glove: Soft Wearable Robot for Hand with a Tendon Routing System

In *et al.* [4] developed a soft wearable glove for grasping assistance (9 DOFs), namely "Exo-Glove" as shown in Figure 2.10(A), employing a soft tendon routing system inspired by human musculoskeletal system. All the elements of the routing system, including the actuator, were designed for operation without pretension, resulting in improved safety, comfort in use, and system efficiency. Authors proposed a novel feeder mechanism, avoiding cable slack and ensuring cable tension around the actuation units. Furthermore to achieve stable grasping using fewer actuators than the number of fingers, an underactuated mechanism for adaptation was employed, aiming to reduce the complexity of the system and enhance the handling of various objects. Considering the control and command, wrist motion has been considered for human-robot interface, and an admittance control was used, making the tendons

act as a virtual compliant spring and guaranteeing the safety of the device. Finally the Exo-Glove was verified on both healthy and impaired subjects, and the results demonstrated that the robot was able to restore grasping function to the disabled subject. The advantages of the Exo-Glove make this an important study for the future design concepts. However there are still several limitations on the control algorithm of the Exo-Glove need to be addressed, such as the sensory systems for the robot and effective compensation control paradigms for inherent backlash and friction in the tendon sheath mechanism.

Soft Robotic Tendon-driven Glove with Synergy-based Actuator

Xiloyannis *et al.* [5] described the design and modelling of tendon-driving actuation unit that empowers a soft wearable glove for grasping assistance. Authors used only one DC motor to actuate simultaneously 8 DOFs (flexion/extension of the thumb, index and middle fingers) of the hand by employing an underactuated mechanism based on the human hand's first postural synergy to design. This aimed to reduce the complexity of the overall system and was able to cover about 60% of activities of daily living. A Bowden-cable transmission was used for motion transmission from the actuation unit which was located on a belt to the fingers' joints. Furthermore taking the advantage of the Exo-Glove, authors employed the feeder mechanism to avoid cable slack around the spool, and proposed an clutch-based mechanism which allows the hand posture to be locked once the object has been grasped, aiming to release the motor's control effort and reduce the associated power assumption. The described actuation unit was tested to verify that it can meet the bandwidth requirement to assist human hand. The result showed a bandwidth of 8Hz which is fully satisfied. Finally a novel position controller based on a machine learning algorithm was introduced to control the system, the obtained results presented a significant improvement in position tracking performance.

2.4 Control Algorithms for the Upper Limb Exoskeleton Robots

The principle to control the exoskeleton robots, especially for assistive technology is to operate according to the user motion intention. This becomes much more important for a physically impaired subject, who is not able to generate the daily motions properly. An exoskeleton robot for assistance purpose consists of two types of controllers: human motion detection and robot controller, working in parallel. The robot controller of the exoskeletons especially aims to low-level control the actuator,

driving the human motions, based on the human motion intention. The conceptual control diagram for the exoskeleton robots with assistive purpose is shown in Figure 2.11 [82]. The motion in a human body can be considered as a feedback loop, where the *Brain* plays a role of control human motions, H represents the musculoskeletal part of the human body. The *Brain* controls the *Muscles* such that H follows an arbitrary desired motion $y_{desired}$. The control output u_h generated by the *Brain* is the motor control signal, sending to the *Muscles* to produce the joint torque τ_h. The input (i.e. human intention) to the exoskeleton robots can be extracted from the *Muscles* signals. By the robot controller, the actuator generates the assistive torque τ_a delivered to the human body H. In the other words, the human body H is actuated by the sum of muscular torque τ_h and assisted by the additional torque τ_a, completing the movements.

Regarding to the control implementation of exoskeleton robots, sensing technologies for detecting the human intention play an important role. However, identifying the exact human motion intention is still the subject of intense research [83]. An effective sensing method is the surface electromyography (sEMG) approach. It is known that the sEMG signals are related to human joint torques and occur prior to the actual motion [84, 85, 86]. Since this sensing method is adaptable for the user, EMG signals have been successfully employed in most of upper limb exoskeleton robots for identifying the human motion intention [9, 74, 87]. In [87] muscle-model oriented EMG-based control method is proposed to control 7 DOFs upper limb exoskeleton robots. Especially in the soft gloves, Delph *et al.* [9] and HK Yap *et al.* [74] simply used the EMG information to activate the robot controller once the signals overcome the certain threshold values. However, the EMG sensors have practical limitations such as subject-dependence, sensitivity to the sensing location, low signal-to-noise-ratio and low repeatability, which does not make them robust enough for daily usage.

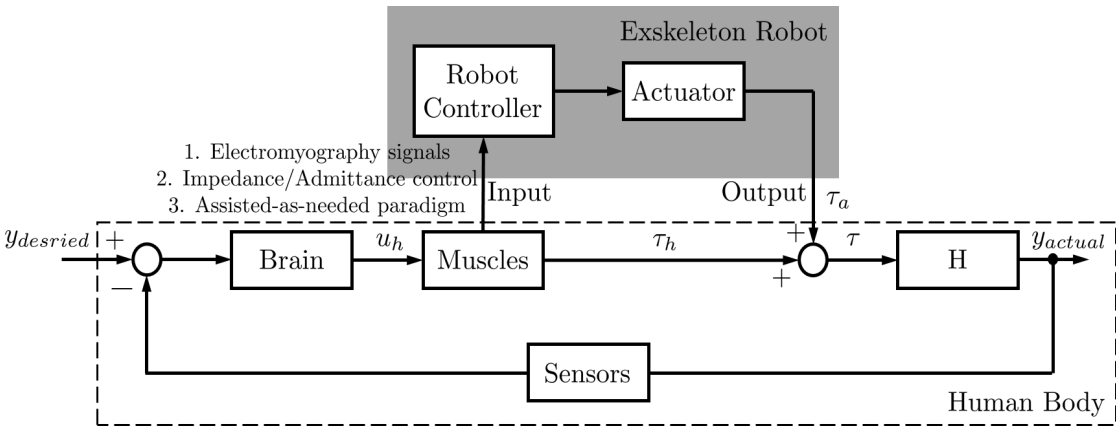

Figure 2.11: Human-exoskeleton robots interaction control system.

Alternative sensing methods, such as muscle fiber expansion sensors [88] or muscle hardness sensors [89], have been developed to overcome such problems, but they do not provide a concrete solution yet.

An alternative common and more robust method consists in extracting the human intention from force/torque sensors at the human-robot interface, combining them with an impedance/admittance controller and a dynamic model of the human limbs [82, 90, 91]; then the robots can deliver the appropriate assistance level to compensate for the user's lack of muscular strength. This approach requires a careful selection of the desired impedance parameters and a good estimation of the dynamic model of the human upper limbs in order to achieve stable performances. However since force/torque sensors cause the system to be expensive and bulky, several researchers have attempted to provide a solution addressing to such problem by introducing sensorless force controlling platforms for human intention detection.

Wolbrecht *et al.* [92] proposed a control method, providing assist-as-needed paradigm, to be used for robot-aided movement training following strokes. Three desirable features of the control method were high mechanical compliance, the ability to assist patients in completing desired movements, and the ability to provide only the minimum assistance required. The control scheme used an adaptive control approach to learn the patient's abilities and delivered the required assistance in completing movements while remaining compliance. Carmichael *et al.* [93] proposed a novel assist-as-needed architecture using the models to estimate the assistance needed by the human operator, where an optimization model was developed utilizing the available musculoskeletal models representing the human upper limb to estimate their strength.

In this thesis, combining the strength of the non-biological signals and assisted-as-needed concept, I propose a high-level control method for the arm exosuit, using the admittance controller and the estimation of the dynamic model of the human arm, to predict the human motion intention and compute the assistive torque required by the user. Moreover the control paradigm is able to adapt to the user's motion ability, meaning that the proposed method should interpret a reduced motion capability, consequently increase the amount of assistance and vice versa.

2.5 Summary

This chapter introduced the background information of the upper limb exoskeleton robots. The biomechanics of human upper limb towards the hardware design of the robots was described. In the literature reviews, the upper limb exoskeleton robots

were classified according to: the applied segments of the upper limb, the active degrees of freedom, the actuation and motion transmission methods, the applications of the robot, and the control algorithms. Here I focus more details on the actuation and motion transmission technologies in the mechanical design. Thus the robotic devices were mainly organized based on the type of actuation such as actuated by electric motor, actuated by pneumatic actuators, and actuated by hydraulic actuators, the advantages and disadvantages of each actuation were provided and discussed. Taking the advantage of the electric motors, the overview on the exoskeletons actuated by the motors were briefly introduced, ranging from traditional rigid exoskeleton robots to a new frontier of wearable devices using soft materials and/or soft actuators. Despite many upper limb exoskeletons and their associated control methods have been widely developed, still many issues need to be identified and addressed such as human-inspired and/or human-mimetic motion generation, safety considering human-in-the-loop interaction, accurate estimation of joint torques using the biological signals, and high precision position and force control for the systems while maintaining the compliance. In the following chapters, the mechanical design and a novel control architecture for a soft exoskeleton driven by the Bowden-cable transmission for human arm assistance will be proposed and described in details.

3 Soft Arm Exoskeleton and Actuation Stage Design

[1]

This chapter describes in details the mechanical hardware design of a soft exoskeleton (or referred as exosuit) for human arm assistance driven by a Bowden-cable transmission. The proposed exosuit comprises an actuation stage and a wearable component. The actuation stage is located distally, i.e. on the back of the wearer, and transmits forces/torques via Bowden cables routed inside the wearable sleeve to the wearer's elbow joint.

3.1 Design Objectives

In this study I assume that the device will be used for assisting people suffering from muscle weakness and having no major spasticity or contractures (Modified Ashworth Scale (MAS) 0–2). The design objectives are based on the average dynamic and kinematic requirements necessary to perform activities of daily living (ADLs); I have also defined reasonable practical considerations on the weight, size and power consumption of the system.

This is done by combining prior studies on the average force/velocities of the elbow during ADLs with a simple mathematical model of the cables routed in the wearable suit. This allows us to project joint torque to motor torque. The requirements are summarized in Table 3.1.

First of all, an assistive device should have enough degree of freedom (DOF) to match the requirements of the user, i.e. in this thesis the exosuit aims to assist elbow flexion/extension motions. Furthermore it is important for the device to span the whole

[1] Part of the work presented in this chapter was published in [94, 95]

Force/Motion Characteristics	Degree of freedom	1 (Elbow flexion/extension)
	Range of motion [deg]	$0^\circ \rightarrow 145^\circ$
	Joint torque [Nm]	4.45
	Bandwidth [Hz]	1.2
Practical consideration	Wearable suit weight [kg]	≤ 0.7
	Actuation stage weight [kg]	≤ 2.5
	Cost [USD]	≈ 1000

Table 3.1: System requirements

range of motion (RoM) of the elbow joint, i.e. $0^\circ \rightarrow 145^\circ$ for elbow flexion/extension. The assistive force requirement is also characterized, many studies have evaluated that in ADLs elbow flexion can require up to 4.45Nm, with a mean value of 1Nm [96, 97]. Lastly, the actuation stage should match the velocities required for human movements in ADLs. Many studies have reported an average elbow flexion velocity of 331°/s [98, 99]. Assuming a sinusoidal motion with a peak-to-peak movement equal to the RoM, this velocity corresponds to a bandwidth of 1.1Hz for the elbow.

Last but not least, portability being one of the main goals when designing the system, I require the total wearable suit weight not to exceed 0.7kg; and the actuation stage, motor controller, and battery should be not over 2.5kg. Finally the overall cost of the exosuit should be kept under USD1000.

3.2 Design of Wearable Sleeve

The sleeve is designed to be both comfortable and functional for the wearer in ADLs [100, 101]. To achieve these goals, I use a combination of fabrics and components with different elastic properties: (1) stretchable fabric made of a mixture of elastane and polyamide is to adapt to the wearer's morphology and increase ergonomics, durability and flexibility, (2) unstretchable fabric (load paths) made of nylon webbing is used to support the tensions T applied by the artificial tendons by redirecting the tensions on the sleeve to normal forces F_N on rigid bone structures (the clavicle), preventing fabric deformation caused by cable tensions. Furthermore in order to maximize motion transmission capability, a pair of rigid braces (3) are tightened around the wearer's arm and forearm using buckles and Velcro straps, thus increasing friction between the suit and the skin, and minimizing undesired slippage. Finally, a harness is used to connect the soft frame to the user's body to bear and distribute the weight of the actuator unit on the user's shoulders. The conceptual sketch of the sleeve is depicted in Figure 3.1.

The first developed prototype of the elbow sleeve is shown in Figure 3.2(A). In Figure 3.2(A) the subject is wearing a harness designed to carry the actuation unit on his torso. The harness, that can be tightened through a set of buckles, loads the weight of the actuator on the wearer's shoulders.

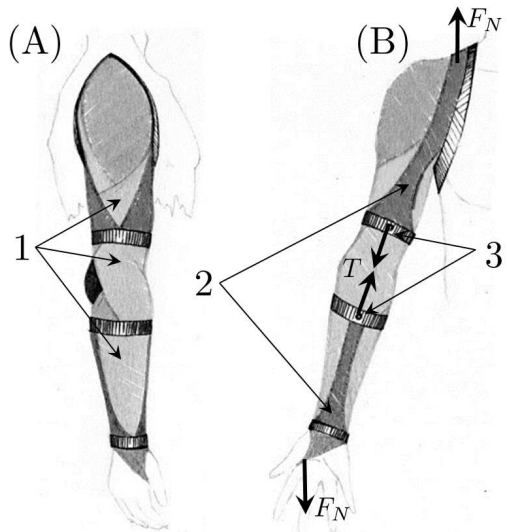

1: Strong stretchable fabric (in light grey)
2: Strong unstretchable fabric (load paths, in dark grey)
3: Rigid braces (anchor points)

Figure 3.1: The conceptual sketch for the sleeve made of different fabrics. (A): Side view. (B): Front view.

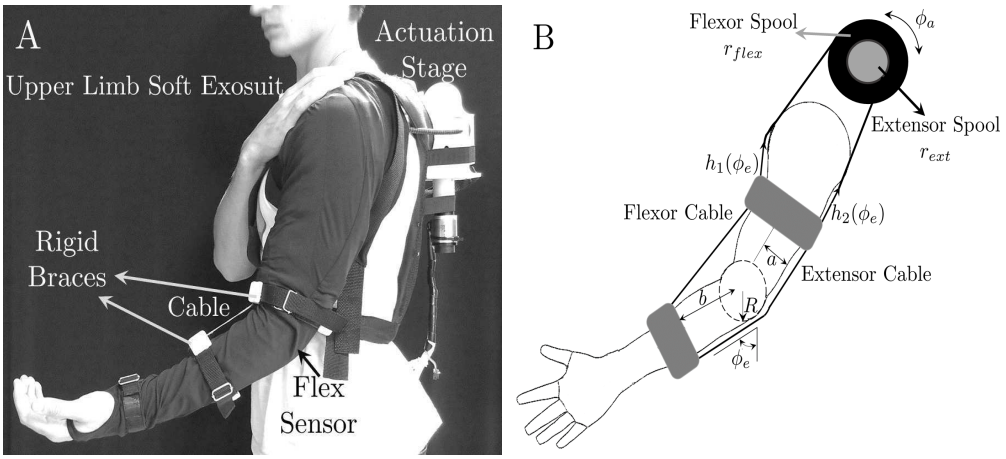

Figure 3.2: First prototype of the sleeve. (A): The exosuit worn by the user, the sleeve, including Bowden cables, weighs less than 400g. (B): Sketch of the cables routed in the human arm and connected to the spool.

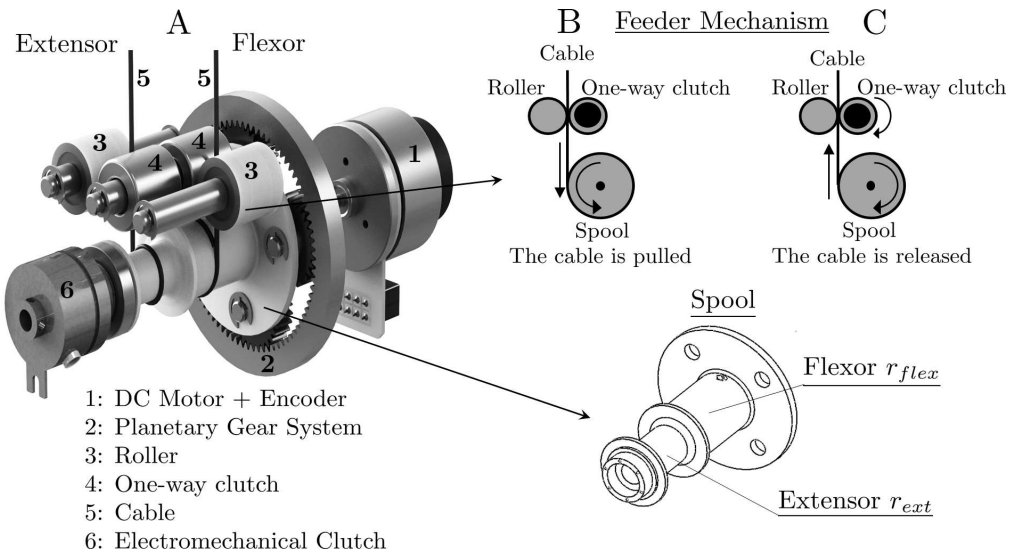

Figure 3.3: (A): CAD drawing for the actuator and the spool, the larger diameter spool for flexor cable and the smaller diameter spool for extensor (the diameter ratio ≈ 1.66). (B)(C): The feeder mechanism aims to prevent cable derailing; when the cable is released the one-way clutch is free to rotate, otherwise it is locked and the spool drags the cable introducing friction.

3.3 Actuation Stage Mechanical Design

The actuation stage is located on the back of the user as shown in Figure 3.2(A). The Bowden-cable transmission routed inside the soft frame, is driven by an actuation unit based on multiple reduction stages: it comprises a DC motor (Maxon EC-i 40 70W, gear ratio 5 : 1) coupled to a custom-designed planetary gear (reduction ratio 5 : 1). The planets drives a spool (shown in Figure 3.3) which pulls the cables in two directions depending on the rotation of the DC motor to actuate elbow flexion and extension movements in agonist-antagonist configuration. The relationship between the displacement of the cables and the joint angle ϕ_e (or extension function [102]) can be formalized using the geometrical relations shown in Figure 3.2(B). Especially, the flexor cable has the extension function h_1 of the form:

$$h_1(\phi_e) = l_1 + 2\sqrt{a^2+b^2}\cos\left(\tan^{-1}\left(\frac{a}{b}\right)+\frac{\phi_e}{2}\right)-2b \tag{3.1}$$

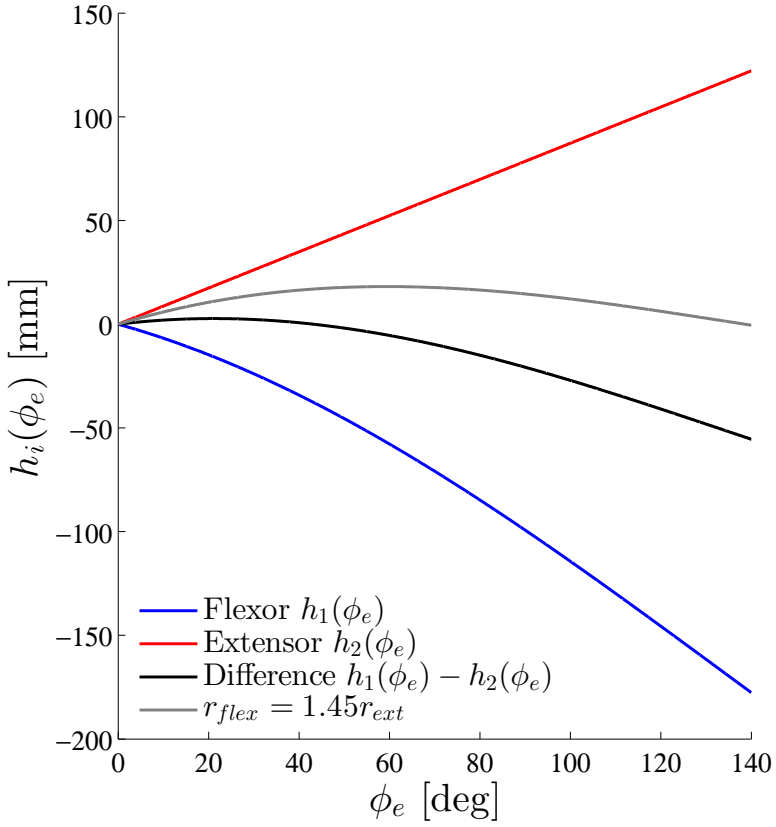

Figure 3.4: The plot shows the displacements of the flexor (h_1) and the extensor cables (h_2) as functions of the full range of motion of the elbow joint ϕ_e [$0° \rightarrow 145°$]. The difference ($\Delta h = h_1(\phi_e) - h_2(\phi_e)$) would cause significant stress on the user's joints. By dimensioning the spool, the mismatch can be minimized (shown in grey). The spool diameters for flexor and extensor are different by a factor ≈ 1.45.

while the extensor cable satisfies:

$$h_2(\phi_e) = l_2 + R\phi_e \tag{3.2}$$

where a is half of the width of the arm, b is the distance from the joint centre of rotation to the anchor points (rigid braces), R is the radius of the elbow joint, ϕ_e is the elbow joint angle (shown in Figure 3.2(B)), and l_i ($i = 1,2$) is the nominal extension when $\phi_e = 0$.

By using the following parameters based on anthropometric data of human elbow [103] ($a = 35$mm, $b = 85$mm, $R = 50$mm and $\phi_e = [0° \rightarrow 145°]$), the resulting displacements of the cables as functions of the joint angle ϕ_e are obtained and depicted in

Figure 3.4. Due to the geometrical differences in human anatomy, the extensor cable $h_2(\phi_e)$ shortens more than the flexor elongation $h_1(\phi_e)$, and a maximum difference Δh of 55mm is generated (shown in black in Figure 3.4). Insufficient release of the extensor cable during motion could cause unnecessary strain on the joint. To avoid this problem, the radius of the flexor and extensor spools are chosen to fit the difference between $h_1(\phi_e)$ and $h_2(\phi_e)$. This results in the flexor spool needing to be approximately 45% larger in radius than the extension one, and a maximum difference Δh is minimized ($\approx$ 3mm) as shown in grey in Figure 3.4. As a result, the spool presents two sections: one for the flexor cable with larger diameter, and one for extensor cable with smaller diameter.

Furthermore in Bowden-cable transmission, it is important to guarantee that the cables do not slack around the spool. Pre-tensioning, a strategy commonly used in cable-driven robots, is not a feasible solution due to the stress that a continuous force would introduce on human joints. Thus in this study I employ a feeder mechanism [104, 105] that confines the cable slack outside of the actuation stage. The feeder mechanism comprising three kingpins has been designed (shown in Figure 3.3(B, C)): the ones on the sides hold one idle rollers while the central one holds two one-way clutches, and the cables pass between the rollers and the clutches. The one-way clutches are oriented such that the free direction is the cable releasing while they are locked when the cables are pulled, coiling around the spool. By doing so they introduce a direction-dependent friction in the mechanism: friction is nearly null

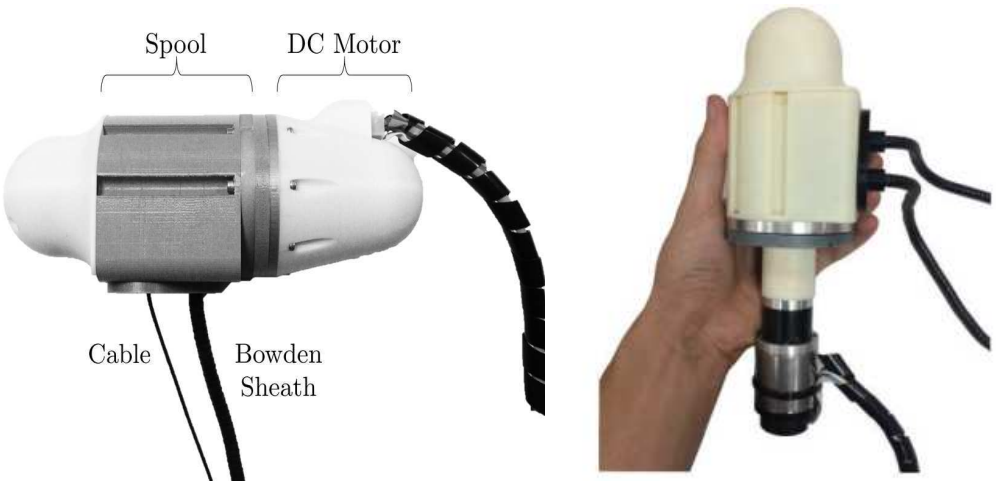

Figure 3.5: Particular of the assembled actuation stage used in the exosuit, a 3D-printed plastic cased in ABS plastic encloses the whole mechanism. The total weight of the actuator, including Bowden cables, is 878g.

when the clutch is free to rotate (i.e. when the cable is released), but is significant when the clutch is locked (i.e. when the cable is coiled). Such friction can be easily won by the motor, but is enough to prevent any slack of the cable around the spool. In order to increase adhesion, a lining of urethane coating was added on the metallic surface of the clutches.

The two flexor and extensor cables, made of tear-resistant Dyneema wire (IGUS Robolink®Dyneema rope), are routed from the spool of the actuation stage on the wearer's back to the elbow joint through the Bowden sheaths (IGUS Robolink®Bowden cable). The whole system are enclosed in a 3D-printed case in ABS plastic shown in Figure 3.5.

3.4 Actuation Stage's Bandwidth

The actuator was tested to verify that it meet the bandwidth required to assist human movements in ADLs. I designed a test bench, illustrated in Figure 3.6, comprising an output spool and a rotary encoder, mounted on the spool's shaft, to monitor its angular position. The cables, routed through the Bowden sheaths from the designed actuation unit to the test bench, was wrapped around the test bench spool.

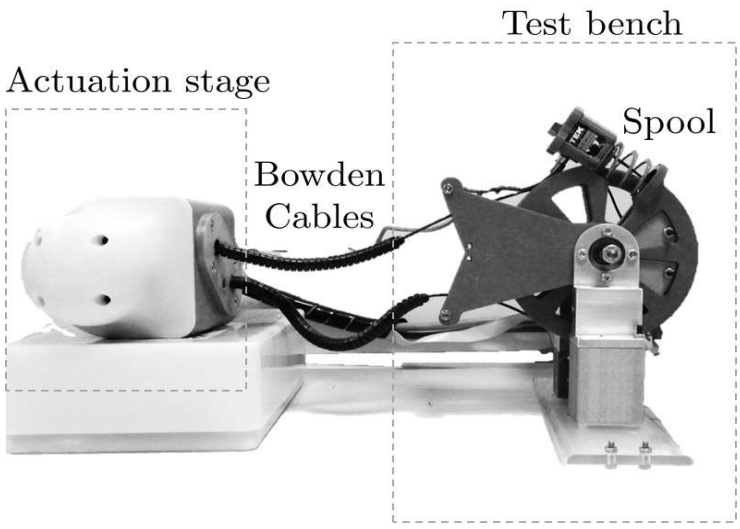

Figure 3.6: The test bench used to evaluate the bandwidth of the designed actuator. The cables were attached to a second spool whose angular position is monitored by a rotary encoder. Upon the application of the input chirp position signal, I measured the output angular displacement and derived the system's transfer function G.

The actuator was then excited with an input linear chirp position signal of the form:

$$\begin{cases} s(t) = S_0 \sin\left(2\pi f(t)\right) \\ f(t) = f_0 + \frac{f_1 - f_0}{T} t \end{cases} \tag{3.3}$$

where $f_0 = 0.1$Hz, $f_1 = 20$Hz, $T = 120$s and S_0 was chosen to span half range of motion of the elbow joint. The angular position of the test bench spool was recorded by means of the encoder attached on the shaft.

Control signal and data acquisition were performed and output using MATLAB/SIMULINK (MathWorks®, USA) interfaced with a Quanser QPIDe acquisition board (Quanser^{TM}) running at a sampling frequency of 1KHz; the low-level position control was handled by a Maxon EPOS2 50/5 motor controller. Figure 3.7 shows the Bode plot of the actuation unit, including magnitude and phase of the system's transfer function G between

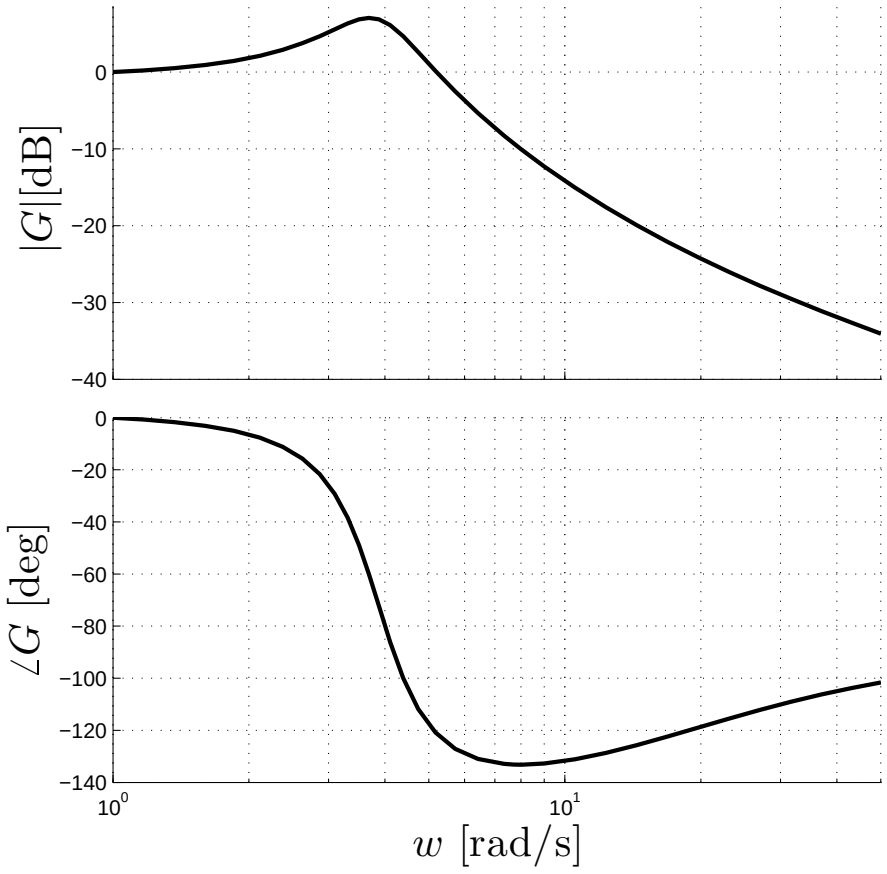

Figure 3.7: Bode plot of the system's transfer function G, between the motor position and the end-effector spool position. The result shows a bandwidth of 6rad/s (≈ 1Hz).

	Cost [USD]
Actuation Stage	
EC motor	285
Planetary gearhead	238
Rotary encoder	106
Servo controller	153
Single board computer	69
Li-Po battery	44
Miscellaneous (gears, clutches, rollers, etc.)	≈ 220
Subtotal	1115
Wearable Suit	
Bowden cables	11
3D-printed parts	24
Fabrics	11
Subtotal	46
Total	1161

Table 3.2: Material cost analysis.

the input position of the actuator and the output spool's position. The system presents a bandwidth of 1Hz, that fully satisfies the characteristic requirements introduced in Table 3.1, that in applications where assistance to impaired subjects is the primary, result to be sufficiently wide.

3.5 Discussion and Summary

In this chapter I presented the hardware design of a soft wearable exosuit for assisting elbow flexion/extension movements. Using fabrics and Bowden cables for motion transmission instead of traditional rigid frames would potentially result in a cheaper solution, making it low profile, lightweight, compliant and less restrictive to the wearer's motions. I based our design on a set of force and motion characteristic requirements, and kept the weight and size of the device as low as possible. As the future work, a stand-alone system is under development, where the actuation stage, the controller architecture and the power supply are redesigned and integrated, fitting compactly in a backpack, to maximize the system biomimetics. Table 3.2 shows the detailed cost analysis of our devices, including electronics and batteries, it is noted that most of the expenses derive from the use of high-quality motors and controllers (96% of the total cost). Thus for mild cases of impairments, the soft exosuit could be a valid low-cost alternative to traditional rigid exoskeletons.

4 High-level Assist-as-needed Control Strategy using Admittance Control

[1]

Regarding to the control strategy of the designed exosuit, this chapter proposes a hierarchical control architecture, starting from the evaluation of the level of assistance requested by the user, then computing the amount of motion delivered to the elbow, and ending to compensating the inherent nonlinear behaviours existing in the Bowden-cable transmission, i.e. backlash and friction. The control scheme shown in Figure 4.1 comprises three main layers: a *high-level*, a *mid-level* and a *low-level* controller. The *high-level* control strategy will be described in details in this chapter, whilst in two following chapters I will explain about the principles of *mid* and *low-level* controller. In this chapter I especially introduce and discuss the general concept of assistance using an admittance controller, regulating the interaction between the exoskeleton robot and the wearer. The objective of the high-level controller is to estimate the amount of assistive torque $\widehat{\tau_a}$ required by the user, decreasing the mechanical impedance perceived by the human arm, and consequently provide an active reference motion ϕ_e^d for the elbow joint based on the admittance control. Furthermore the level of assistance is supposed to be dependent on the wearer's residual motion capacity, meaning the assistive torque $\widehat{\tau_a}$ provided by the exosuit can be modulated according to the wearer's motion speed (i.e. motion ability). This strategy somewhat resembles the "assist-as-needed" paradigm.

4.1 Mechanical Impedance/Admittance Control

Mechanical impedance is the relationship between the net forces applying on a mechanical system and the system's resulting kinematics, i.e. position, velocity, and

[1] Part of the work presented in this chapter was published in [106]

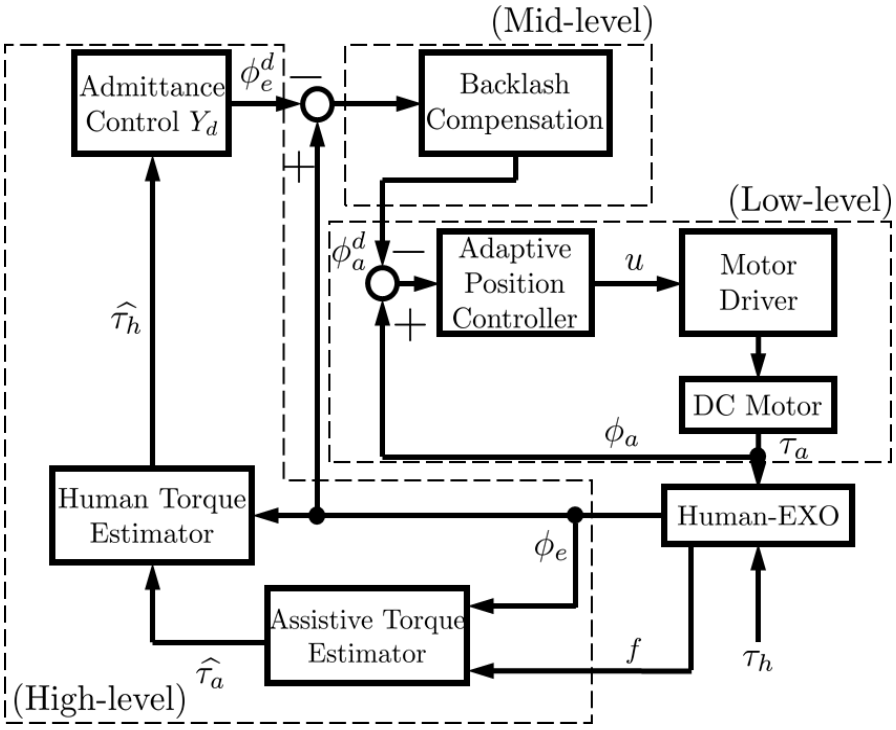

Figure 4.1: The hierarchical control architecture consists in several blocks devoted to different tasks: ranging from model-based admittance control (*high-level*) for assistance modulation, to compensation of nonlinear behaviours in Bowden-cable transmission (i.e. backlash and friction) and desired trajectory tracking (*mid* and *low-level*).

acceleration as shown in Figure 4.2 [107, 108]. For example, in this chapter, the overall

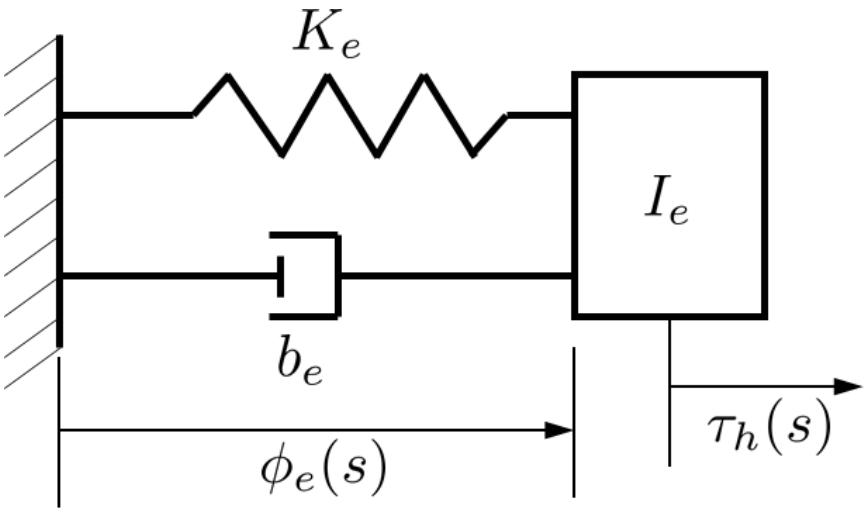

Figure 4.2: A linear model of a one DOF system with its mechanical impedance.

impedance of the human elbow can be expressed in the Laplace domain second-order transfer function $Z_e(s)$, relating the angular position $\phi_e(s)$ and the applying net torque $\tau_h(s)$:

$$Z_e(s)\phi_e(s) = (I_e s^2 + b_e s + K_e)\phi_e(s) = \tau_h(s) \tag{4.1}$$

The parameters I_e, b_e, and K_e represent the physical mechanical properties of the system, i.e. the human elbow, which are passive and constant. Under the assistance of the exoskeleton robot, the actual dynamic behaviour of the elbow can be modified and replaced by a set of desired impedance parameters I_e^d, b_e^d, and K_e^d. This form of control is referred as impedance/admittance control which is able to modify the force-position relation (mechanical impedance) in a desired configuration. Shaping the desired mechanical impedance not only effectively provides an assistance but also allows the user to safely interact with the robot.

In Figure 4.3(A), the mechanical impedance perceived by the user, acting a torque τ_h is $Z_e(s) = I_e s^2 + b_e s + K_e$, that is the natural impedance of the elbow joint. In Figure 4.5(B) the elbow is subject to an assistive torque τ_a from the exosuit in addition to the human torque τ_h. The impedance/admittance control adjusts the assistive torque τ_a such that the user now feel a different (desired) impedance, i.e. $Z_e^d(s) = I_e^d s^2 + b_e^d s + K_e^d$ as shown in Figure 4.3(C). From the wearer's perspective, the coupled systems, consisting of the exosuit and its wearer, shown in Figure 4.3(B) and 4.3(C) behave the exact same dynamic performance [109, 110].

This study investigates and implements the admittance control, selecting appropriate desired impedance parameters to tune assistance to the exosuit's user. The interaction torque $\widehat{\tau_h}$ is estimated and used as input to the admittance control block Y_d shown in Figure 4.1, yielding a desired trajectory ϕ_e^d for the elbow joint. In the *mid-level* controller, a backlash compensation block translates the user's motion intention ϕ_e^d to the desired actuator motion ϕ_a^d, while the *low-level* controller is devoted to accurately track that actuator's motion reference. The inherent backlash in the Bowden cable-driven system introduces significant time delay and inaccuracy in joint position tracking. Hence, in the absence of the transmission mode (*mid-level* controller) that accounts for that nonlinear behaviour, control performances are extremely poor. Finally, the desired motion of the actuation stage is passed to the *low-level* controller, which computes the control signal u and sends it to the DC motor, to improve the tracking effectively, overcome the friction effect from the cable and provide the correct assistive torque τ_a to the human-exosuit system.

4.2 High-level Controller Design: Subject Assistance Evaluation

4.2.1 Sensors Calibration

In order to measure the elbow joint angle and the cable tensions needed for designing the high-level admittance controller, a flex sensor and two load cells are used. The flex sensor (Spectrasymbol®, USA, accuracy ±1°) is embedded in the sleeve at correspondence of the joint, while the load cells (Futek®, USA) are attached in the anchor points, connecting one end of the cables, as shown in Figure 4.4(A). The flex sensor acts like a variable resistor whose output voltage is changed by flexing it. A simple voltage divider is used to convert a change in resistance into a change in voltage. The relationship between the output voltage and the bending angle ϕ_e is assumed to be linear [111]. A calibration step is necessary before the experiment to render the measurement, obtaining a linear regression model to map the measured voltage to the joint angle ϕ_e.

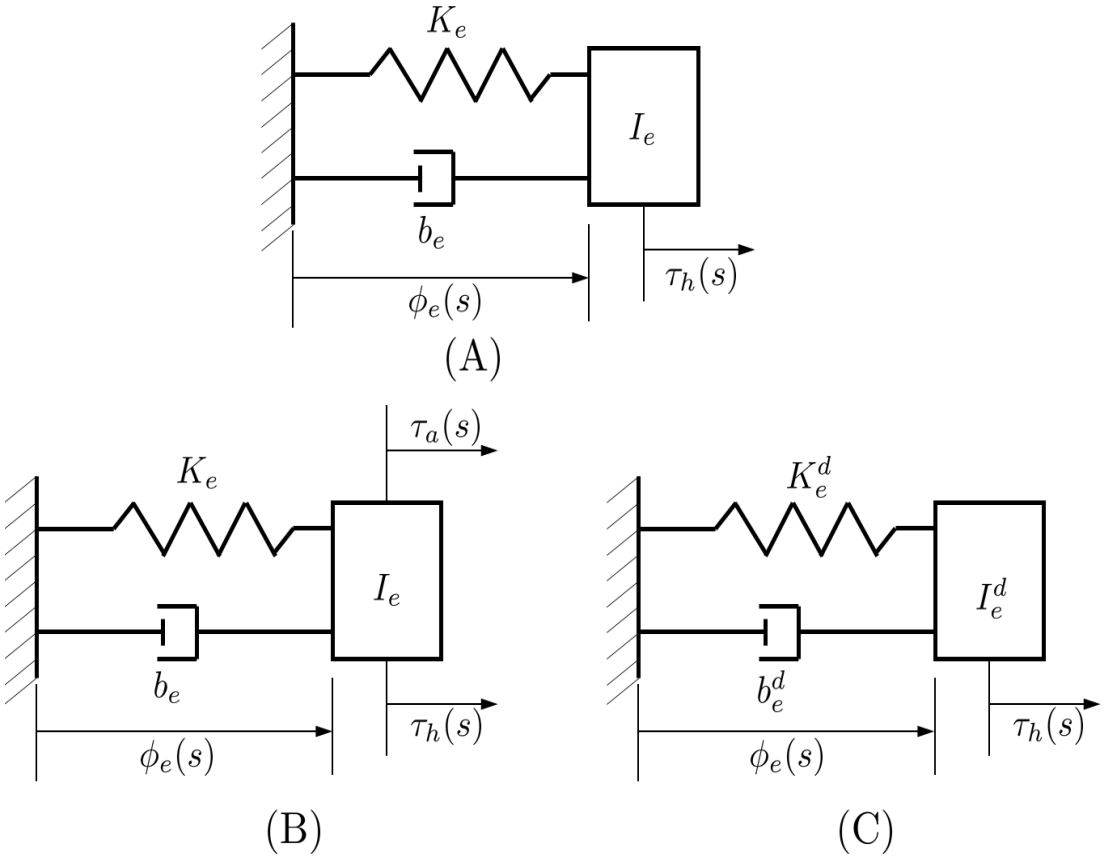

Figure 4.3: General desired impedance parameters of the coupled system including exosuit and its wearer, through the impedance/admittance control.

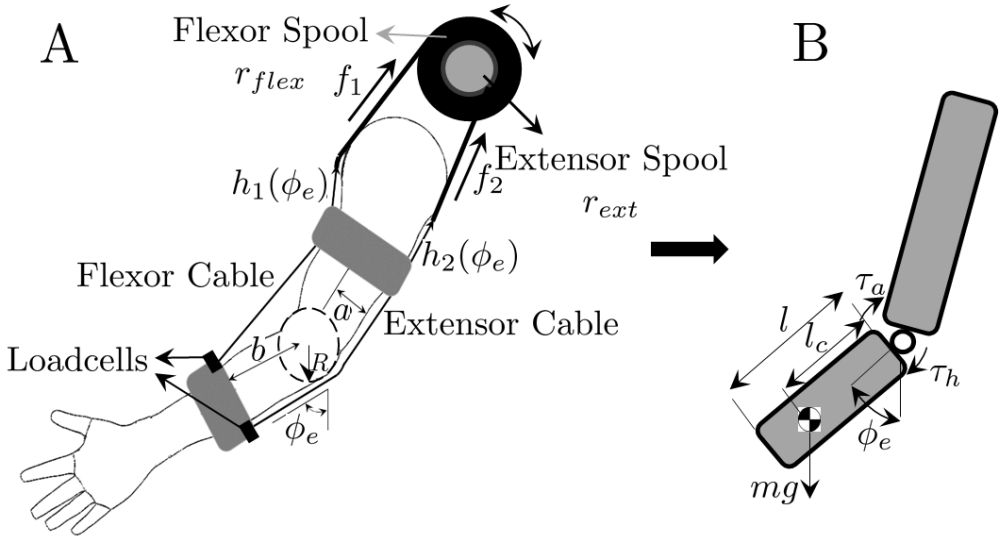

Figure 4.4: (A): Cable routing and the extension functions $h_i(\phi_e)$ $(i = 1,2)$ relating the cables (flexor and extensor) displacement to the joint angle ϕ_e, and the assistive torque $\widehat{\tau_a}$ provided by the exosuit can be estimated based on the cable tensions f_i $(i = 1,2)$ measured by two loadcells. (B): Human arm model presenting the forces/torques acting on the elbow joint.

A similar calibration is applied to the load cell, relating the recorded voltage as a linear function of the force/cable tension. These procedures are repeated for each subject at the beginning of each experiment.

Sensor noise in the measured angular position ϕ_e is attenuated using a Butterworth second order low-pass filter with a cut-off frequency of 8Hz. Then the angular velocity $\dot{\phi}_e$ and acceleration $\ddot{\phi}_e$ are estimated using a numerical differentiation followed by the same low-pass Butterworth filter.

4.2.2 Assistive Torque Estimator $\widehat{\tau_a}$

The intrinsic compliance of the exosuit does not allow to estimate the torque generated by the actuation unit by classical robotic approach. We used a mathematical model for bowden-cable transmission which provides an acceptable estimation of the torque, from the cable tensions [112] measured by the two load cells. Similar to the previous chapter, Figure 4.4(A) shows the human arm model, depicting the cable routing and the descriptive extension functions $h_i(\phi_e)$ $(i = 1,2)$ mapping the cables (flexor and extensor) displacement to the joint angle ϕ_e. Again, the flexor cable has an extension

function $h_1(\phi_e)$ defined as:

$$h_1(\phi_e) = l_1 + 2\sqrt{a^2+b^2}\cos\left(\tan^{-1}\left(\frac{a}{b}\right)+\frac{\phi_e}{2}\right) - 2b \tag{4.2}$$

and the extensor cable is described by:

$$h_2(\phi_e) = l_2 + R\phi_e \tag{4.3}$$

where a is half of the width of the arm, b is the distance from the joint centre of rotation to the anchor points (rigid braces), and R is the radius of the elbow joint. ϕ_e is the bending angle of the elbow joint, referencing the forearm to the upper arm which is assumed to be vertical and aligned with gravity, and l_i $(i = 1,2)$ is the nominal extension when $\phi_e = 0$.

Once computing the two extension functions $h_i(\phi_e)$ we can determine the relationship between the cable tensions f_i, recorded by the load cells and the assistive torque $\widehat{\tau_a}$ delivered to the elbow joint. By defining the coupling matrix **J** as:

$$\mathbf{J}(\phi_e) = \frac{\partial \mathbf{h}^T}{\partial \phi_e}(\phi_e) = \begin{bmatrix} -\sqrt{a^2+b^2}\sin\left(\tan^{-1}\left(\frac{a}{b}\right)+\frac{\phi_e}{2}\right) & R \end{bmatrix} \tag{4.4}$$

where $\mathbf{h} = \begin{bmatrix} h_1(\phi_e) & h_2(\phi_e) \end{bmatrix}^T$ represents the vector of cable function extensions, the estimated assistive torque $\widehat{\tau_a}$ generated by bowden-cable transmission is finally evaluated by the equation:

$$\widehat{\tau_a} = \mathbf{J}(\phi_e)\mathbf{f} = \sqrt{a^2+b^2}\sin\left(\tan^{-1}\left(\frac{a}{b}\right)+\frac{\phi_e}{2}\right)f_1 + Rf_2 \tag{4.5}$$

where $\mathbf{f} = \begin{bmatrix} f_1 & f_2 \end{bmatrix}^T$ represents the vector of the measured cable tensions obtained by the two load cells.

4.2.3 Human Joint Torque Estimator $\widehat{\tau_h}$

The human arm dynamics can be obtained by the Lagrangian formulation [113], by defining the kinetic K and the potential P energies of the arm as follows:

$$K = \frac{1}{3} m l^2 \dot{\phi_e}^2 \tag{4.6}$$

$$P = m g l_c \left(1 - \cos \phi_e\right) \tag{4.7}$$

where the forearm can be assumed to be a uniformly distributed mass m, with a total length l and a distance from the joint to the center of gravity (COG) l_c as shown in Figure 4.4(B).

By defining the Lagrangian equation: $L = K - P$ and introducing a damping force for elbow opposing to the elbow motion, a simplified dynamic model of the human arm can be expressed as follow:

$$\tau = \frac{d}{dt}\left(\frac{\partial L}{\partial \dot{\phi_e}}\right) - \frac{\partial L}{\partial \phi_e} = \tau_h + \tau_a = \frac{2}{3} m l^2 \ddot{\phi_e} + b_e \dot{\phi_e} + m g l_c \sin \phi_e \tag{4.8}$$

where τ is the resulting torque of the human action τ_h and the assistive torque from the exosuit τ_a, b_e is the viscous damping constant, and $g = 9.81 [\mathrm{m/s^2}]$ represents the gravity constant.

The estimated torque deriving from the human muscles $\widehat{\tau_h}$ can be obtained from the inverse dynamic model expressed by (4.8), i.e.,

$$\widehat{\tau_h} = I_e \ddot{\phi_e} + b_e \dot{\phi_e} + m g l_c \sin \phi_e - \widehat{\tau_a} \tag{4.9}$$

where $\widehat{\tau_a}$ is the estimated assistive torque obtained from (4.5), and $I_e = \frac{2}{3} m l^2$ represents the inertia of the elbow joint.

The parameters in (4.9) can be empirically measured and opportunely tuned on each individual subject following the simple known rules listed below [114, 115]:

- The forearm mass m as 2.2% of the total body weight M, i.e., $m = 0.022M$[kg]
- The length l_c from the elbow joint to the center of gravity as 68.2% of the total forearm length l, i.e., $l_c = 0.682l$[m]
- The human elbow viscous damping coefficient b_e can be tuned according to the damping ratio ξ: $b_e = 2I_e\Omega_0\xi$ where $\Omega_0 = \sqrt{\frac{mgl_c}{I_e}}$ is the resonance frequency. In this work, we chose $\xi = 1.2$, ensuring a stable and overdamped dynamic behaviour.

4.2.4 Assistance through Admittance Controller

The exosuit which is used in the present research has been conceived as a device to provide assistance to impaired people, in particular to stroke subjects who do not preserve enough residual voluntary capacity of motion to lift their elbow. Hence after the human joint torque $\widehat{\tau_h}$ has been estimated by the aforementioned model, a successive block in the controller must generate a reference trajectory ϕ_e^d which the actuation stage must deliver to the human elbow joint. In order to provide a smooth intervention of the actuation on the user, an admittance controller has been used. The admittance controller plays the role of changing the overall dynamics, increasing the transparency of the exosuit itself and decreasing the mechanical impedance perceived by the user. The result is an assistance which is gradually modulated and depends on the mutual interaction between the device and the wearer. The admittance control block can be defined as follows:

$$I_e^d\ddot{\phi}_e^d + b_e^d\dot{\phi}_e^d + K_e^d\sin\phi_e^d = \widehat{\tau_h} \tag{4.10}$$

where I_e^d, b_e^d, and K_e^d denote the desired inertia, viscous damping and gravitational torque acting at the elbow joint, respectively, while $\widehat{\tau_h}$ represents the estimated human torque obtained from (4.9).

It can be noticed that in order to reduce the human joint torque $\widehat{\tau_h}$, the desired parameters must be tuned in such a way that the desired impedance is lower than the real one of the human arm [108] (i.e. $I_e^d \leq I_e$, $b_e^d \leq b_e$, and $K_e^d \leq mgl_c$). In this study, we want to verify how the exosuit can assist the wearer by a gravity compensation paradigm. The desired parameters of the admittance controller (I_e^d, b_e^d, and K_e^d) are chosen based on the actual human elbow joint dynamics defined in (4.11), and the level of assistance is regulated by a compensation factor α ($0 < \alpha \leq 1$) which multiples the gravitational effect mgl_c. With such selection, the dynamics of the admittance

controller can be proven to be stable and overdamped.

$$\begin{cases} I_e^d = I_e = \frac{2}{3}ml^2 \\ b_e^d = b_e = 2I_e\Omega_0\xi \\ K_e^d = \alpha mgl_c \\ \alpha = \alpha_0 \tanh\left(\frac{\dot{\phi}_e}{\epsilon_\alpha}\right) + \alpha_1 \end{cases} \tag{4.11}$$

where α_0 and α_1 are two constants experimentally chosen to bound the intervention of the assistance; and ϵ_α denotes the sensitivity coefficient of the hyperbolic function tanh(.). It is highlighted that the factor α increases with the measured joint velocity $\dot{\phi}_e$ [116], meaning that the level of assistance is strictly dependent on the user's residual motion capacity: a high motion speed from the user (i.e. high motor ability) corresponds to a low assistive torque provided by the exosuit and vice versa, and the device is therefore able to gradually tune the assistive torque $\widehat{\tau_a}$ based on the real-time estimation of the subject's motion ability.

4.3 Experimental Evaluations

4.3.1 Experimental Protocol

The experiment was performed on a group of three healthy subjects (males, age: 26.6±1.5 years) wearing the exosuit. They all provided written informed consents prior to the experiment, and the procedures were approved by the Institutional Review Board at Nanyang Technological University, Singapore. The parameters of the subject's arm and the exosuit (i.e. a, b, R, m, l, and l_c) are obtained as described in the subsection 4.2.3 and shown in Table 4.1 in terms of mean and standard deviation.

The experiment aims at demonstrating that the proposed high-level admittance controller is accurate, stable and provides a smooth assistance to the users, modulating the amount of assistive torque provided to the elbow depending on the capacity of

Parameters	Values [unit]
a, b	0.035[m], 0.085[m]
R	0.05[m]
m, l	1.55 ± 0.12[kg], 0.24 ± 0.03[m]
l_c	0.2 ± 0.02[m]

Table 4.1: Average identified parameters

motion of the subject and decreasing the muscular effort during load manipulation. During the experiment the subjects were instructed to flex/extend their forearm, following the motion of a virtual avatar on a screen to match the range of motion and speed (as shown in Fig. 4.5) while holding a 1kg load in their right hand, in two distinct task phases. The visual input was used as a way to standardize the velocity and amplitude of the movements across subjects, allowing across-subjects comparisons of muscular effort.

- Performing 10 repetitive elbow flexion/extension movements with and without assistance delivered by the exosuit in order to prove that the use of the proposed device/controller effectively decrease the muscular activity, helping the wearer to complete the task;
- Performing 10 repetitive elbow flexion/extension movements at two different speeds ($\dot{\phi}_e^1 = 18°/s$ and $\dot{\phi}_e^2 = 36°/s$), in order to show that the intervention of the exosuit is based on the subject's motion ability. It is commonly accepted that kinematics in stroke subjects are dramatically jeopardized and a lower motion speed is associated to a reduced voluntarily capacity of motion. For this reason, asking subjects to move at a lower and higher speed implies that the proposed high-level controller should interpret a lower speed motion as a reduced motion capacity and consequently increase the amount of the assistive torque $\widehat{\tau_a}$ and vice versa, as described in the subsection 4.2.4.

Muscular effort can be estimated by the Root Mean Square (RMS) of the EMG signal of the main muscle involved in performing elbow flexion movements, i.e. the biceps brachii of the right arm. The raw EMG signal was acquired using Trigno wireless

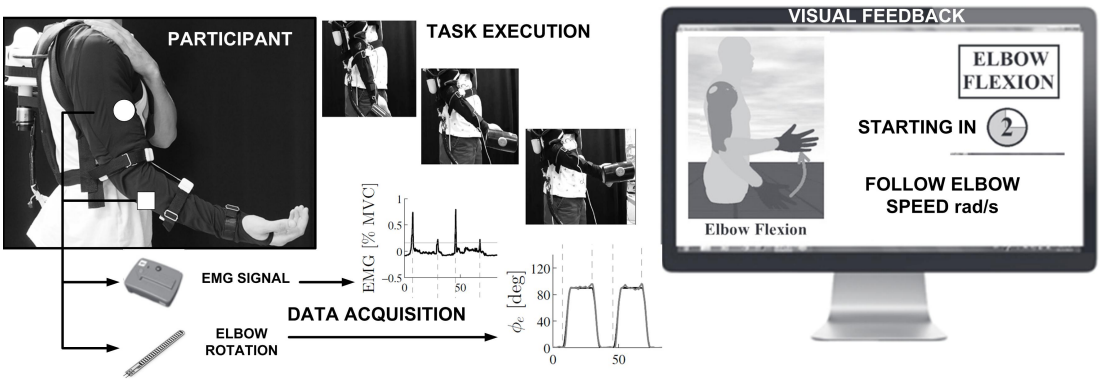

Figure 4.5: The experiment was conducted by instructing the subjects to replicate the elbow flexion/extension movements of a virtual avatar on the screen, trying to match the motion speed.

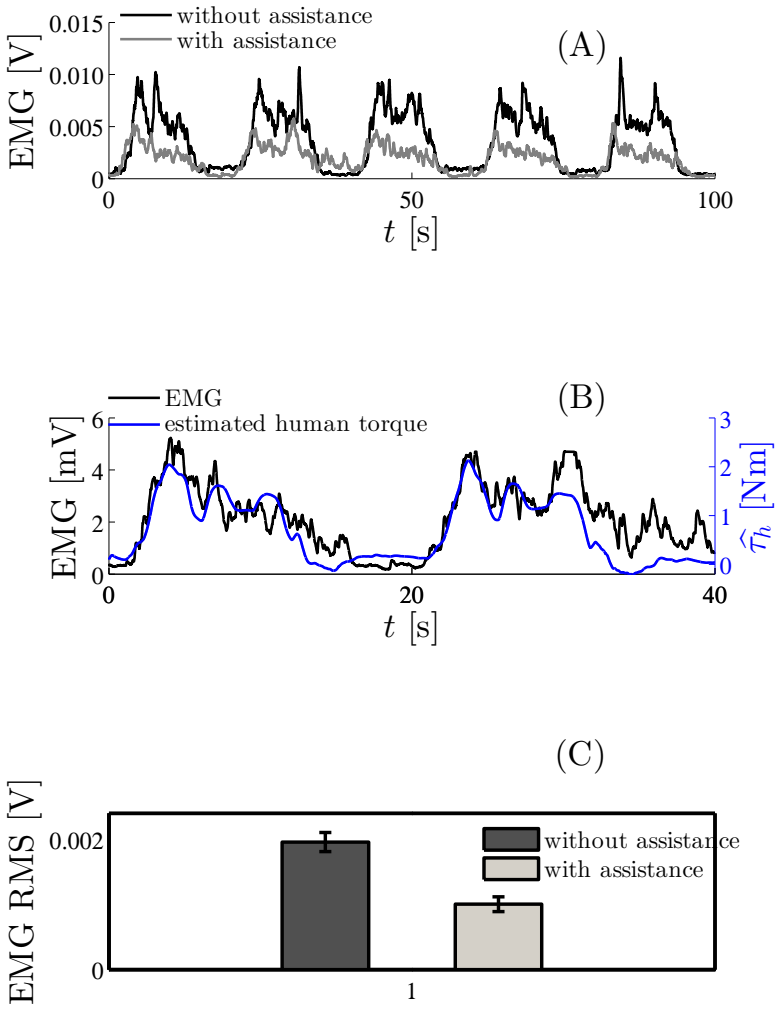

Figure 4.6: **First experiment** (A): EMG amplitude comparison on a single subject with and without the exosuit's assistance. (B): EMG amplitude of a single subject under assistance and corresponding estimated human joint torque $\widehat{\tau_h}$, as computed from (4.9). (C): Bar plot showing the mean and standard deviation of the RMS value of the EMG activity, averaged over repetitions and subjects.

sensors (Delsys®Inc., USA) and was pre-processed using a full-wave rectification, followed by a low-pass second-order Butterworth filter with a 8Hz cut-off frequency.

4.3.2 Experimental Results

Results of the first experiment comparing the EMG amplitude of one subject with and without the assistance are depicted in Figure 4.6(A), showing a clear decrease in the amplitude of the EMG signal when the exosuit is assisting the elbow motion. Figure 4.6(B) shows the estimated human torque $\widehat{\tau_h}$, as computed from (4.9) and the recorded EMG activities during two elbow flexion/extension repetitions from one of the participants, it can be seen that the estimated human torque shows a similar curve as the processed EMG signal. Finally the analysis of the RMS value of the EMG signal, averaged over repetitions and subjects, is shown in Figure 4.6(C). The latter shows an average drop in RMS value of 48.3% between the non-assisted and assisted case.

The second experiment examines the efficacy of the controller in adapting its contribution to the user's capacity of motion. The subjects performed the elbow movement at two different angular velocities ($\dot{\phi}_e^1 = 0.3$rad/s and $\dot{\phi}_e^2 = 0.6$rad/s) and the exosuit was able to modulate the degree of assistance, i.e. the estimated assistive torque $\widehat{\tau_a}$, based on the speed of the subjects. Figure 4.7(A-B) show the EMG activities and the delivered assistive torques $\widehat{\tau_a}$ respectively for one typical subject at the two execution speeds: it is observable that at lower speed (meaning lower capacity of motion) the controller provides a higher assistive torque $\widehat{\tau_a}$ than when the subject moves at the higher speed (which corresponds to a higher capacity of motion). Similar results are observed for the whole group of subjects. An analysis of the estimated assistive torque $\widehat{\tau_a}$ supports these results: Figure 4.7(C) shows that the mean and standard deviation of the RMS value of the estimated assistive torque $\widehat{\tau_a}$, averaged over subjects and trials, is lower at a higher speed of motion, confirming that the controller has adapted to the lower motor ability of the subjects by providing higher assistance.

4.4 Discussion and Summary

In the present chapter I introduced the problem of motion intention detection by formulating a geometry model of the human arm which can be used to predict the human joint torque from only simple load cells. An admittance control block was dedicated to increase the transparency of the device, reduce the mechanical impedance perceived by the wearer, and also define the reference motion delivered to the elbow joint. The results have shown that the muscular effort of subjects using the exosuit and the associated high-level controller is lower than performing the same action with no assistance. It is worth highlighting that the reduction of muscular activity was not provided by a predominant action of the device replacing entirely the human voluntary motion, but rather by a coordinated interaction between the exosuit and the

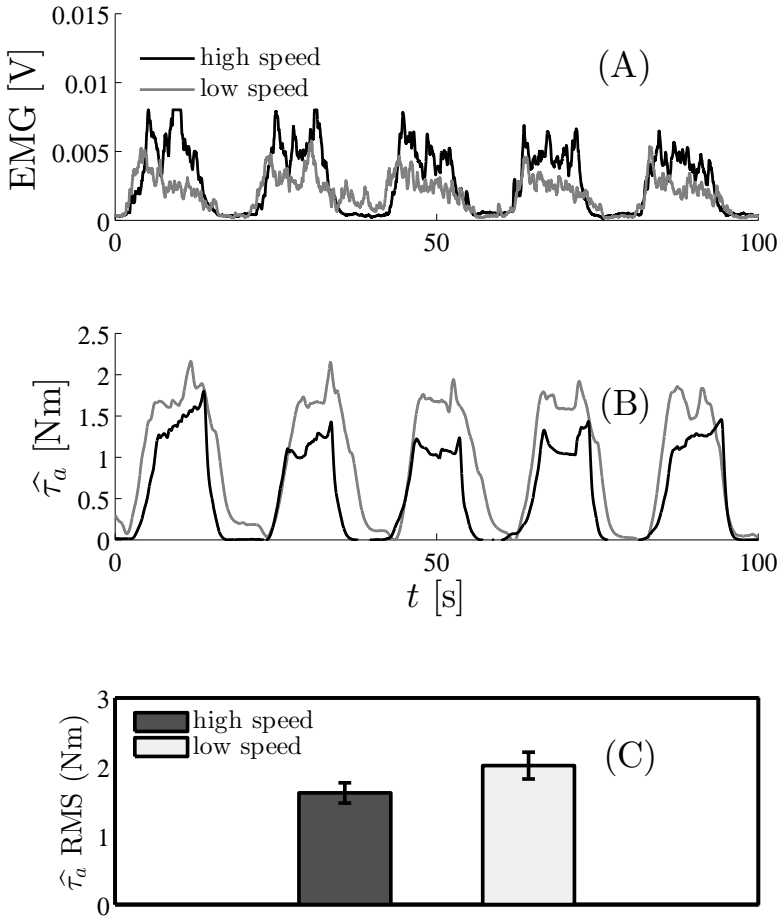

Figure 4.7: **Second experiment:** evaluation of the effectiveness of the assistance modulation at different elbow motion speeds. (A): The amplitude of the EMG activities are shown when a single subject performed the elbow motions at two different velocities. (B): The estimated assistive torques $\widehat{\tau_a}$ at low (light grey) and high (dark grey) elbow speed motions. (C): Bar plot showing the mean and standard deviation of the RMS of $\widehat{\tau_a}$, averaged over repetitions and subjects.

user. I further showed that the proposed velocity-dependent admittance control architecture was able to tune the level of assistance depending on the voluntary motion capacity of the subjects. This strategy somewhat resembles the "assist-as-needed" paradigm [117], and to our knowledge it is the first time that this kind of approach is being formulated for a wearable exosuit rather than for end-effector robotics device. Keeping in mind that the users of assistive devices, who are mainly hemiplegic or impaired subjects, must rely very intimately on the exosuit which is attached to their bodies, and the "gentle intervention" from the controller represents a delicate and

pivotal goal.

In this study, I assumed that the upper arm was aligned with the direction of gravity and the forearm moved on the sagittal plane only, neglecting the shoulder movements. For the future work, the proposed hierarchical controller can be extended to assist the arm with shoulder flexion/extension by using a sensor (i.e. IMU) to measure the orientation of the upper arm with gravity, allowing to update the Lagrangian equation and controller accordingly. In addition, a more comprehensive model of the elbow joint on the transverse plane, i.e. 90° shoulder abduction, can be defined such that the proposed controller can be applied to assist the arm horizontally. Finally, in the two following chapters, the principles of mid-level and low-level control schemes will be described in details. They are both based on a nonlinear adaptive controller in order to compensate for the time-varying backlash and friction effects in the Bowden-cable transmission and effectively improve the control robustness and accuracy in system's position tracking performance.

5 Mid-level Nonlinear Backlash Compensation Control

[1]

This chapter describes the design of the mid-level controller in details, investigating the accurate position control of Bowden-cable transmission of the exosuit through analysis of its performance limitations. In spite of many significant benefits of Bowden cable-driven actuation, the presence of nonlinearities, especially backlash and friction, challenges the system control and limits the performance. Inherent backlash and friction in Bowden cable-driven system impact on control robustness, introducing a delay in the transmission and inaccuracy in force and position tracking. In this chapter I focus on the backlash effect, introducing a mathematical model to capture the associated hysteresis, and implementing a control algorithm for backlash compensation. Since the backlash is strictly dependent on the total curvature angle of the outer Bowden sheath which is time-varying and totally unknown, the proposed control algorithm is based on a nonlinear adaptive controller to deal with the uncertainties in the backlash parameters and the changes of the system's configuration during human arm motion. Furthermore the backlash compensation control scheme in the mid-level layer also plays a role of translating the user's motion intention ϕ_e^d generated from the high-level to the desired motion for the actuation stage ϕ_a^d to drive the exosuit. The proposed adaptive control paradigm is then validated on a custom-designed test bench. Finally, it is embedded into the soft exosuit and applied in a preliminary clinical trial on an impaired subject affected by bilateral brachial plexus injury.

[1] Part of the work presented in this chapter was published in [94, 118]

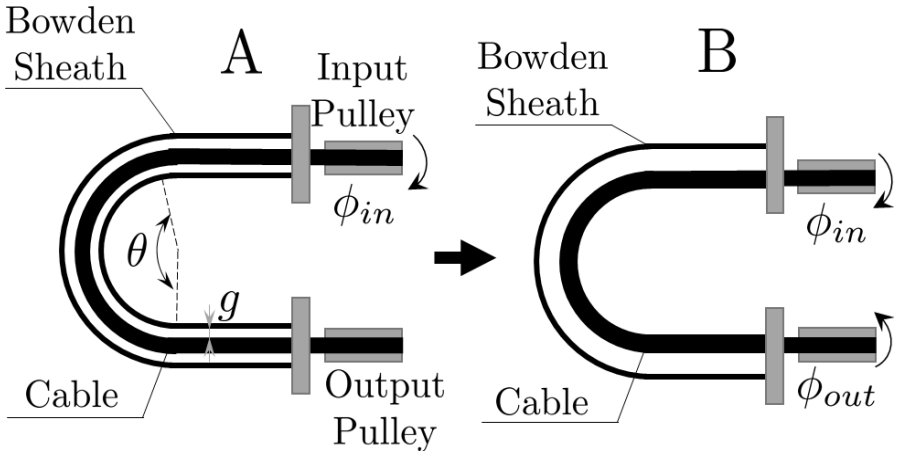

Figure 5.1: Cable position in the Bowden sheath. (A): Backlash behaviour is created by cable slack in the Bowden sheath. (B): Under tension the backlash effect is eliminated, the motion is transmitted from the input to the output pulley.

5.1 Overview on Backlash in Bowden-cable Transmission, Associated Hysteresis and Compensation Control Strategy

The soft exosuit presented in this study combines the use of fabrics and a Bowden cable-driven actuation stage for motion transmission to directly apply torques at the joints level. Being flexible and compliant, this kind of systems allow to place the actuation unit away from human articulations (i.e. in a backpack), and the assistive torque can be transmitted via cables from the actuators to the end-effector.

In spite of many significant benefits, the presence of nonlinearities, especially backlash phenomenon [14], challenges the system control and limits its performances. Inherent backlash effect in the Bowden cable-driven system impacts on control robustness, introducing a time delay in the transmission and inaccuracy in position tracking performance. In the absence of a transmission model that accounts for this nonlinear behaviour [18, 19], control performances are extremely poor. In Figure 5.1, a conceptual representation of backlash caused by the gap between the cable and the inner wall of the Bowden sheath [119] is depicted. The amount of backlash is directly proportional to the curvature angle θ of the sheath and the gap size g. Since these values cannot be directly measured, the backlash effect is unpredictable and continuously changes during operation due to geometrical variation of the Bowden sheath.

A wealth of analytical models have been proposed to address the nonlinear backlash

characteristics of Bowden-cable transmission. Kaneko *et al.* [16] presented a parametric lumped mass model for describing the transmission of tendon tension and Palli improved it with the introduction of a dynamic model (Dahl model) to account for anomalous behaviour in the stationary condition [11]. Similar approaches were carried out by Tian *et al.* [120] and Agrawal *et al.* [20], where a set of partial differential equations are discretized to model the partially-moving, partially-sticking cable motion inside the Bowden sheath. However, these approaches still suffer from the discontinuity at near-zero cable velocity and a high degree of complexity. In [20] the authors discussed a method to compensate for the backlash-induced hysteresis in the motion-control of a robotic arm. Their approach was based on a smooth backlash inverse model, where a new desired trajectory was generated by adding the tracking error to the original desired trajectory. This suffers from the limitation of assuming that the required offset to be added is constant and not velocity-dependent. In [119], Kesner demonstrated that a model-based compensation strategy, where the hysteresis profile is analytically modelled, achieves better performance than the backlash inverse model-based compensation one. This approach required physical model and evaluation of backlash parameters, and the system's configuration was assumed to be fixed which is not suitable in the practical applications. In addition, Wu *et al.* [121] introduced a cascaded PID controller to enhance the performance of trajectory tracking tasks in a lower limb exoskeleton driven by Bowden cables. However, the relation between the controller and the backlash effect, which is an inherent issue in Bowden-cable transmissions, is still missing and the fixed PID gains thus might fail to compensate for the nonlinear variable backlash during motion. Hence a model-based approach for backlash compensation is required.

Several mathematical formalisms exist for modelling backlash-induced hysteresis, including the Bouc-Wen model, Preisach model, Prandtl-Ishlinskii (PI) model [122]. The PI and Preisach were modelled as a sum of many elementary hysteresis, which increase the complexity in computation and implementation. The Bouc-Wen model has been proven to capture a wide range of hysteresis phenomena whilst retaining a low level of complexity and computational effort [123, 124], and has been successfully used for accurate position control of flexible endoscopic systems with the variable geometry [14, 15, 125].

5.2 Backlash Compensation Controller Design based on Nonlinear Adaptive Controller

5.2.1 Test Bench Set-up

In order to model the backlash hysteresis in the Bowden cable-driven system and test the compensation control algorithm, a test bench has been designed as shown in Figure 5.2(A). A DC motor (Maxon EC-i 40 70W motor) connected to a pulley drives a cable routed in an outer Bowden sheath. The angular position of the input pulley ϕ_{in} is monitored using an incremental encoder mounted on the motor shaft. The cable passes through the Bowden sheath and wraps around a secondary pulley whose position ϕ_{out} is obtained by a second encoder. A spring at the distal end pretensions the cable by providing a resisting force to simulate a conservative force field to resemble the gravity force applied on human elbow. Dyneema cables (IGUS Robolink®Dyneema rope) are used to transmit forces. The feedback and control signals are acquired and output by MATLAB SIMULINK from MathWorks®and inter-

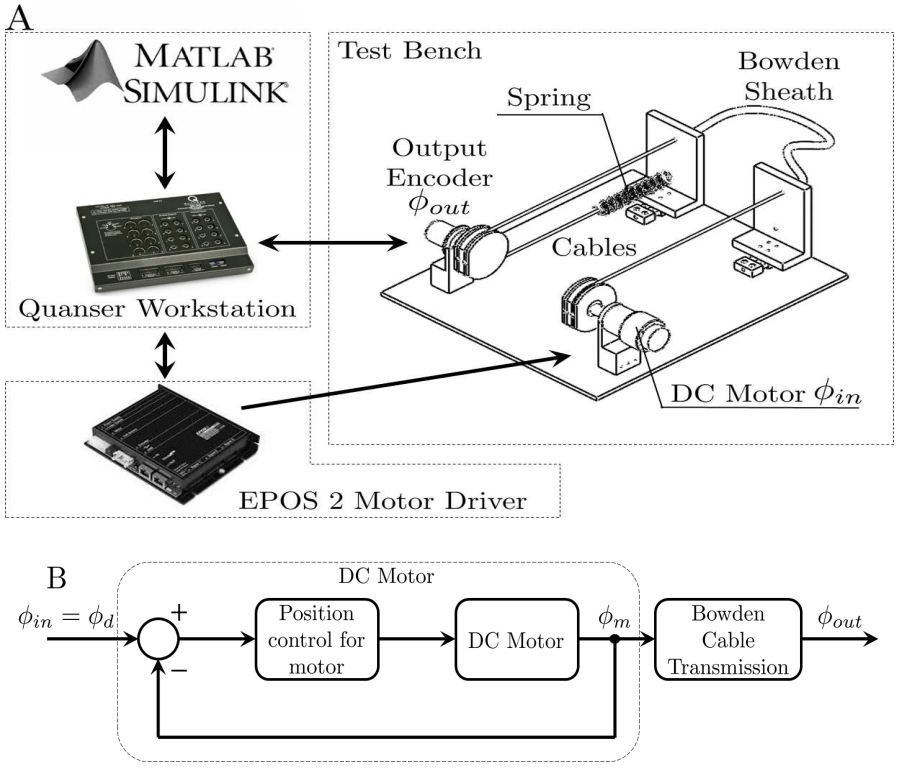

Figure 5.2: (A): The custom-built test bench to measure the effects of backlash in position tracking. (B): Control scheme for the Bowden-cable transmission without backlash compensation.

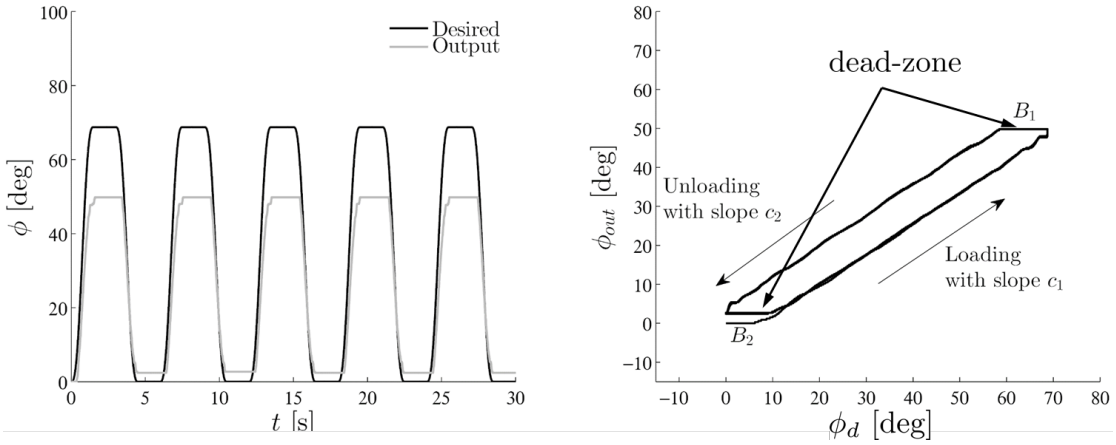

Figure 5.3: Tracking performance of the test bench when no backlash compensation is active. (A): Desired motion ϕ_d and measured output motion ϕ_{out} versus time t; (B): Example of hysteresis between the desired motion ϕ_d and measured output motion ϕ_{out}.

faced with Quanser Quarc^{TM} real-time control architecture running at 1kHz refresh rate.

An initial pretension force is applied to the cable to prevent it from slacking. The output displacement ϕ_{out} is supposed to accurately follow a desired motion ϕ_d which is a periodic minimum jerk trajectory ranging from 0° to 70°. This desired motion is commanded to the DC motor ($\phi_{in} = \phi_d$) to actuate the system. The initial control scheme with no backlash compensation is shown in Figure 5.2(B). As the cable is pulled at the input pulley driven by the DC motor (loading), the tension in the cable increases according to the resisting force generated by the spring. When the DC motor reverses the direction of motion (unloading), due to the resisting force, the cable is pulled back at the output pulley. The detrimental effect of the backlash on the position tracking performance and the associated hysteresis are shown in Figure 5.3, where the plots of the desired motion ϕ_d and the output motion ϕ_{out} versus time show a significant mismatch and time delay between the input and the output. This effect comes from a combination of backlash and cable deflection which play a major role in reliability of the Bowden-cable transmission and need to be opportunely modelled and compensated.

5.2.2 Backlash Hysteresis based on normalized Bouc-Wen model

The backlash leads to a hysteresis between the input ϕ_{in} and the output displacement ϕ_{out} [126] resulting in two straight lines (upward and downward sides) and

horizontal segments describing the *dead-zone* (Figure 5.3(B)). The hysteresis can be approximated mathematically by the following discontinuous functions:

$$\dot{\phi}_{out} = \begin{cases} c_1\dot{\phi}_{in}(t) & (\dot{\phi}_{in}(t) > 0) \\ c_2\dot{\phi}_{in}(t) & (\dot{\phi}_{in}(t) < 0) \end{cases} \tag{5.1}$$

or

$$\phi_{out} = \begin{cases} c_1(\phi_{in}(t) - B_1) & (\dot{\phi}_{in}(t) > 0) \\ c_2(\phi_{in}(t) + B_2) & (\dot{\phi}_{in}(t) < 0) \end{cases} \tag{5.2}$$

where $c_1 > 0$, $c_2 > 0$ are the backlash slopes; $B_1 > 0$, $B_2 > 0$ are the widths of the backlash profile; $\phi_{in}(t)$, $\dot{\phi}_{in}(t)$, $\phi_{out}(t)$, $\dot{\phi}_{out}(t)$ are angular displacements and velocities of the input and the output, respectively.

However, the model described by (5.1) and (5.2) is discontinuous and to estimate the unknown descriptive constants and improve the position tracking accuracy, a complex nonlinear algorithm implementation is needed. In the present paper we introduce a description of the backlash and the associated hysteresis by using the Bouc-Wen formulation. The resulting model is continuous, and it may represents a suitable option for the implementation of the compensation controller. The Bouc-Wen model has been adopted in several applications providing a versatile description of hysteresis shapes. The model is formulated by a first-order nonlinear differential equation containing several parameters that need to be identified to approximate the behaviour of a system presenting hysteresis. In this paper, the following formulation for the Bouc-Wen model is used to predict the hysteresis in the Bowden-cable transmission [123, 127, 124]:

$$\phi_{out} = \alpha_\phi \phi_{in} + \alpha_h h \tag{5.3}$$

$$\dot{h} = \rho\left(\dot{\phi}_{in} - \sigma|\dot{\phi}_{in}||h|^{n-1}h - (\sigma - 1)\dot{\phi}_{in}|h|^n\right) \tag{5.4}$$

where ϕ_{out} is the measured output displacement of the Bowden cable-driven system,

ϕ_{in} is the input displacement. The variable h is the solution of a differential equation (5.4). The dimensionless parameters ρ, σ, n adjust the shape and size of the backlash hysteresis profile; and α_ϕ, α_h represent the ratio of the output displacement ϕ_{out} to the input displacement ϕ_{in} and to the variable h, respectively.

5.2.3 Nonlinear Adaptive Backlash Compensation Controller

While the model defined by (5.3) has been formulated for a fixed configuration of the Bowden cable, one needs to account for the variation of the Bowden cable curvature angle caused by the motion of the exosuit: an additional term D is introduced in (5.3) to describe the backlash uncertainty:

$$\phi_{out} = \alpha_\phi \phi_{in} + D \rightarrow \beta \phi_{out} = \phi_{in} + \beta D \tag{5.5}$$

where α_ϕ is a positive coefficient representing the slope of the backlash hysteresis profile; and $\beta = \frac{1}{\alpha_\phi}$ which is the inverse of the slope. We define D_m to be the bounded value of the model uncertainties D such that $|D| \leq D_m$.

Adopting the notation from [128], I define the tracking error e between the output motion ϕ_{out} and the desired motion ϕ_d, the filtered tracking error s and the reference motion ϕ_r as:

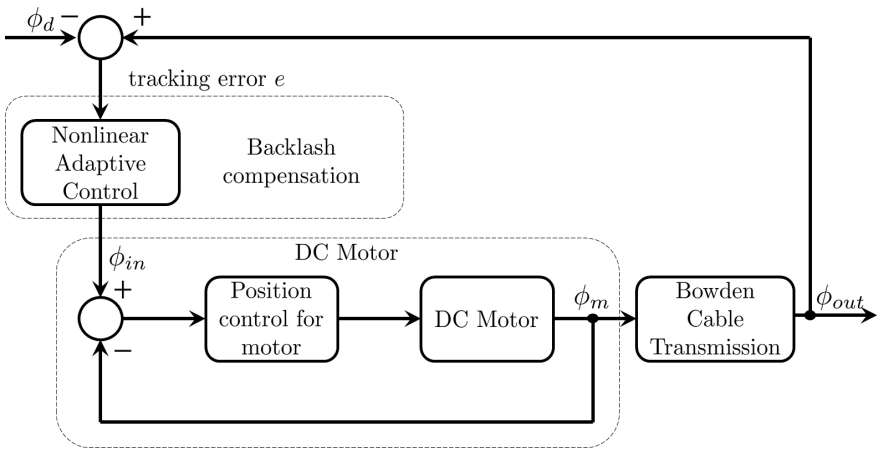

Figure 5.4: The proposed control scheme using a nonlinear adaptive controller for backlash compensation in the test bench.

$$\begin{cases} e = \phi_{out} - \phi_d \\ s = \lambda e + \int_0^t e(\tau) d\tau \rightarrow \dot{s} = \lambda \dot{e} + e \\ \phi_r = \phi_d - \lambda \dot{e} \end{cases} \tag{5.6}$$

where λ is selected to be positive such that the polynomial equation $p = \lambda q + 1$ with Laplace variable q is stable according to Hurwitz criteria.

The control law ϕ_{in} can be chosen as:

$$\phi_{in} = \widehat{\beta}\left(\phi_r - \widehat{D_m}\tanh\left(\frac{s}{\epsilon}\right)\right) - \kappa s \tag{5.7}$$

where $\widehat{\beta}$ is the estimated value of β; $\widehat{D_m}$ is the estimated value of D_m; and κ is a positive constant. The hyperbolic tangent function tanh(.) is used to alleviate the problems of chattering and mechanical resonance [129, 130], and ϵ denotes the sensitivity coefficient of the tanh(.) function.

Replacing the control law ϕ_{in} from (5.7) to (5.5):

$$\beta\phi_{out} = \widehat{\beta}\left(\phi_r - \widehat{D_m}\tanh\left(\frac{s}{\epsilon}\right)\right) - \kappa s + \beta D \tag{5.8}$$

Adjusting (5.8) leads to the dynamics of tracking error as:

$$\beta\dot{s} + \kappa s = \widetilde{\beta}\overline{\phi_{in}} - \beta\widetilde{D_m}\tanh\left(\frac{s}{\epsilon}\right) - \beta\left(D_m\tanh\left(\frac{s}{\epsilon}\right) - D\right) \tag{5.9}$$

where $\overline{\phi_{in}} = \phi_r - \widehat{D_m}\tanh\left(\frac{s}{\epsilon}\right)$; $\widetilde{\beta} = \widehat{\beta} - \beta$ is the estimated error of β; and $\widetilde{D_m} = \widehat{D_m} - D_m$ is the estimated error of D_m

According to [131] the parameters adaptation law is given by:

$$\begin{cases} \dot{\widehat{\beta}} = -\delta_1\overline{\phi_{in}}s - \delta_1\sigma_1\widehat{\beta} \\ \dot{\widehat{D_m}} = \delta_2\beta\tanh\left(\frac{s}{\epsilon}\right)s - \delta_2\sigma_2\widehat{D_m} \end{cases} \tag{5.10}$$

where δ_1, δ_2 are positive adaptation gains; and the initial values for $\widehat{\beta}$ and $\widehat{D_m}$ are set to be zero. The additional terms ($\sigma_1 > 0$ and $\sigma_2 > 0$, σ modification) ensure the boundedness of $\widehat{\beta}$ and $\widehat{D_m}$ which guarantees the robustness of the closed-loop system in the presence of approximation errors.

In order to prove the stability of the closed-loop system shown in Figure 5.4, I consider a Lyapunov function candidate as:

$$V = \frac{1}{2}\beta s^2 + \frac{1}{2\delta_1}\widetilde{\beta}^2 + \frac{1}{2\delta_2}\widetilde{D_m}^2 \tag{5.11}$$

Appendix A.1 will prove that the Lyapunov function is decreasing; and the filtered tracking error s, the tracking error e, and the estimated errors of β and D_m are guaranteed to be uniformly ultimately bounded (u.u.b).

5.3 Experimental Evaluations and Comparisons

5.3.1 Backlash Compensation for the Test Bench with Constant Curvature Angle

In order to demonstrate the effectiveness of the assumed Bouc-Wen model and the proposed control scheme for backlash compensation, an initial test has been run on

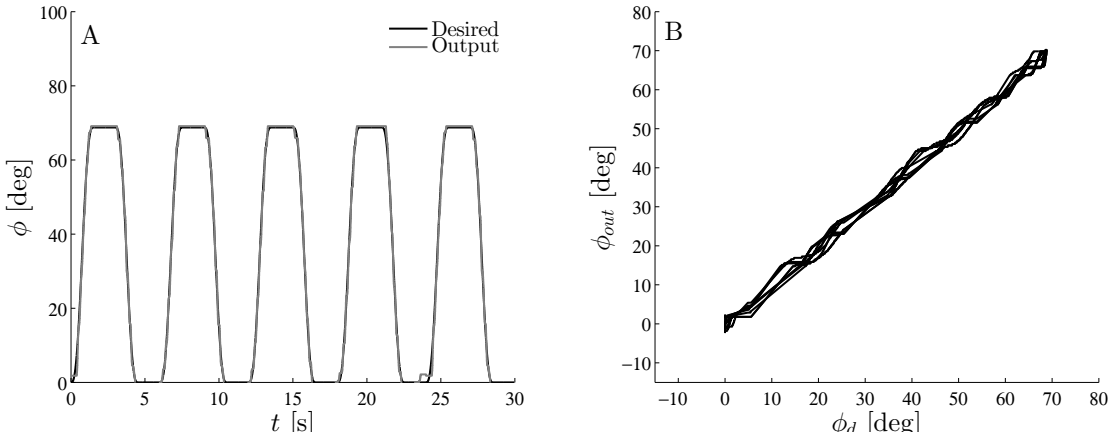

Figure 5.5: **Nonlinear adaptive controller** for backlash compensation for the test bench in the case of constant curvature of the bowden sheath. (A): Desired motion ϕ_d and measured output motion ϕ_{out} versus time t. (B): Desired motion ϕ_d versus measured output motion ϕ_{out}.

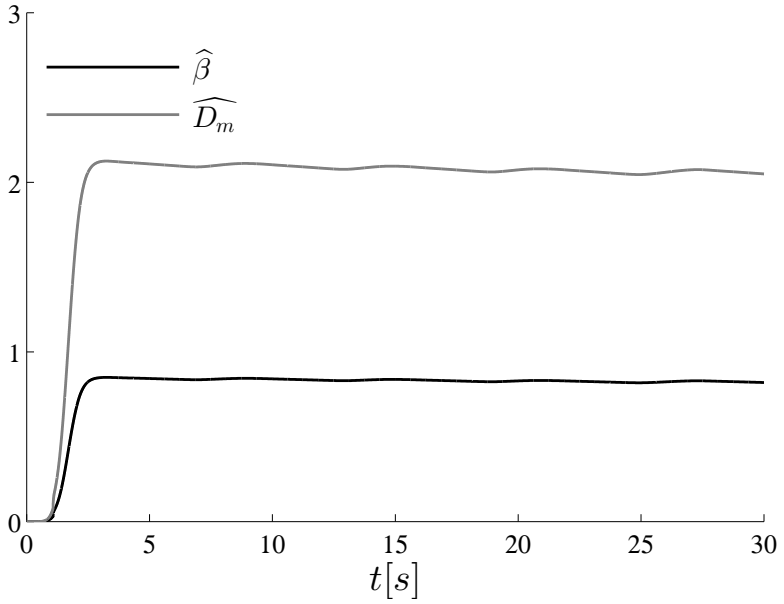

Figure 5.6: The estimated backlash model parameters $\widehat{\beta}$ and $\widehat{D_m}$ are updated online according to the adaptation law described in (5.10) and converges to the actual values after $t = 2.5s$.

the previously described test bench. In this initial experiment, the Bowden sheath curvature angle was kept constant, and the position controller for the DC motor is a linear high-gain PD controller.

The parameters for the adaptation law (5.10) were set as follow: $\lambda = 2$, $\kappa = 10$, $\epsilon = 0.01$, $\delta_1 = \delta_2 = 2$, and $\sigma_1 = \sigma_2 = 0.005$ (practical advices on how to choose these values are described in Appendix A.1). As shown in Figure 5.5 the proposed backlash compensation strategy based on nonlinear adaptive controller allows to significantly reduce the backlash hysteresis *dead-zone*, and the relationship between the desired trajectory ϕ_d and the measured output displacement ϕ_{out} is almost linear. Moreover a significant reduction of the tracking error e and time delay t_d is also achieved. The proposed nonlinear control for backlash compensation gradually tunes the estimated values $\widehat{\beta}$ and $\widehat{D_m}$ of the backlash model parameters which at the beginning of the process are unknown (Figure 5.6) (converging time $t \approx 2.5s$).

5.3.2 Backlash Compensation for the Test Bench under Varying Curvature Angle

To examine the efficacy of the nonlinear adaptive controller for backlash compensation under varying Bowden cable configurations, the Bowden sheath was manually

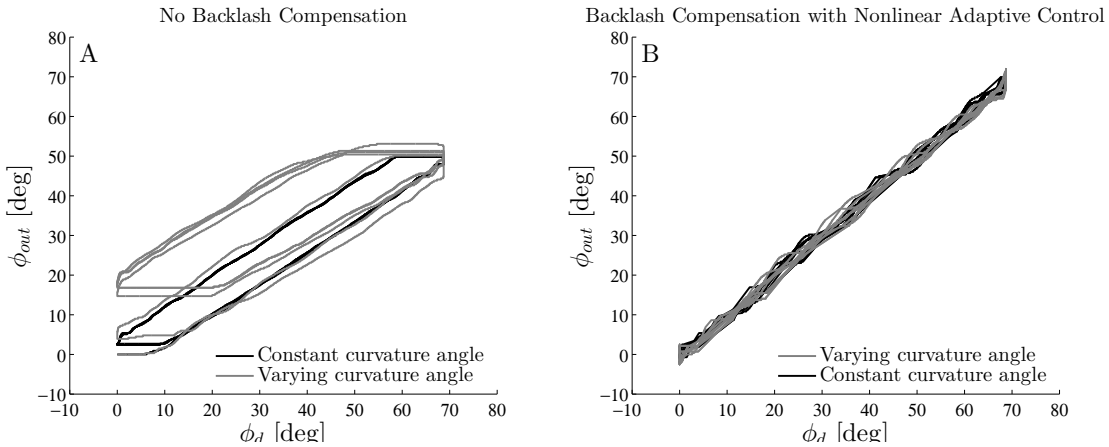

Figure 5.7: Tracking performance comparison between with and without the backlash compensation adaptive controllers in case of variable curvature angle of the Bowden sheath. (A): In case of simple position controller a change in curvature angle of the Bowden sheath leads to a significant increase and variable hysteresis. (B): When the nonlinear adaptive controller is active, even changing the Bowden cable curvature angle the linearity between the desired motion ϕ_d and the output ϕ_{out} is still preserved.

RMSE[deg]	**No Compensation**	**Nonlinear Adaptive Compensation**
Constant curvature angle	8.745	0.425
Varying curvature angle	15.561	1.087

Table 5.1: Root Mean Square Error (RMSE) of position tracking performance of Bowden-cable transmission without and with nonlinear adaptive backlash compensation controller.

moved during online operation. The position tracking performances acquired from the test bench under varying curvature angles with and without the compensation control architecture are depicted and compared in Figure 5.7.

It is evident from Figure 5.7(A) that without backlash compensation, the backlash hysteresis width increases as the curvature of the Bowden sheath is varying (the *dead-zone* changes from 10° increasing to 20°), resulting in a decreasing motion transmitted from the motor to the output pulley. In the second case (Figure 5.7(B)), with the proposed backlash compensation controller, despite the curvature angle is varying unpredictably, the transmission of motion between the input motor and the output pulley is kept constant and the undesirable effect of the backlash is dramatically compensated. The proposed adaptive controller is able to estimate and update online the backlash model parameters, and provides an appropriate compensation to drive the input ϕ_{in} to the DC motor for minimizing the tracking error e and time delay t_d.

For detailed numerical results and comparison, Table 5.1 shows the root mean square error (RMSE) obtained from the desired trajectory ϕ_d and the measured output displacement ϕ_{out} defined as (5.12). It is worth highlighting that the nonlinear adaptive controller significantly reduces the backlash effect in the Bowden-cable transmission and effectively decreases the tracking error e regardless of the Bowden cable configuration variation.

$$\text{RMSE} = \sqrt{\frac{\sum_{i=1}^{n} \left(\phi_d^i - \phi_{out}^i\right)^2}{n}} \tag{5.12}$$

5.4 Preliminary Clinical Trial

To test the effectiveness of the proposed adaptive backlash compensation controller in a clinical scenario, we applied and tested the controller on the soft exosuit worn by an impaired subject who volunteered to test the device. The control architecture used in the clinical trial is shown in Figure 5.8, the reference motion for the elbow joint ϕ_e^d was chosen as a minimum jerk trajectory with a amplitude from 0° to 90°. By similarly applying the notation from (5.6), the desired trajectory for the actuation stage ϕ_a^d can be computed as in (5.14). The adaptation law for the backlash parameters is exactly as same as (5.10). In order to accurately track the desired motion ϕ_a^d of the actuator, a low-level PD position controller with high gains is used to overcome the friction force in the Bowden-cable transmission.

$$\begin{cases} e = \phi_e - \phi_e^d \\ s = \lambda e + \int_0^t e d\tau \rightarrow \dot{s} = \lambda \dot{e} + e \\ \phi_e^r = \phi_e^d - \lambda \dot{e} \end{cases} \tag{5.13}$$

where e represents the tracking error between the desired elbow joint angle ϕ_e^d and the measured one ϕ_e by the flex sensor.

$$\phi_a^d = \widehat{\beta}\left(\phi_e^r - \widehat{D_m}\tanh\left(\frac{s}{\epsilon}\right)\right) - \kappa s \tag{5.14}$$

Due to its intrinsic soft nature, the exosuit relies on the wearer's skeletal structure to transmit compressive forces and is hence limited in the amount of assistance it can

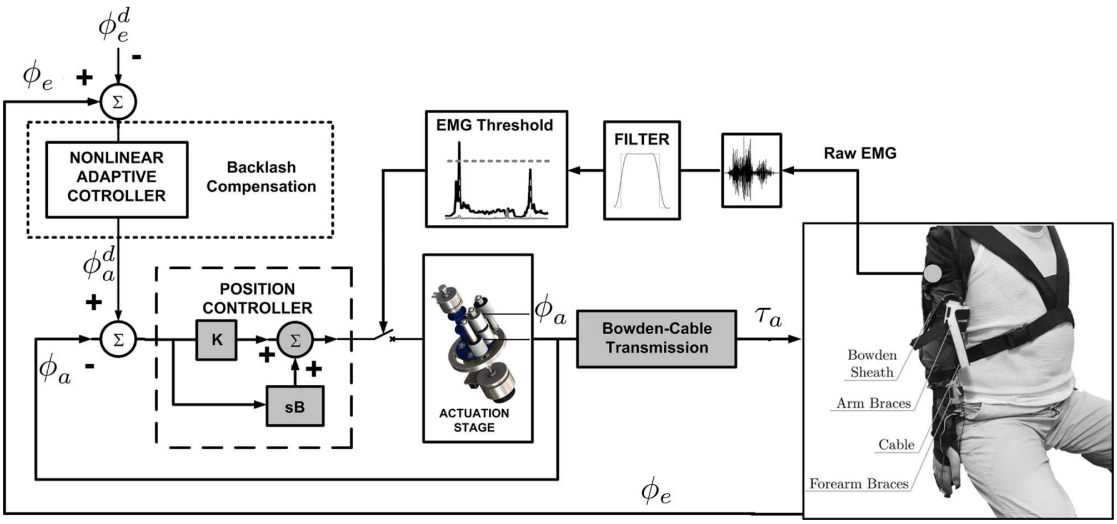

Figure 5.8: Embedded control used in the preliminary clinical trial: The raw EMG acquired from the patient engages the assistive control once a threshold has been overcome. The nonlinear adaptive controller compensates for the backlash effect during motion, assuring the desired motion ϕ_e^d of the patient's elbow joint to be accurately followed.

provide. It is thus likely that this solution would be inadequate for patients with severe contractures or spasticity (Modified Ashworth Scale of the biceps or triceps muscles greater than 2) and/or suffering from disuse osteoporosis (a common co-morbodity of neuromuscular impairments). Unfortunately no experimental method has yet been used to rigorously assess for whom and for how long a soft exosuit could be used with no counter effects. Hence, future studies in this direction are needed.

The reported pilot study was conducted on a patient suffering from neither contractures/spasticity in the upper limbs nor disuse osteoporosis. He is affected by a severe bilateral brachio radialis plexus injury, having thus nearly completely lost motor-sensory innervations of the upper limbs. Voluntary capacity of motion was severely affected and muscular atrophy limited the range of motion to a portion lower than 20°. The experiment was approved by the Institutional Review Board at SINAPSE Institute for Neuro-technology (Singapore). The research conformed to the ethical standards laid down in the 1964 Declaration of Helsinki that protect research subjects. The participant signed a consent form prior to the experiment. The preliminary test consisted in assisting the patient in moving his elbow: residual EMG signals have been used to trigger the exosuit actuation stage and drive the elbow joint to a 90° configuration starting from a resting position (Figure 5.8).

The EMG signals (Trigno wireless EMG electrodes, Delsys®Inc.) were recorded from

a single channel acquiring biceps muscular activity: raw signals were pre-processed using a full-wave rectification and following by a low-pass second-order Butterworth filter with a 8Hz cut-off frequency, and they were used to activate the elbow flexion/extension once a pre-set threshold was crossed (20% of maximum voluntary contraction). Due to the severe clinical conditions, the subject retained residual muscular activity only in the biceps, while other muscles being affected by atrophy, presented a degraded electromyogram which was not suitable for triggering the device. As shown in Figure 5.8, once the EMG signal overcomes the threshold, the position controller is engaged and drives the actuation stage. Figure 5.9(A) shows the EMG bursts triggering flexion and extension: once the assistive effort by the exosuit is engaged the EMG activities noticeably decrease, meaning that the elbow motion is almost fully supported by the device. Figure 5.9(B) represents the corresponding measured joint angle (ϕ_e) during seven flexion/extension tasks with a respective amplitude ranging from 0° to 90°. Accuracy in tracking the desired motion ϕ_e^d is depicted in Figure 5.9(C), showing that the maximum tracking error e between ϕ_e and ϕ_e^d is bounded in a compact set ranging between ±5°, furthermore the time delay between EMG signal and assistance initiation is almost eliminated ($t_d \approx 0.2s$). It is worth highlighting that during elbow motion flexing and extending, the curvature of the Bowden sheath is subjected to unpredictable variations leading to a change in the amount of backlash and the associated hysteresis: despite these nonlinear dynamics are not directly measurable, we showed in our experiments that the proposed mid-level controller implementation with adaptive backlash compensation results in a much improved accuracy in position tracking performance.

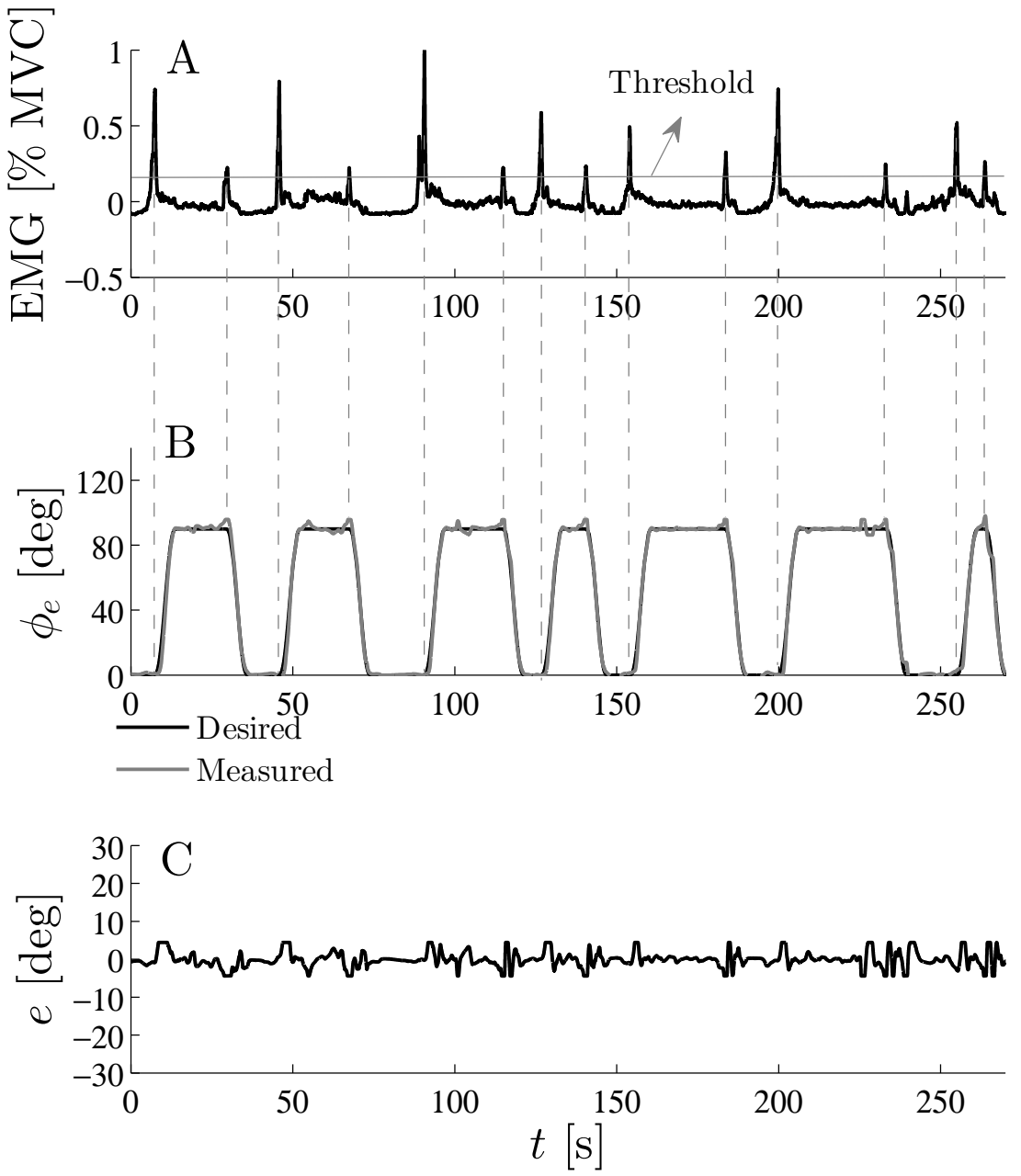

Figure 5.9: Results from the clinical trial for arm motion assistance. (A) The patient's EMG is processed and compared with a threshold set as a percentage of the maximum voluntary contraction (MVC). The EMG burst activates the assistance and the actuation stage drives the elbow from the rest configuration 0° to a 90° configuration. (B): Set of seven flexion and extension movements are depicted and time delay between the EMG signal and movement initiation negligible due to the action of nonlinear adaptive algorithm. (C): Tracking error between the desired ϕ_e^d and the actual ϕ_e elbow angle is below 5°.

5.5 Discussion and Summary

In this study, I presented a novel nonlinear adaptive compensation controller that continuously updates the parameters of the backlash model and it is able to adapt online to the system's configuration, taking into account the time-varying curvature of the Bowden sheath due to the motion of the human arm. I then implemented the nonlinear adaptive controller on a custom-designed test bench. The results show that the proposed control scheme with the adaptation law is able to achieve a significant improvement in position tracking; even when the Bowden sheath shape is variable, the linearity between the output and desired motion is still preserved, respecting the primary requirements of stability and robustness. I also embedded the proposed nonlinear adaptive algorithm for backlash compensation into the soft exosuit and tested its efficacy in a clinical scenario. The results are promising in terms of joint's position tracking performance, considering the severity of the patient, who presented a reduced motion capacity. The present contribution is intended to be framed in a wider context, where backlash compensation is just one aspect which must be addressed in the design of wearable assistive devices. The main goal is not only to identify a particular aspect such as backlash but to succeed in formulating a robust control paradigm.

Although the tracking performance is significantly enhanced, the inherent friction in Bowden-cable transmission still limits the control robustness of the system. The backlash compensation controller in mid-level layer converts the reference motions ϕ_e^d of the elbow joint into the desired trajectory ϕ_a^d of the actuator which would be fed in the low-level position controller, at which the nonlinear friction effect need to be compensated. In this chapter, a high-gain PD control is employed to overcome the friction, reducing the steady-state position error of the DC motor. However the high control gains cause the less compliance of the system, making the exosuit unstable and less safe for the wearer as well as increasing energy consumption. Thus in order to achieve high precision motion control, the friction effect must be appropriately modelled and compensated. In the next chapter, the low-level position controller with adaptive friction compensation will be explained and implemented to guarantee the system robustness and achieve high-level of tracking accuracy.

6 Low-level Nonlinear Friction Compensation Control

[1]

This chapter presents the design principle of the low-level controller, compensating for the friction effect occurring when the cable slides along the inner wall of the Bowden sheath and computing the control signal u for the DC motor to drive the actuation stage. The undesirable friction in Bowden-cable transmission affects on the performance of the system, leading to unexpected vibration and loss in transmitted force and motion to the end-effector. However, similarly to the backlash, it is a challenge to deal with the cable friction, which is hard to model and unpredictably varies with respect to the curvature angle of the Bowden sheath. Thus in this study, I present a dynamic model for accurately capture the friction characteristics. Furthermore, based on the one degree of freedom model of the actuator, another nonlinear adaptive controller is proposed to take account of the nonlinear friction and compute the control command u for the DC motor, accurately tracking the desired trajectory ϕ_a^d obtained from the mid-level control block. Finally it is embedded into the overall hierarchical controller presented in Chapter 4 and applied on the exosuit, assisting a healthy subject's arm motions, comparisons on position tracking performance are then presented to verify the effectiveness of the proposed friction compensation method.

6.1 Overview on Friction in Bowden-cable Transmission and Compensation Control Methods

Friction is a complex phenomenon which exists in all mechanical systems, arising when having relative motion [132, 133]. The friction force depends on many factors such as materials, lubrication, velocity, temperature, and force orthogonal to the

[1] Part of the work presented in this chapter was published in [106]

relative motion. Friction is highly nonlinear and results in steady-state error, limit cycles, and extremely poor performance in motion control. Thus in order to deal with the undesired effects of friction, many friction models have been introduced in the literature review.

Friction can be classified into two categories: static and dynamic [129, 134, 135]. Conventionally, friction is modelled as a static function of velocity and the external applied force. However the simple static models, such as Coulomb and viscous, cannot properly describe all the dynamic effects of the friction, such as the pre-sliding displacement, the friction lag, and the Stribeck effect. In the applications with high precision position tracking, in order to take account for these effects, the dynamic friction model is required to capture the friction characteristics and design the appropriate compensation control algorithm. The Dahl model was introduced in [136], where several experiments on friction in servo systems with ball bearings were conducted. In the sliding displacement, the Dahl model can be considered as a generalization of ordinary Coulomb friction. Moreover, it can approximates the pre-sliding displacement by introducing a first order function of displacement and the direction of motion. However the Dahl model is not able to describe the Stribeck effect. Motivated by Dahl model, Canudas de Wit *et al.* [137, 138] presented a new dynamic friction model, namely LuGre model, which can capture all the observed static and dynamic characteristics of the friction. Also the LuGre model can provides a smooth transition when the motion velocity is reversed. The LuGre model is expressed in the following form:

$$F_f = \sigma_{f0} z + \sigma_{f1} \dot{z} + \sigma_{f2} \dot{x} \tag{6.1}$$

$$\dot{z} = -\alpha(x, \dot{x}) |\dot{x}| z + \dot{x} \tag{6.2}$$

where F_f denotes the friction force, z represents an internal variable of the LuGre model. σ_{f0}, σ_{f1} and σ_{f2} are friction force parameters describing the stiffness of bristles, damping coefficient and viscous coefficient. $\alpha(x, \dot{x})$ is a function characterizing the dynamic effects of the friction force.

Replacing (6.2) into (6.1), the dynamic friction F_f can be re-written as:

$$\begin{aligned} F_f &= \sigma_{f1}\dot{x} + \sigma_{f2}\dot{x} + \sigma_{f0}z - \sigma_{f1}\alpha(x,\dot{x})|\dot{x}|z \\ &= \theta\dot{x} + F_z(x,\dot{x},z) \end{aligned} \tag{6.3}$$

where $\theta = \sigma_{f1} + \sigma_{f2}$, $\theta\dot{x}$ represents the viscous friction force. $F_z(x,\dot{x},z) = \sigma_{f0}z - \sigma_{f1}\alpha(x,\dot{x})|\dot{x}|z$ is the dynamic effect of the friction, depending on the variable z.

The friction in the Bowden cable-driven system occurs when the cable is sliding inside the flexible Bowden sheath, resulting in the lost of the assistive torque τ_a to the elbow joint. The conceptual representation of the friction in the Bowden-cable transmission is shown in Figure 6.1, where F_f and F_N are the friction force and the normal force acting between the cable and the outer sheath respectively, τ_f is the resistive torque caused by the corresponding friction. As shown in Figure 6.2, the normal force F_N varies as the curvature angle of the Bowden sheath is changed, resulting in the variation of the cable friction. In Figure 6.2(A), the normal force F_N is approximately to zero, the friction force between the cable and the sheath is negligible. As the curvature of the Bowden sheath increases from Figure 6.2(A-D), the magnitude of F_N and F_f also increase. Thus if the varying friction is not compensated, then some of the generated torque is resisted during transmission, leading to inaccuracy in motion transmission.

A physical design has been shown to deal with the friction in the Bowden-cable transmission: a PTFE lining on the cable and/or housing can reduce the friction phenomenon, but this choice can only improve the system performance in a certain degree. In order to obtain higher and reliable accuracy, it must rely on effective compensation control algorithms. Bae *et al.* [139] estimated the varying friction by assuming that all the difference between the generated force in the actuator and the transmitted force in the end-effector is caused by the cable friction. The estimated friction was then fed in to the controller for compensation. This approach could evaluate and compensate the friction in real-time, but it requires two force sensors in the input and output sides, making the system bulky and complicated. In [140], authors proposed a method, namely "loop routing", to maintain the cable friction by fixing the bending angle of the Bowden sheath, allowing the tension control with feedforward friction compensation. Palli *et al.* [11] presented a parametric lumped mass model and a dynamic friction model (Dahl model) for describing the transmission of tendon tension. Both of these methods assumed the Bowden sheath's configuration to be fixed, meaning the constant friction. However in the applications of the exosuit, where complex and configuration-dependent friction arises, making the existing control

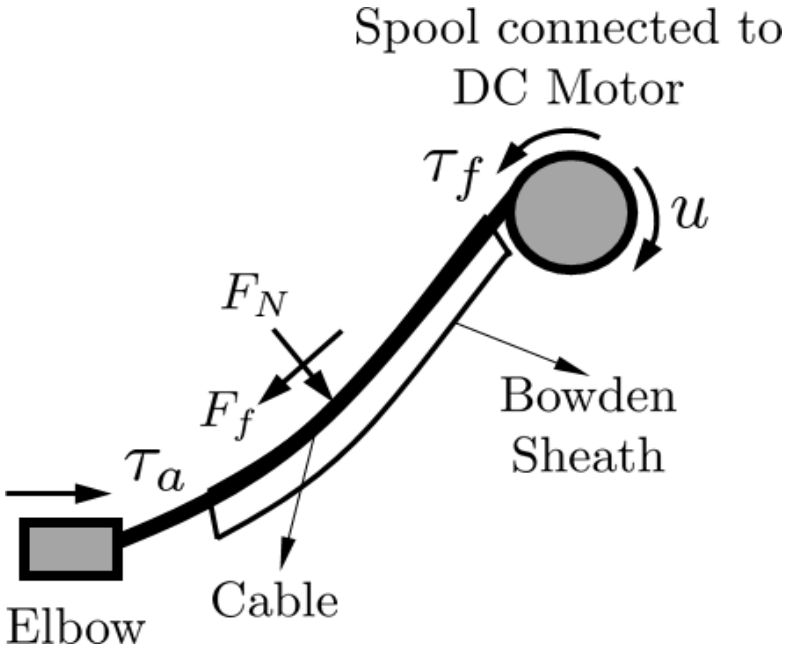

Figure 6.1: Varying friction F_f occurring when the cable slides along the inner wall of the Bowden sheath resulting in the lost of the assistive torque τ_a.

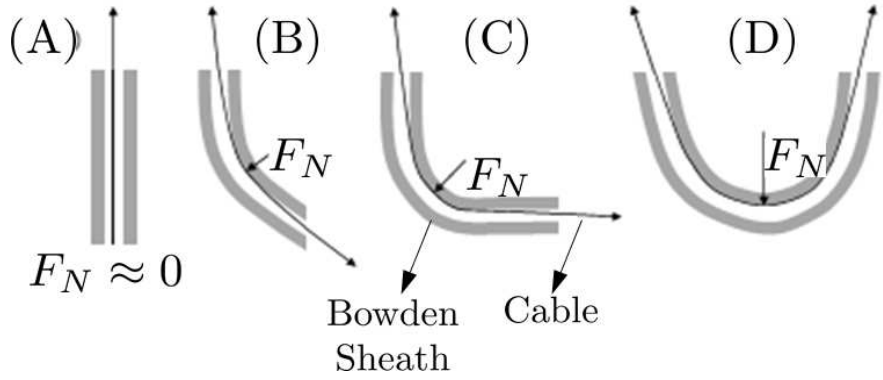

Figure 6.2: Change of the curvature angle of the Bowden sheath, leading to the change of the normal force F_N and the friction force F_f.

approaches insufficient for achieving a reliable performance.

Hence in this chapter I employ the dynamic LuGre model to estimate the friction in the Bowden-cable transmission and then propose another adaptive compensation control technique for the low-level controller to compensate for the variable friction, ensuring the compliance of the system and still achieving an improved position tracking performance for the actuation stage.

6.2 Actuation Stage Position Controller with Adaptive Friction Compensation

The low-level control layer is intended to drive the actuator by sending the control command u to the DC motor and compensate for the nonlinear friction force acting between the cable and the Bowden sheath (Figure 6.1). Alike the backlash, the friction continuously and unpredictably changes according to the curvature angle of the flexible outer sheath which moves with the wearer's arm motion; if not compensated, the torque and the motion generated by the actuator is partly lost during operation. An adaptive algorithm compensates for the friction and controls the DC motor in correctly tracking the desired trajectory ϕ_a^d. From Figure 6.1 the actuation stage in the presence of the friction can be modeled as follows:

$$J\ddot{\phi}_a + B\dot{\phi}_a + \tau_f = u \tag{6.4}$$

where J and B represent the inertia and damping coefficient of the DC motor, τ_f the corresponding friction torque, and u is the control signal to be sent to the DC motor. The dynamic parameters of the actuation stage comprising the DC motor and the Bowden cable and the friction variability are unknown: the LuGre model for the dynamic friction force in (6.3), allows to express the resistive torque τ_f as follows:

$$\tau_f = B_v\dot{\phi}_a + \tau_z\left(\phi_a, \dot{\phi}_a, z\right) \tag{6.5}$$

where z is an internal variable in the LuGre model; $B_v\dot{\phi}_a$ represents the viscous friction; and $\tau_z\left(\phi_a, \dot{\phi}_a, z\right)$ represents the dynamic effects caused by the friction force. It is assumed that τ_z to be bounded by: $|\tau_z\left(\phi_a, \dot{\phi}_a, z\right)| \leq \tau_{zm}$.

Before designing the control signal u, we define the tracking error e_1, reference motion ϕ_a^r and filtered tracking error s_1 for the actuator as [128, 141]:

$$\begin{cases} e_1 = \phi_a - \phi_a^d \\ s_1 = \dot{e}_1 + \lambda_1 e_1 \\ \dot{\phi}_a^r = \dot{\phi}_a^d - \lambda_1 e_1 \end{cases} \tag{6.6}$$

where ϕ_a^d denotes the desired rotation of the actuator obtained from the mid-level

backlash compensation controller, while ϕ_a is the measured value monitored by the incremental encoder mounted on the motor's shaft; and λ_1 is an arbitrary positive constant.

The control signal u for the DC motor is designed as:

$$u = \widehat{J}\ddot{\phi}_a^r + \left(\widehat{B} + \widehat{B_v}\right)\dot{\phi}_a - \widehat{\tau_{zm}}\tanh\left(\frac{s_1}{\epsilon_1}\right) - \kappa_1 s_1 \tag{6.7}$$

where $\widehat{J}$ is the estimated value of J; $\widehat{B}$ and $\widehat{B_v}$ denote respectively the estimated values of B and B_v; $\widehat{\tau_{zm}}$ denotes the estimated value of τ_{zm}; and ϵ_1 and κ_1 are two positive constants.

Substituting (6.5) and (6.7) to (6.4), and replacing $B_t = B + B_v$ (total viscous coefficient) result in the dynamics of the tracking error s_1 as:

$$\begin{aligned} J\dot{s}_1 + \kappa_1 s_1 = \widetilde{J}\ddot{\phi}_a^r + \widetilde{B_t}\dot{\phi}_a - \widetilde{\tau_{zm}}\tanh\left(\frac{s_1}{\epsilon_1}\right) \\ - \tau_{zm}\tanh\left(\frac{s_1}{\epsilon_1}\right) - \tau_z\left(\phi_a, \dot{\phi}_a, z\right) \end{aligned} \tag{6.8}$$

where $\widetilde{J} = \widehat{J} - J$ is the estimated error of J; $\widetilde{B_t} = \widehat{B_t} - B_t$ is the estimated error of B_t; and $\widetilde{\tau_{zm}} = \widehat{\tau_{zm}} - \tau_{zm}$ is the estimated error of τ_{zm}.

Therefore, the unknown parameters $\widehat{J}$, $\widehat{B_t}$, and $\widehat{\tau_{zm}}$ are updated at each period by [129, 130, 142]:

$$\begin{cases} \dot{\widehat{J}} = -\delta_3\ddot{\phi}_a^r s_1 - \delta_3\sigma_3\widehat{J} \\ \dot{\widehat{B_t}} = -\delta_4\dot{\phi}_a s_1 - \delta_4\sigma_4\widehat{B_t} \\ \dot{\widehat{\tau_{zm}}} = \delta_5\tanh\left(\frac{s_1}{\epsilon_1}\right)s_1 - \delta_5\sigma_5\widehat{\tau_{zm}} \end{cases} \tag{6.9}$$

where δ_3, δ_4, and δ_5 are positive adaptation gains; and the initial values of $\widehat{J}$, $\widehat{B_t}$, and $\widehat{\tau_{zm}}$ are set to be zero. The positive terms σ_3, σ_4 and σ_5 ,which are the σ modification, are added to guarantee the boundedness of the corresponding parameters $\widehat{J}$, $\widehat{B_t}$ and $\widehat{\tau_{zm}}$, leading to the stability of the closed-loop system.

Finally the closed-loop nonlinear adaptive controller of the actuator with the control

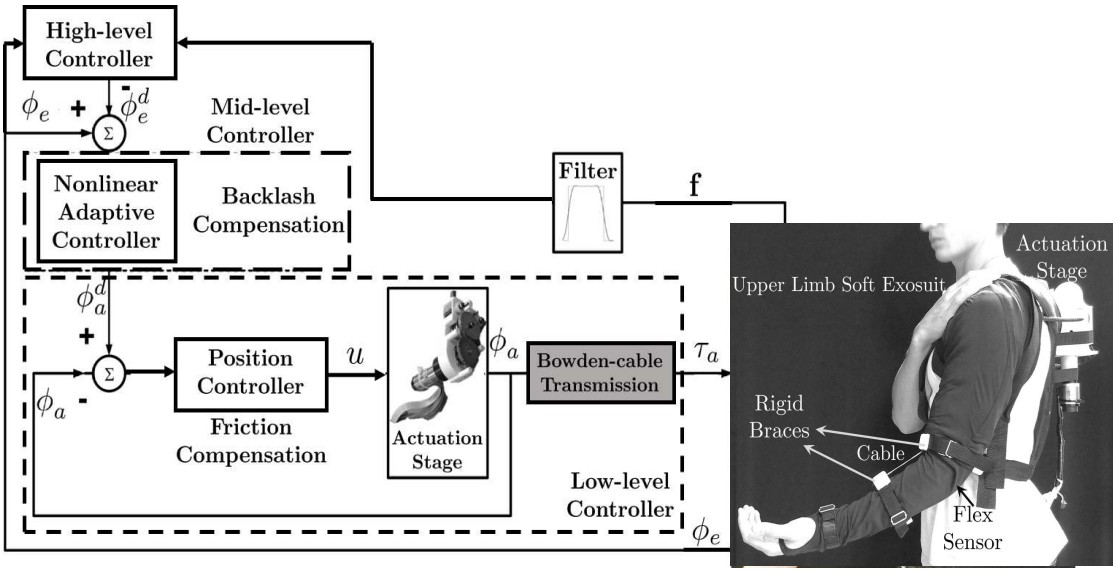

Figure 6.3: Overall hierarchical controller used in the exosuit worn by a healthy subject: ranging from human motion detection by admittance controller and (high-level) ending to the adaptive compensation for the nonlinear behaviours of the Bowden-cable transmission (i.e. backlash in mid-level and friction in low-level).

input u defined in (6.7) can be verified to be stable with a Lyapunov function candidate as in (6.10) (see Appendix A.2).

$$V_1 = \frac{1}{2}Js_1^2 + \frac{1}{2\delta_3}\widetilde{J}^2 + \frac{1}{2\delta_4}\widetilde{B_t}^2 + \frac{1}{2\delta_5}\widetilde{\tau_{zm}}^2 \tag{6.10}$$

6.3 Experimental Results

In order to demonstrate the efficacy of the described nonlinear adaptive position controller, a test has been conducted on the exosuit worn by a healthy subject. The exosuit assists the wearer's arm in ten elbow flexion/extension movements, the proposed hierarchical controller was embedded into the device, ranging from human motion detection by admittance controller and ending to the adaptive compensation for the nonlinear behaviours of the Bowden-cable transmission (i.e. backlash and friction). Especially the mid-level backlash compensation controller converts the desired trajectory ϕ_e^d of the elbow joint generated by the high-level control layer to the desired rotation ϕ_a^d for the actuation stage by (5.14) which is fed in the low-level controller to track. The embedded overall control architecture used in the test is shown in Figure 6.3, the measured elbow joint ϕ_e and cable tensions **f** were input to the high-level

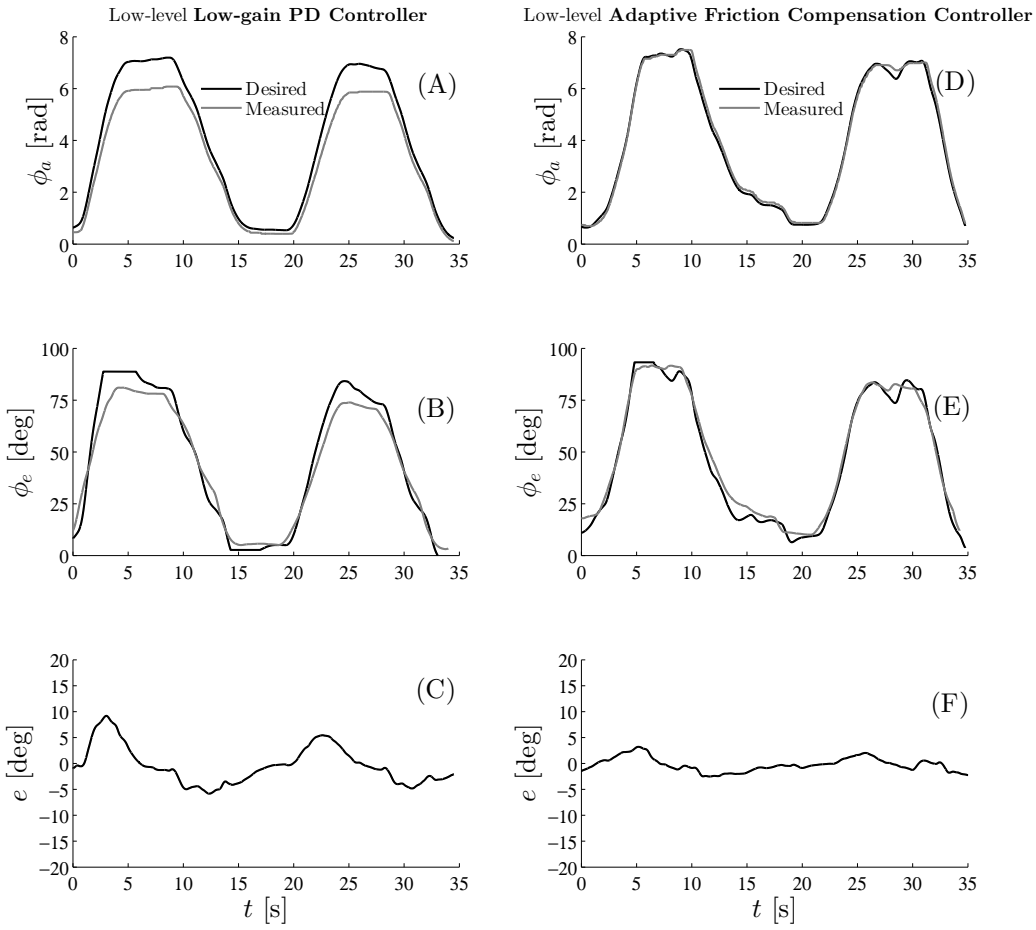

Figure 6.4: Comparisons on position tracking performance. (A)(B)(C): Desired and measured rotation ϕ_a^d and ϕ_a of the actuator, reference and actual motion ϕ_e^d and ϕ_e of the elbow joint, and the elbow joint tracking error $e = \phi_e - \phi_e^d$ respectively when the low-gain PD position controller is used in the low-level control layer. (D)(E)(F): Similar descriptions when the proposed nonlinear adaptive controller with the friction compensation is active.

control layer for motion detection. Comparisons on position tracking performance has been illustrated between using a linear low-gain PD position controller with using the proposed adaptive friction compensation control algorithm in the low-level control block. The parameters for the adaptation law for the friction parameters in defined (6.9) were set as follows: $\lambda_1 = 1.5$, $\kappa_1 = 5$, $\epsilon_1 = 0.01$, $\delta_3 = \delta_4 = \delta_5 = 1$, and $\sigma_3 = \sigma_4 = \sigma_5 = 0.0025$. When the low-gain PD position controller is used to control the actuation stage, Figure 6.4(A) shows the desired rotation ϕ_a^d for the actuator and the measured value obtained from the mounted encoder, (B) represents the corresponding reference and actual motions for the elbow joint, and (C) shows the joint

	RMSE [deg]
Low-level **Low-gain PD Position Controller**	7.128 ± 1.376
Low-level **Adaptive Friction Compensation Algorithm**	2.387 ± 0.643

Table 6.1: Root Mean Square Error (RMSE) of tracking performance of the Bowden-cable transmission without and with friction compensation low-level controller.

tracking error $e = \phi_e - \phi_e^d$. It is worth highlighting that although the mid-level backlash compensation controller significantly enhances the tracking performance, it is not sufficient to overcome the detrimental effect of the friction force, making the tracking error e not to be totally eliminated, with the RMSE is 7.128 ± 1.376[deg] over ten tasks. When the proposed nonlinear adaptive friction compensation control method is active, it is observed that the joint tracking error e is almost reduced to zero, the RMSE value is 2.387 ± 0.643[deg] over ten movements. The RMSE values in two cases are summarized in Table 6.1. The experimental results are promising, showing that by combining the adaptive compensation controllers for the nonlinear behaviours in the exosuit, i.e. backlash and friction, a high-level tracking accuracy can be achieved, while ensuring the control robustness and compliant human-robot interaction.

6.4 Discussion and Summary

Nonlinear friction force in the Bowden-cable transmission causes a lost in transmitted force/motion, resulting in inaccuracy in the assistive torque τ_a delivered to the wearer's elbow joint. Conventionally in order to achieve high accurate motion control, a linear PD position controller with high gains is used to compensate for the undesired effect of the friction force. However, it does not guarantee the compliance of the system, especially in the application with human-in-the-loop, reducing the safety in human-robot interaction. Some authors proposed several methods to estimate the friction force and feed it to the compensation controller, but these approaches required some assumptions which were not practical i.e. the system's configuration must be fixed or constant friction. However in the applications of the exosuit, the curvatures angle of the flexible Bowden sheath and cable are unpredictably changed during the arm motions, leading to the variation in the friction force/torque. Thus in this chapter I introduced a dynamic model, namely LuGre model, to capture all the effects of the friction, and based on this model, implemented an nonlinear adaptive controller for friction compensation in the low-level layer. The proposed low-level position controller is able to update the friction parameters in real-time and accordingly compute the control signal u, sending to the DC motor to drive the exosuit and enhance the overall system's performance, i.e. minimizing the tracking error and

increasing the system robustness and compliance.

7 Discussion and Conclusion

This chapter discusses the contributions of this thesis and future directions for further research.

7.1 Major Contributions

It has been almost three decades that robot-aided rehabilitation and assistive robotics introduced the new concept of gentle human-robot interaction based on soft actuations and materials, yet many questions on ergonomic design and control implementation remain unanswered. Despite the wide spectrum of possible applications, soft robotics with human-in-the-loop is still far from reaching the same performance of the classical approach based on rigid materials and frames. If on one side rigid exoskeletons for assistive technology present insurmountable drawbacks in terms of ergonomics, yet the classical wearable robots are able to model and predict the dynamics at the interface between the robot and the human user.

Soft robotics for human assistance and interaction, has been introduced to answer the questions regarding a more gentle interaction and a higher transparency of the technology which should not modify the user's biomechanics by a large perceived mechanical impedance. Despite promising results, we are still far from the optimal human–robot co-existence, where the lack of functionality caused by neurological damages can be complemented or replaced by soft wearable assistive technology. The main problem can be identified in the missing link between human biomechanics and actuation: the biomimetic approach, based on mimicking the working principles underlying the mechanisms of motion, is often promising but inaccurate and not robust. Nonlinear phenomenons and unpredictable dynamics, which are difficult to model and observe during operations, are the main reasons why the soft wearable assistive technology is still lacking of a large diffusion. In the specific case of

cable-driven actuation, which is the most widely adopted solution to transfer motion from the actuation unit to the human joints, the presence of backlash and friction is detrimental, and may severely affect the assistive effort resulting inaccurate in terms of both dynamics and kinematics. Thus this thesis addressed major issues related to the hardware mechanical design and control implementation of an upper limb soft exoskeleton driven by the Bowden-cable transmission to assist arm motions of physically weak individuals in activities of daily living. The main contributions presented in the thesis are summarized as follow:

- **Mechanical Design of an Actuation Stage and Soft Wearable Suit:**
  In chapter 3 I presented the design and a preliminary bandwidth testing of an actuation stage and a soft wearable exosuit for assisting elbow movements. Using fabrics and Bowden cables for motion transmission instead of traditional rigid transmissions would potentially result in cheaper devices, moreover making the device low profile, lightweight, compliant and less restrictive to the wearer's motion. We based our design on a set of documented force and motion requirements and kept the weight and size of the actuators as low as possible. The actuation unit is located on the user's back, transmitting the force/torque to the elbow joint. It was designed to drive a set of two Bowden cables operating in angonist-antagonist fashion with accordance to elbow flexion/extension tasks. The spool radius for two cables are different by a certain ratio to minimize the cables' elongation mismatch, reducing the stress acting on the human joint. Finally a feeder mechanism was employed to prevent the cables from slacking wrapped around the spool, making the system stable.

- **High-level Controller based on Assisted-as-needed Admittance Controller:**
  In chapter 4 I introduced the problems of sensing human intention of conventional methods using the biological signals, i.e. surface electromyography sEMG. In order to overcome such issues, I presented a non-biological method for human intention detection based on the admittance control combined with the assisted-as-needed algorithm in the high-level controller. As a result, it allows the controller to adapt to the user's motion ability and correspondingly provide an appropriate assistance to the elbow motions. The obtained results have shown that the muscular effort of subjects using the exosuit and the associated controller is lower than performing actions with no assistance. I further showed that the proposed high-level controller was able to tune the level of assistance depending on the voluntary motion capacity of the subjects. This strategy somewhat resembles the "assist-as-needed" paradigm [22], and to our knowledge it is the first time that this kind of approach is being formulated for a wearable exosuit rather than for end-effector robotics device. Finally it is

worth to highlight that the reduction of muscular activation was not provided by a predominant action of the device replacing entirely the human voluntary motion, but rather by a coordinated interaction between the exosuit and the user.

- **Mid-level Controller with Adaptive Backlash Compensation:**
  Chapter 5 introduced the limitation in the Bowden-cable transmission caused by the presence of the backlash, showing a significant time delay and amplitude mismatch in position tracking performance. Many approaches have existed for backlash compensation [20, 119, 121] but they required physical modelization and evaluation of parameters, such as the gap size in the Bowden cable, or also the sheath curvature which plays a fundamental role in affecting the amount of the backlash. Hence, these solutions present limitation in the application of soft exosuit where the backlash hysteresis in the bowden-cable transmission continuously unpredictably varies during the arm motion. Backlash in bowden-cable transmission increases as a function of the bending angle, but decrease as function of the gap size, which also decides the backlash *dead-zone*. Thus I proposed a novel nonlinear adaptive backlash compensator that continuously updates the parameters of the backlash model and it is able to adapt online to the system's configuration, taking into account the time-varying curvature angle of the flexible Bowden sheath due to the human arm motions. Furthermore the adaptive backlash compensation controller was used in the mid-level controller to compute the desired trajectory ϕ_a^d from the elbow's reference motion ϕ_e^d, fed into the actuator to drive the elbow flexion/extension movements. I finally applied the adaptive backlash compensation algorithm in the soft arm exosuit and tested in a real clinical scenario on an impaired subject, where the controller required an EMG activation to trigger the assistance. The results showed a considerable reduction of time delay and amplitude mismatch between the desired and measured trajectory. It implies that the proposed backlash compensation method for the mid-level controller is promising, also considering the severity of the patient, who presented an extremely reduced motion capacity and a degraded electromyographic activity.

- **Low-level Position Controller with Adaptive Friction Compensation:**
  The low-level position controller for the actuator presented in chapter 6 attempted to address the issues related to the friction occurring in the Bowden-cable transmission. Although traditional high-gain PD controller was successfully employed to overcome the detrimental effects of the friction, the performance was still limited, especially in the applications with human-in-the-loop which are required the compliant human-robot interaction. Thus this chapter

introduced the LuGre model to capture the dynamic effects of the friction force and sequentially proposed a friction compensation control method based on another nonlinear adaptive control which was able to online update the actuator and friction parameters, computing the right amount of the control input u and actuating the DC motor. The position controller with adaptive friction compensation was embedded to the overall hierarchical control and validated its efficacy on the exosuit worn by a healthy subject. Comparisons in the tracking performance of both the actuator and the elbow joint demonstrated that the friction compensation control scheme aided to minimize the tracking error to be kept below ±3[deg], while still maintain the compliant interaction and system robustness.

7.2 Ongoing and Future Works

Ongoing and future works will be devoted to develop the proposed hierarchical control paradigm for assisting the human arm movements not only in the sagittal plane but also in the transverse plane. A new hardware design of the actuation unit and the exosuit which is more compact, lightweight, and optimal will be also developing. In addition, the application of the proposed controller with assist-as-needed concept will be extended to not only the arm exosuit but also our developing soft glove for grasping assistance.

7.2.1 A More Comprehensive Model for the Human Arm

In this thesis, the forearm motion was assumed to be in the sagittal plane, and the flex sensor measured the bending angle of the elbow joint ϕ_e, referencing the forearm to the upper arm which we assumed to be vertical and aligned with gravity. Under such conditions the presented Lagrangian formulation in (4.8) described in Chapter 4 was successful and no sensor at the shoulder was required. For future work, in order to increase the degree of freedom, i.e. shoulder flexion/extension, the proposed controller with gravity compensation can be extended by using a sensor (e.g. IMU) to measure the orientation of the upper arm with respect to gravity. This would allow us to update the Lagrangian equation accordingly and thus re-obtain the dynamic model of the elbow joint.

Furthermore as mentioned in the dynamic parameters of the human arm, i.e. inertia, damping, and stiffness are dependent on the arm posture, i.e. horizontal or vertical movements. The dynamic model of the human arm obtained in this thesis was only accurate with an assumption that the forearm only moved vertically and the shoulder

was fully adducted, neglecting the shoulder abduction. With this assumption, the inertia of the elbow joint $I_e = \frac{2}{3}ml^2$, with the forearm mass m and the total forearm length l, is constant which is consistent with previous measurements [6], the damping coefficient b_e is also assumed to be constant, and the stiffness K_e is related to the load from the gravity and the joint angle ϕ_e. In the other words, the stiffness K_e is proportional to $mgl_c \sin\phi_e$, with the length l_c from the elbow joint to the centre of gravity. In the present paper, I wanted to assess whether the exosuit can assist the user's arm by gravity compensation, implying stiffness compensation. Furthermore, the hierarchical controller presented in the thesis can be extended to arm assistance by stiffness compensation in horizontal movements, i.e. 90° shoulder abduction, as long as the dynamic model of the arm can be obtained on the horizontal plane.

7.2.2 New Mechanical Design of the Actuation Unit and Exosuit

As an ongoing project, an advanced development of the wearable suit and the actuation stage for assisting the elbow has been introduced. The new design of the wearable sleeve is designed to be as simple as possible using several pre-tensioning buckles so that it can be easily worn, allows to adapt to different arm morphology, and increases the comfort to the user. The webbing load paths is also re-designed, increasing the ability to withstand larger cable tension. Moreover the new prototype of the actuation unit is more compact, lightweight and ergonomic so that it can be fitted compactly in a backpack, while the operating principle and components are similar to the current one, i.e. spool and feeder mechanism. In order to reduce the friction force in the cable

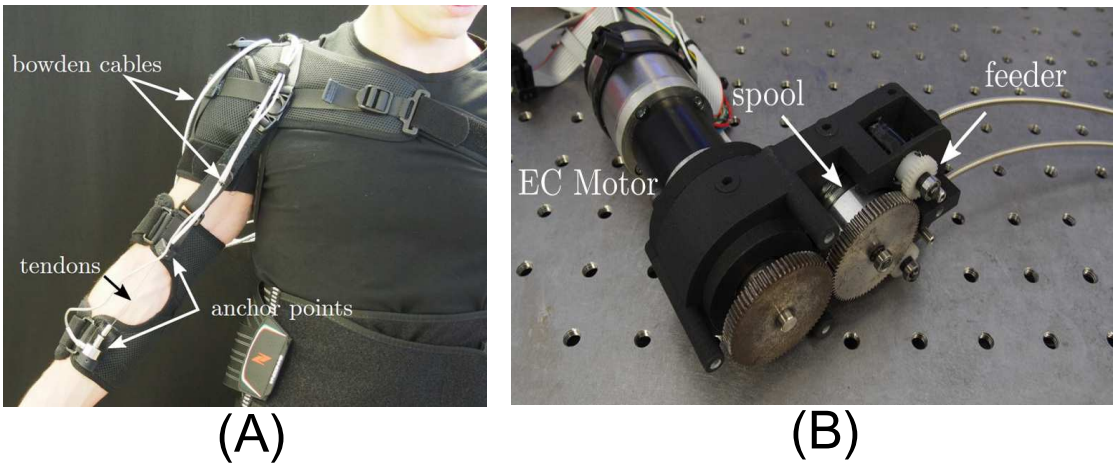

Figure 7.1: (A): New prototype of soft robotic exosuit for arm assistance. (B): More compact and lightweight actuation stage, consisting of a DC motor, spool and feeder mechanism, weighs less than 800g.

path, an alternative tension spring is used for the outer sheath, a Teflon tube is then inserted inside the sheath, and finally a Nitinol cable routed inside the Teflon tube is used to transmit force and motion. By such way, the friction force acting between the inner cable and the outer sheath is significantly decreased. Last but not least, a mechanism using an electromechanical clutch for locking the transmission and keeping the arm in a desired position with minimal power consumption [143], and a custom, low-power electronic system are still ongoing and under development. The new designs of the exosuit as well as the actuation unit are shown in Figure 7.1.

7.2.3 Application of the Hierarchical Controller to Soft Glove for Grasping Assistance

As perspective for this thesis, the proposed control structure can be applied to different upper limb movements such as in a soft glove for hand open/close and grasping assistance, due to the fact that each layer of the presented hierarchical controller was designed in a general way. Especially by using the same approach, i.e. the fabric frames and the Bowden-cable transmission, a low-profile and functional soft glove has been developed as shown in Figure 7.2(A). The fundamental components of the actuation unit for the soft glove are similar to the one used in the elbow-driving actuator. The only difference is that the under-actuated actuator drives three pairs of tendons instead of one by using only an array of spools, consisting of three cylinders with different radius around which three tendons for thumb, index and middle fingers are wrapped. Tendons slack from the spool is also avoided using the feeder mechanism described in the actuator driving the elbow. The first prototype of the actuation

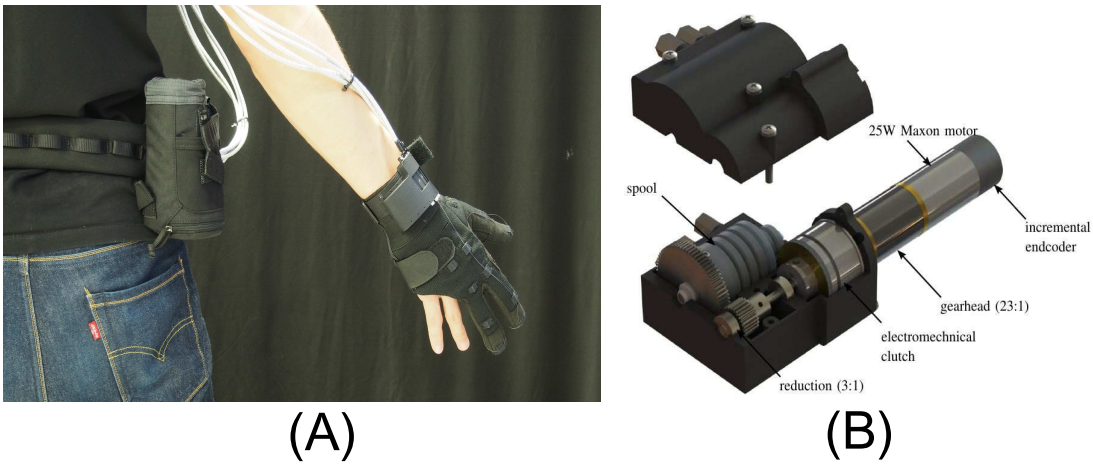

Figure 7.2: (A): Soft robotic glove for grasping assistance. (B): Tendon-driving actuation unit located on the belt driving the robotic glove is enclosed in a 3D printed case.

unit for the developing soft glove is shown in Figure 7.2(B). Finally the proposed hierarchical control architecture with assist-as-needed paradigm can be applied for assisting human hand by modelling the dynamics of each finger, while the nonlinear adaptive controller is responsible for compensating for the undesirable effects caused backlash and friction occurring in the Bowden-cable transmission, and improving the hand tracking performance and grasping ability.

A Appendix

A.1 Appendix: Stability Analysis for the Nonlinear Adaptive Backlash Compensation Control

This appendix proves the stability of the nonlinear adaptive controller for backlash compensation in the mid-level layer presented in chapter 5 and the boundedness of the filtered tracking error s, the tracking error e, and the estimated errors of β and D_m

Considering the Lyapunov function candidate defined in (5.11):

$$V = \frac{1}{2}\beta s^2 + \frac{1}{2\delta_1}\tilde{\beta}^2 + \frac{1}{2\delta_2}\widetilde{D_m}^2$$

The time derivative of V is:

$$\begin{aligned}
\dot{V} &= \beta \dot{s} s + \frac{1}{\delta_1}\dot{\tilde{\beta}}\tilde{\beta} + \frac{1}{\delta_2}\dot{\widetilde{D_m}}\widetilde{D_m} \\
&= \left[\widetilde{\beta\phi_{in}} - \beta\widetilde{D_m}\tanh\left(\frac{s}{\epsilon}\right) - \beta\left(D_m\tanh\left(\frac{s}{\epsilon}\right) - D\right) - \kappa s\right] s \\
&\quad + \frac{1}{\delta_1}\dot{\tilde{\beta}}\tilde{\beta} + \frac{1}{\delta_2}\dot{\widetilde{D_m}}\widetilde{D_m} \\
&= \tilde{\beta}\left(\overline{\phi_{in}} s + \frac{1}{\delta_1}\dot{\tilde{\beta}}\right) - \widetilde{D_m}\left(\beta s\tanh\left(\frac{s}{\epsilon}\right) - \frac{1}{\delta_2}\dot{\widetilde{D_m}}\right) - \kappa s^2 \\
&\quad - \beta s\left(D_m\tanh\left(\frac{s}{\epsilon}\right) - D\right)
\end{aligned} \tag{A.1}$$

Noting that $\dot{\widetilde{\beta}} = \dot{\widehat{\beta}}$, $\dot{\widetilde{D_m}} = \dot{\widehat{D_m}}$, and substituting the adaptation law for the backlash parameters (5.10) into (A.1):

$$\begin{aligned} \dot{V} &= -\kappa s^2 - \sigma_1 \widetilde{\beta}\widehat{\beta} - \sigma_2 \widetilde{D_m}\widehat{D_m} + D\beta s - D_m \beta s \tanh\left(\frac{s}{\epsilon}\right) \\ &\leq -\kappa s^2 - \sigma_1 \widetilde{\beta}\widehat{\beta} - \sigma_2 \widetilde{D_m}\widehat{D_m} + \left|D_m \beta s\right| - D_m \beta s \tanh\left(\frac{s}{\epsilon}\right) \end{aligned} \tag{A.2}$$

Remarking the following property of the hyperbolic tangent function tanh(.):

$$0 \leq |\alpha| - \alpha \tanh\left(\frac{s}{\epsilon}\right) \leq 0.2785\epsilon \qquad (\forall \alpha \in R) \tag{A.3}$$

Combining (A.2) and (A.3) leads to:

$$\dot{V} \leq -\kappa s^2 - \sigma_1 \widetilde{\beta}\widehat{\beta} - \sigma_2 \widetilde{D_m}\widehat{D_m} + 0.2785\epsilon \tag{A.4}$$

Noting that $\widehat{\beta} = \widetilde{\beta} + \beta$ and $\widehat{D_m} = \widetilde{D_m} + D_m$, and according to the complete square inequality for $-\sigma_1 \widetilde{\beta}\widehat{\beta}$:

$$-\sigma_1 \widetilde{\beta}\widehat{\beta} \leq -\sigma_1 \widetilde{\beta}^2 + \sigma_1 |\widetilde{\beta}||\beta| \leq -\frac{\sigma_1 \widetilde{\beta}^2}{2} + \frac{\sigma_1 |\beta|^2}{2} \tag{A.5}$$

The same argument is applied for $-\sigma_2 \widetilde{D_m}\widehat{D_m}$:

$$-\sigma_2 \widetilde{D_m}\widehat{D_m} \leq -\frac{\sigma_2 \widetilde{D_m}^2}{2} + \frac{\sigma_2 |D_m|^2}{2} \tag{A.6}$$

Substituting (A.5) and (A.6) into (A.4), the time derivative of the Lyapunov function can be rewritten as:

$$\dot{V} \leq -\kappa s^2 - \frac{\sigma_1 \widetilde{\beta}^2}{2} - \frac{\sigma_2 \widetilde{D_m}^2}{2} + \frac{\sigma_1 |\beta|^2}{2} + \frac{\sigma_2 |D_m|^2}{2} + 0.2785\epsilon \tag{A.7}$$

Adding and subtracting the term ρV with $\rho > 0$:

$$\dot{V} \leq -\rho V - \left(\kappa - \frac{\rho\beta}{2}\right)s^2 - \left(\sigma_1 - \frac{\rho}{\delta_1}\right)\frac{\widetilde{\beta}^2}{2} - \left(\sigma_2 - \frac{\rho}{\delta_2}\right)\frac{\widetilde{D_m}^2}{2} + f \tag{A.8}$$

where $f = \frac{\sigma_1|\beta|^2}{2} + \frac{\sigma_2|D_m|^2}{2} + 0.2785\epsilon$

If I choose $\rho \leq \min\{\frac{2\kappa}{\beta}, \sigma_1\delta_1, \sigma_2\delta_2\}$, I have:

$$\dot{V} \leq -\rho V + f \tag{A.9}$$

which implies that for $V \geq V_0 = \frac{f}{\rho}$, the negative definiteness of $\dot{V}$ can be assured.

I now prove that the filtered tracking error s, the tracking error e, and the estimated errors of β and D_m are guaranteed to be uniformly ultimately bounded (u.u.b).

Let's introduce a Lemma: Let f, V: $[0,\infty) \mapsto R$. Then

$$\dot{V} \leq -\rho V + f, \quad \forall\, t \geq t_0 \geq 0 \tag{A.10}$$

implies that

$$V(t) \leq e^{-\rho(t-t_0)}V(t_0) + \int_{t_0}^{t} e^{-\rho(t-\tau)}f(\tau)d\tau, \quad \forall\, t \geq t_0 \geq 0 \tag{A.11}$$

Applying this Lemma to (A.9) with $f = \frac{\sigma_1|\beta|^2}{2} + \frac{\sigma_2|D_m|^2}{2} + 0.2785\epsilon$ and $t_0 = 0$:

$$0 \leq V(t) \leq \left(V(0) - \frac{f}{\rho}\right)e^{-\rho t} + \frac{f}{\rho} \tag{A.12}$$

where $V(0)$ is the initial value of the Lyapunov function

From the Lyapunov function ((5.11)), I have:

$$\frac{1}{2}\beta s^2 \leq V \leq \left(V(0) - \frac{f}{\rho}\right)e^{-\rho t} + \frac{f}{\rho} \tag{A.13}$$

The filtered tracking error s can be expressed as follow:

$$|s| \leq \sqrt{\frac{2}{\beta}\left(V(0) - \frac{f}{\rho}\right)e^{-\rho t} + \frac{2f}{\beta\rho}} \tag{A.14}$$

which implies that s converges exponentially to the residual set:

$$\Omega_s = \left\{s \in R, |s| \leq \sqrt{\frac{2f}{\beta\rho}}\right\} \tag{A.15}$$

The same proof can be applied for the estimated errors $\widetilde{\beta}$ and $\widetilde{D_m}$.

For the tracking error e, it is noted that:

$$|s| = |\lambda e + \int_0^t e(\tau)d\tau| \leq \sqrt{\frac{2f}{\beta\rho}} \tag{A.16}$$

Defining $e_1 = \int_0^t e(\tau)d\tau$ and $\dot{e_1} = e$:

$$|\lambda\dot{e_1} + e_1| \leq \sqrt{\frac{2f}{\beta\rho}} \tag{A.17}$$

Case 1: $\lambda\dot{e_1} + e_1 \leq \sqrt{\frac{2f}{\beta\rho}}$. The solution is:

$$e_1 \leq \left(e_1(0) - \sqrt{\frac{2f}{\beta\rho}}\right)e^{-\frac{1}{\lambda}t} + \sqrt{\frac{2f}{\beta\rho}} \tag{A.18}$$

where $e_1(0)$ is the initial value of e_1

Case 2: $-\sqrt{\frac{2f}{\beta\rho}} \leq \lambda\dot{e}_1 + e_1$. The solution can be obtained by:

$$\left(e_1(0) + \sqrt{\frac{2f}{\beta\rho}}\right)e^{-\frac{1}{\lambda}t} - \sqrt{\frac{2f}{\beta\rho}} \leq e_1 \tag{A.19}$$

Hence, the variable e_1 converges to the compact set:

$$\Omega_{e_1} = \left\{e_1 \in R, |e_1| \leq \sqrt{\frac{2f}{\beta\rho}}\right\} \tag{A.20}$$

As a result, the tracking error $e = \dot{e}_1$ can be proven to be bounded:

$$\lambda|\dot{e}_1| - |e_1| \leq |s| = |\lambda\dot{e}_1 + e_1| \leq \sqrt{\frac{2f}{\beta\rho}} \tag{A.21}$$

or

$$\lambda|\dot{e}_1| \leq |e_1| + \sqrt{\frac{2f}{\beta\rho}} \leq 2\sqrt{\frac{2f}{\beta\rho}} \tag{A.22}$$

Then, the tracking error e can be easily expressed as follow:

$$|e| = |\dot{e}_1| \leq \frac{2}{\lambda}\sqrt{\frac{2f}{\beta\rho}} \tag{A.23}$$

Finally, the adaptation law with the σ-modification given by (5.10) can guarantee that the tracking error e, and the estimated errors $\widetilde{\beta}$ and $\widetilde{D_m}$ are uniformly ultimately bounded (u.u.b). From (A.9) and the compact set Ω_{e_1}, it can be seen that the performances and stability of the proposed control scheme depend on the values of f and ρ, in other words the selection of the designed parameters such as the adaptation gains δ_1, δ_2, σ_1, σ_2 and the constant κ. We want to minimize the tracking error e or the size of the compact set Ω_{e_1}, and the size of this set can be reduced by increasing δ_1, δ_2, and κ. However high values of these parameters can cause chattering problems. In practice we empirically increase the value of κ by trial and error to an acceptable value, and the positive adaptation gains δ_1, δ_2 can be respectively adjusted thereafter. Two other positive parameters σ_1 and σ_2 are added to guarantee the convergence of the tracking error e and the robustness of the closed-loop control system (they regulate the *stiffness* in the backlash parameters adaptation law (5.10)). If the modification gains σ_1 and σ_2 are chosen to be too small, the estimated backlash parameters $\widehat{\beta}$ and

$\widehat{D_m}$ might not converge to the actual values. In contrast, if they are too large, the values of $\widehat{\beta}$ and $\widehat{D_m}$ can present oscillations before the convergence. Thus, the terms σ_1 and σ_2 should be selected considering this trade-off between converging time and accuracy [131]. This completes the proof.

A.2 Appendix: Stability Analysis for the Nonlinear Adaptive Friction Compensation Position Control

I apply the similar proof procedure of previous section to demonstrate the Lyapunov function V_1 decreases (i.e. $\dot{V}_1 \leq 0$) and the tracking error e_1 converges to a compact set, resulting in the stability for the closed-loop low-level position controller with the friction compensation.

The time derivative of V_1 is obtained as:

$$\begin{aligned}
\dot{V}_1 &= J s_1 \dot{s}_1 + \frac{1}{\delta_3}\widetilde{J}\dot{\widetilde{J}} + \frac{1}{\delta_4}\widetilde{B_t}\dot{\widetilde{B_t}} + \frac{1}{\delta_5}\widetilde{\tau_{zm}}\dot{\widetilde{\tau_{zm}}} \\
&= \frac{1}{\delta_3}\widetilde{J}\dot{\widetilde{J}} + \frac{1}{\delta_4}\widetilde{B_t}\dot{\widetilde{B_t}} + \frac{1}{\delta_5}\widetilde{\tau_{zm}}\dot{\widetilde{\tau_{zm}}} \\
&+ s_1\left(\widetilde{J}\ddot{\phi}_a^r + \widetilde{B_t}\dot{\phi}_a - \widetilde{\tau_{zm}}\tanh\left(\frac{s_1}{\epsilon_1}\right)\right. \\
&\left. - \tau_{zm}\tanh\left(\frac{s_1}{\epsilon_1}\right) - \tau_z\left(\phi_a, \dot{\phi}_a, z\right) - \kappa_1 s_1\right)
\end{aligned} \tag{A.24}$$

Substituting the adaptation law (6.9) to (A.24), and it is noted that $\dot{\widetilde{J}} = \dot{\widehat{J}}$, $\dot{\widetilde{B_t}} = \dot{\widehat{B_t}}$ and $\dot{\widetilde{\tau_{zm}}} = \dot{\widehat{\tau_{zm}}}$. Hence $\dot{V}_1$ is rewritten as following:

$$\begin{aligned}
\dot{V}_1 &= -\kappa_1 s_1^2 - s_1\left(\tau_{zm}\tanh\left(\frac{s_1}{\epsilon_1}\right) - \tau_z\left(\phi_a, \dot{\phi}_a, z\right)\right) - \sigma_3\widetilde{J}\widehat{J} - \sigma_4\widetilde{B_t}\widehat{B_t} - \sigma_5\widetilde{\tau_{zm}}\widehat{\tau_{zm}} \\
&\leq -\kappa_1 s_1^2 + \left|s_1\tau_z\left(\phi_a, \dot{\phi}_a, z\right)\right| - s_1\tau_{zm}\tanh\left(\frac{s_1}{\epsilon_1}\right) - \sigma_3\widetilde{J}\widehat{J} - \sigma_4\widetilde{B_t}\widehat{B_t} - \sigma_5\widetilde{\tau_{zm}}\widehat{\tau_{zm}} \\
&\leq -\kappa_1 s_1^2 + \left|s_1\tau_{zm}\right| - s_1\tau_{zm}\tanh\left(\frac{s_1}{\epsilon_1}\right) - \sigma_3\widetilde{J}\widehat{J} - \sigma_4\widetilde{B_t}\widehat{B_t} - \sigma_5\widetilde{\tau_{zm}}\widehat{\tau_{zm}}
\end{aligned} \tag{A.25}$$

Reminding the property of the hyperbolic tangent function tanh(.):

$$0 \leq |\alpha| - \alpha \tanh\left(\frac{s_1}{\epsilon_1}\right) \leq 0.2785\epsilon_1 \qquad (\forall \alpha \in R) \tag{A.26}$$

Combining (A.25) and (A.26):

$$\dot{V}_1 \leq -\kappa_1 s_1^2 - \sigma_3 \widetilde{J}\widehat{J} - \sigma_4 \widetilde{B_t}\widehat{B_t} - \sigma_5 \widetilde{\tau_{zm}}\widehat{\tau_{zm}} + 0.2785\epsilon_1 \tag{A.27}$$

Noting that $\widehat{J} = \widetilde{J} + J$, $\widehat{B_t} = \widetilde{B_t} + B_t$ and $\widehat{\tau_{zm}} = \widetilde{\tau_{zm}} + \tau_{zm}$. Applying the complete square inequality:

$$-\sigma_3 \widetilde{J}\widehat{J} \leq -\sigma_3 \widetilde{J}^2 + \sigma_3 |\widetilde{J}||J| \leq -\frac{\sigma_3 \widetilde{J}^2}{2} + \frac{\sigma_3 |J|^2}{2} \tag{A.28}$$

$$-\sigma_4 \widetilde{B_t}\widehat{B_t} \leq -\sigma_4 \widetilde{B_t}^2 + \sigma_4 |\widetilde{B_t}||B_t| \leq -\frac{\sigma_4 \widetilde{B_t}^2}{2} + \frac{\sigma_4 |B_t|^2}{2} \tag{A.29}$$

$$-\sigma_5 \widetilde{\tau_{zm}}\widehat{\tau_{zm}} \leq -\sigma_5 \widetilde{\tau_{zm}}^2 + \sigma_5 |\widetilde{\tau_{zm}}||\tau_{zm}| \leq -\frac{\sigma_5 \widetilde{\tau_{zm}}^2}{2} + \frac{\sigma_5 |\tau_{zm}|^2}{2} \tag{A.30}$$

Substituting the inequalities (A.28), (A.29) and (A.30) to (A.27):

$$\dot{V}_1 \leq -\kappa_1 s_1^2 - \frac{\sigma_3 \widetilde{J}^2}{2} - \frac{\sigma_4 \widetilde{B_t}^2}{2} - \frac{\sigma_5 \widetilde{\tau_{zm}}^2}{2} + \frac{\sigma_3 |J|^2}{2} + \frac{\sigma_4 |B_t|^2}{2} + \frac{\sigma_5 |\tau_{zm}|^2}{2} + 0.2785\epsilon_1 \tag{A.31}$$

Adding and subtracting the term $\rho_1 V_1$ with $\rho_1 > 0$:

$$\dot{V}_1 \leq -\rho_1 V_1 - \left(\kappa_1 - \frac{\rho_1 J}{2}\right) s_1^2 - \left(\sigma_3 - \frac{\rho_1}{\delta_3}\right) \frac{\widetilde{J}^2}{2} - \left(\sigma_4 - \frac{\rho_1}{\delta_4}\right) \frac{\widetilde{B_t}^2}{2} - \left(\sigma_5 - \frac{\rho_1}{\delta_5}\right) \frac{\widetilde{\tau_{zm}}^2}{2} + f_1 \quad \text{(A.32)}$$

where $f_1 = \frac{\sigma_3 |J|^2}{2} + \frac{\sigma_4 |B_t|^2}{2} + \frac{\sigma_5 |\tau_{zm}|^2}{2} + 0.2785\epsilon_1$

If I choose $\rho_1 \leq \min\left\{\frac{2\kappa_1}{J}, \sigma_3\delta_3, \sigma_4\delta_4, \sigma_5\delta_5\right\}$, I have:

$$\dot{V}_1 \leq -\rho_1 V_1 + f_1 \quad \text{(A.33)}$$

The time derivative of the Lyapunov function $\dot{V}_1 \leq 0$ whenever $V_1 \geq \frac{f_1}{\rho_1}$.

By applying the exact same argument in Appendix A.1, I can prove that the tracking error e_1 and the estimated errors $\widetilde{J}$, $\widetilde{B_t}$ and $\widetilde{\tau_{zm}}$ are uniformly ultimately bounded (u.u.b). Thus it can be concluded that the nonlinear adaptive position controller for the friction compensation is stable and the tracking error e_1 converges to a small neighbourhood of zero whose size is adjustable by the constant κ_1. It is noted that the size of the set Ω_{s_1} can be minimize by increasing the value of κ_1. However the high value of κ_1 can cause the vibration issue. Hence I empirically increase κ_1 by trial and error and fix to an acceptable value, the adaptation gains δ_3, δ_4 and δ_5 can be adjusted thereafter. This completes the proof.

Author's Publications

Book Chapter

1. Michele Xiloyannis, **Binh Khanh Dinh**, Leonardo Cappello, Chris Wilson Antuvan and Lorenzo Masia. 'Design Guidelines for Upper Limb Soft Wearable Exosuits', submitted to *Wearable Technology for Medicine and Healthcare*, Elsevier, (in press).

2. Lorenzo Masia, Michele Xiloyannis, **Binh Khanh Dinh**, Chris Wilson Antuvan, Sara Contu and Yongtae Kim. 'Actuation for Robot-Aided-Rehabilitation: Design and Control Strategies', submitted to *Rehabilitation Robotics*, Elsevier, (in press).

3. Lorenzo Masia, Irfan Hussain, Michele Xiloyannis, Claudio, Pacchierotti, Leonardo Cappello, Monica Malvezzi, Giovanni Spagnoletti, Chris Wilson Antuvan, **Binh Khanh Dinh**, Maria Pozzi and Domenico Prattichizzo. 'Soft Wearable Assistive Robotics: Exosuits and Supernumerary Limbs', Springer, (in press).

Submitted Journal Publications

1. **Binh Khanh Dinh**, Leonardo Cappello, and Lorenzo Masia. 'Novel Series Elastic Actuator employing Multistable Composite Structures: Application of Machine Learning to Predict Stable Positions and System Reconfiguration Control Implementation', submitted to *Mechatronics* 2017 (submitted).

2. Leonardo Cappello, **Binh Khanh Dinh** (co-first author), Alberto Pirrera, Filippo Mattioni, and Lorenzo Masia. 'Novel Series Elastic Actuator employing Multistable Composite Structures: Characterization and Control Implementation', submitted to *Mechatronics* 2017 (under review).

3. **Binh Khanh Dinh**, Michele Xiloyannis, Chris Wilson Antuvan, Leonardo Cappello, and Lorenzo Masia. 'Hierarchical Cascade Controller for Assistance Mod-

ulation in a Soft Wearable Arm Exoskeleton' submitted to *Robotics Automation Letters* 2017 (accepted for publication).

4. **Binh Khanh Dinh**, Michele Xiloyannis, Leonardo Cappello, Chris Wilson Antuvan, Shih-Cheng Yen, and Lorenzo Masia. 'Adaptive Backlash Compensation in Upper Limb Soft Wearable Exoskeleton' submitted to *Robotics and Autonomous Systems* 2017 (accepted for publication in the special issue: Human-oriented Approaches for Assistive and Rehabilitation Robotics).

5. Michele Xiloyannis, Leonardo Cappello, **Binh Khanh Dinh**, Chris Wilson Antuvan, and Lorenzo Masia. 'Preliminary design and control of a soft exosuit for assisting elbow movements and hand grasping in activities of daily living' submitted to *Journal of Rehabilitation and Assistive Technologies Engineering (RATE)* 2016 (accepted for publication).

Refereed Conference Publications

1. **Binh Khanh Dinh**, Michele Xiloyannis, Chris Wilson Antuvan, Leonardo Cappello, and Lorenzo Masia. 'Hierarchical Cascade Controller for Assistance Modulation in a Soft Wearable Arm Exoskeleton'. IEEE International Conference on Robotics and Automation ICRA 2017, Singapore 29^{th} May-03^{rd} June 2017

2. **Binh Khanh Dinh**, Leonardo Cappello, Michele Xiloyannis, and Lorenzo Masia. 'Position Control using Adaptive Backlash Compensation for Bowden Cable Transmission in Soft Wearable Exoskeleton'. IEEE International Conference on Intelligent Robots and Systems IROS 2016, Daejeon, South Korea $9^{th} - 14^{th}$ October 2016

3. **Binh Khanh Dinh**, Leonardo Cappello, and Lorenzo Masia. 'Localized Extreme Learning Machine for Online Inverse Dynamic Model Estimation in Soft Wearable Exoskeleton'. IEEE International Conference on Biomedical Robotics and Biomechatronics BIOROB 2016, Singapore $26^{th} - 29^{th}$ June 2016.

4. **Binh Khanh Dinh**, Leonardo Cappello, Lorenzo Masia. Control Implementation of Compliant Composite Material Actuators for Wearable Robotic Exoskeletons IEEE International Conference on Robotic Rehabilitation ICORR 2015, Singapore $11^{th} - 14^{th}$ August 2015

5. Leonardo Cappello, **Binh Khanh Dinh**, and Lorenzo Masia. 'Design of SARCOMEX: a Soft ARm COMpliant Exoskeleton'. IEEE International Conference on Biomedical Robotics and Biomechatronics BIOROB 2016, Singapore $26^{th} - 29^{th}$ June 2016

6. Michele Xiloyannis, Leonardo Cappello, **Binh Khanh Dinh**, Chris Wilson Antuvan, and Lorenzo Masia. 'Design and Preliminary Testing of a Soft Exosuit for Assisting Elbow Movements and Hand Grasping'. International Conference on Neurorehabilitation ICNR 2016, Spain 18^{th} – 21^{st} 2016.

7. Michele Xiloyannis, Leonardo Cappello, **Binh Khanh Dinh** and Lorenzo Masia. 'Towards the Design of an Underactuated Soft Exoskeleton for Grasp Assistance'. IEEE International Conference on Biomedical Robotics and Biomechatronics BIOROB 2016, Singapore 26^{th} – 29^{th} June 2016

8. Jeong-Yean Yang, **Binh Khanh Dinh**, Han-Gyeol Kim, and Dong-Soo Kwon. 'Development of emotional attachment on a cleaning robot for the long-term interactive affective companion'. IEEE International Symposium on Robot and Human Interactive Communication RO-MAN 2013, South Korea 26^{th} – 29^{th} August 2013

Bibliography

[1] N. Jarrassé and G. Morel, "Connecting a human limb to an exoskeleton," *IEEE Transactions on Robotics*, vol. 28, no. 3, pp. 697–709, 2012.

[2] A. T. Asbeck, K. Schmidt, and C. J. Walsh, "Soft exosuit for hip assistance," *Robotics and Autonomous Systems*, vol. 73, pp. 102–110, 2015.

[3] V. Bartenbach, K. Schmidt, M. Naef, D. Wyss, and R. Riener, "Concept of a soft exosuit for the support of leg function in rehabilitation," in *Rehabilitation Robotics (ICORR), 2015 IEEE International Conference on*. IEEE, 2015, pp. 125–130.

[4] H. In, B. B. Kang, M. Sin, and K.-J. Cho, "Exo-glove: A wearable robot for the hand with a soft tendon routing system," *IEEE Robotics & Automation Magazine*, vol. 22, no. 1, pp. 97–105, 2015.

[5] M. Xiloyannis, L. Cappello, D. B. Khanh, S.-C. Yen, and L. Masia, "Modelling and design of a synergy-based actuator for a tendon-driven soft robotic glove," in *6th IEEE International Conference on Biomedical Robotics and Biomechatronics (BIOROB)*, June 2016, pp. 1213–1219.

[6] H. In, B. Kang, M. Sin, and K.-J. Cho, "Exo-glove: A wearable robot for the hand with a soft tendon routing system," *Robotics Automation Magazine, IEEE*, vol. 22, no. 1, pp. 97–105, March 2015.

[7] D. Bennett, J. M. Hollerbach, Y. Xu, and I. Hunter, "Time-varying stiffness of human elbow joint during cyclic voluntary movement," *Experimental Brain Research*, vol. 88, no. 2, pp. 433–442, 1992.

[8] J. Ueda, M. Hyderabadwala, V. Krishnamoorthy, and M. Shinohara, "Motor task planning for neuromuscular function tests using an individual muscle control technique," in *IEEE International Conference on Rehabilitation Robotics (ICORR)*, 2009, pp. 133–138.

[9] M. A. Delph, S. A. Fischer, P. W. Gauthier, C. H. M. Luna, E. A. Clancy, and G. S. Fischer, "A soft robotic exomusculature glove with integrated sEMG sensing for hand rehabilitation," in *IEEE International Conference on Rehabilitation Robotics*, 2013, pp. 1–7.

[10] S. W. Lee, K. A. Landers, and H.-S. Park, "Development of a biomimetic hand exotendon device (biomhed) for restoration of functional hand movement post-stroke," *IEEE Transactions on Neural Systems and Rehabilitation Engineering*, vol. 22, no. 4, pp. 886–898, 2014.

[11] G. Palli and C. Melchiorri, "Model and control of tendon-sheath transmission systems," in *IEEE International Conference on Robotics and Automation (ICRA)*, May 2006, pp. 988–993.

[12] D. Chen, Y. Yun, and A. D. Deshpande, "Experimental characterization of bowden cable friction," in *IEEE International Conference on Robotics and Automation (ICRA)*, May 2014, pp. 5927–5933.

[13] T. N. Do, T. Tjahjowidodo, M. Lau, and S. Phee, "Adaptive control of position compensation for cable-conduit mechanisms used in flexible surgical robots," in *Informatics in Control, Automation and Robotics (ICINCO), 2014 11th International Conference on*, vol. 1. IEEE, 2014, pp. 110–117.

[14] T. N. Do, T. Tjahjowidodo, M. W. S. Lau, and S. J. Phee, "Adaptive control for enhancing tracking performances of flexible tendon–sheath mechanism in natural orifice transluminal endoscopic surgery (notes)," *Mechatronics*, vol. 28, pp. 67 – 78, 2015.

[15] ——, "Real-time enhancement of tracking performances for cable-conduit mechanisms-driven flexible robots," *Robotics and Computer-Integrated Manufacturing*, vol. 37, pp. 197 – 207, 2016.

[16] M. Kaneko, W. Paetsch, and H. Tolle, "Input-dependent stability of joint torque control of tendon-driven robot hands," *IEEE Transactions on Industrial Electronics*, vol. 39, no. 2, pp. 96–104, 1992.

[17] W. Townsend and J. Salisbury, "The effect of coulomb friction and stiction on force control," in *IEEE International Conference on Robotics and Automation (ICRA)*, 1987, pp. 883–889.

[18] J. Veneman, R. Ekkelenkamp, R. Kruidhof, F. Van der Helm, and H. Van der Kooij, "Design of a series elastic-and bowden cable-based actuation system for use as torque-actuator in exoskeleton-type training," in *9th International Conference on Rehabilitation Robotics (ICORR)*. IEEE, 2005, pp. 496–499.

[19] A. Schiele, P. Letier, R. Van Der Linde, and F. Van Der Helm, "Bowden cable actuator for force-feedback exoskeletons," in *IEEE/RSJ International Conference on Intelligent Robots and Systems*, 2006, pp. 3599–3604.

[20] V. Agrawal, W. Peine, B. Yao, and S. Choi, "Control of cable actuated devices using smooth backlash inverse," in *IEEE International Conference on Robotics and Automation (ICRA)*, May 2010, pp. 1074–1079.

[21] R. S. Mosher, "Force-reflecting electrohydraulic servomanipulator," *Electro-Technology, Dec.*, pp. 138–141, 1960.

[22] W. Cloud, "Man amplifiers: Machines that let you carry a ton," *Popular Sci.*, vol. 187, no. 5, pp. 70–73, 1965.

[23] R. S. Mosher, "Handyman to hardiman," SAE Technical Paper, Tech. Rep., 1967.

[24] V. L. Nickel, A. Karchak, and J. Allen, "Electrically powered orthotic systems," *J Bone Joint Surg Am*, vol. 51, no. 2, pp. 343–351, 1969.

[25] G. Schmeisser and W. Seamone, "An upper limb prosthesis-orthosis power and control system with multi-level potential," *J Bone Joint Surg Am*, vol. 55, no. 7, pp. 1493–1501, 1973.

[26] N. Benjuya and S. B. Kenney, "Hybrid arm orthosis." *JPO: Journal of Prosthetics and Orthotics*, vol. 2, no. 2, pp. 155–163, 1990.

[27] H. Kazerooni and S. Mahoney, "Dynamics and control of robotic systems worn by humans," in *Robotics and Automation, 1991. Proceedings., 1991 IEEE International Conference on*. IEEE, 1991, pp. 2399–2405.

[28] K. K. R. A. R. C. Gopura and E. Horikawa, "A study on human upper-limb muscles activities during daily upper-limb motions," *International Journal of Bioelectromagnetism*, pp. 54–61, 2010.

[29] V. M. Zatsiorsky, *Kinetics of human motion*. Human Kinetics, 2002.

[30] K.-N. An, "Kinematic analysis of human movement," *Annals of Biomedical Engineering*, vol. 12, no. 6, pp. 585–597, 1984.

[31] A. Engín, "On the biomechanics of the shoulder complex," *Journal of biomechanics*, vol. 13, no. 7, pp. 575 583–581 590, 1980.

[32] K. Kiguchi, K. Iwami, M. Yasuda, K. Watanabe, and T. Fukuda, "An exoskeletal robot for human shoulder joint motion assist," *IEEE/ASME transactions on mechatronics*, vol. 8, no. 1, pp. 125–135, 2003.

[33] K. Kiguchi, "Active exoskeletons for upper-limb motion assist," *International Journal of Humanoid Robotics*, vol. 4, no. 03, pp. 607–624, 2007.

[34] J. London, "Kinematics of the elbow." *J Bone Joint Surg Am*, vol. 63, no. 4, pp. 529–535, 1981.

[35] K. Kiguchi, S. Kariya, K. Watanabe, K. Izumi, and T. Fukuda, "An exoskeletal robot for human elbow motion support-sensor fusion, adaptation, and control," *IEEE Transactions on Systems, Man, and Cybernetics, Part B (Cybernetics)*, vol. 31, no. 3, pp. 353–361, 2001.

[36] K. Kiguchi, R. Esaki, and T. Fukuda, "Development of a wearable exoskeleton for daily forearm motion assist," *Advanced Robotics*, vol. 19, no. 7, pp. 751–771, 2005.

[37] R. A. R. C. Gopura and K. Kiguchi, "Development of a 6dof exoskeleton robot for human upper-limb motion assist," in *Information and Automation for Sustainability, 2008. ICIAFS 2008. 4th International Conference on.* IEEE, 2008, pp. 13–18.

[38] C. Neu, J. Crisco, and S. Wolfe, "In vivo kinematic behavior of the radio-capitate joint during wrist flexion–extension and radio-ulnar deviation," *Journal of biomechanics*, vol. 34, no. 11, pp. 1429–1438, 2001.

[39] Y. Youm, R. McMurthy, A. E. Flatt, and T. E. Gillespie, "Kinematics of the wrist. i. an experimental study of radial-ulnar deviation and flexion-extension." *J Bone Joint Surg Am*, vol. 60, no. 4, pp. 423–431, 1978.

[40] B. D. Ferris, J. Stanton, and J. Zamora, "Kinematics of the wrist," *Bone & Joint Journal*, vol. 82, no. 2, pp. 242–245, 2000.

[41] B. Buchholz, T. J. Armstrong, and S. A. Goldstein, "Anthropometric data for describing the kinematics of the human hand," *Ergonomics*, vol. 35, no. 3, pp. 261–273, 1992.

[42] J. M. Landsmeer, "Anatomical and functional investigations on the articulation of the human fingers." *Acta anatomica. Supplementum*, vol. 25, no. 24, pp. 1–69, 1954.

[43] J. Barmakian, "Anatomy of the joints of the thumb." *Hand clinics*, vol. 8, no. 4, pp. 683–691, 1992.

[44] A. Hollister, W. L. Buford, L. M. Myers, D. J. Giurintano, and A. Novick, "The axes of rotation of the thumb carpometacarpal joint," *Journal of Orthopaedic Research*, vol. 10, no. 3, pp. 454–460, 1992.

[45] R. Gopura, D. Bandara, K. Kiguchi, and G. K. Mann, "Developments in hardware systems of active upper-limb exoskeleton robots: A review," *Robotics and Autonomous Systems*, vol. 75, pp. 203–220, 2016.

[46] E. Papadopoulos and G. Patsianis, "Design of an exoskeleton mechanism for the shoulder joint," 2007.

[47] M. Mulas, M. Folgheraiter, and G. Gini, "An emg-controlled exoskeleton for hand rehabilitation," in *Rehabilitation Robotics, 2005. ICORR 2005. 9th International Conference on*. IEEE, pp. 371–374.

[48] J. Rosen, M. Brand, M. B. Fuchs, and M. Arcan, "A myosignal-based powered exoskeleton system," *IEEE Transactions on systems, Man, and Cybernetics-part A: Systems and humans*, vol. 31, no. 3, pp. 210–222, 2001.

[49] J. C. Perry, J. Rosen, and S. Burns, "Upper-limb powered exoskeleton design," *IEEE/ASME transactions on mechatronics*, vol. 12, no. 4, pp. 408–417, 2007.

[50] H. Kawasaki, S. Ito, Y. Ishigure, Y. Nishimoto, T. Aoki, T. Mouri, H. Sakaeda, and M. Abe, "Development of a hand motion assist robot for rehabilitation therapy by patient self-motion control," in *Rehabilitation Robotics, 2007. ICORR 2007. IEEE 10th International Conference on*. IEEE, 2007, pp. 234–240.

[51] A. Gupta and M. K. O'Malley, "Design of a haptic arm exoskeleton for training and rehabilitation," *IEEE/ASME Transactions on mechatronics*, vol. 11, no. 3, pp. 280–289, 2006.

[52] A. Frisoli, F. Rocchi, S. Marcheschi, A. Dettori, F. Salsedo, and M. Bergamasco, "A new force-feedback arm exoskeleton for haptic interaction in virtual environments," in *Eurohaptics Conference, 2005 and Symposium on Haptic Interfaces for Virtual Environment and Teleoperator Systems, 2005. World Haptics 2005. First Joint*. IEEE, 2005, pp. 195–201.

[53] A. Frisoli, L. Borelli, A. Montagner, S. Marcheschi, C. Procopio, F. Salsedo, M. Bergamasco, M. C. Carboncini, M. Tolaini, and B. Rossi, "Arm rehabilitation with a robotic exoskeleleton in virtual reality," in *Rehabilitation Robotics, 2007. ICORR 2007. IEEE 10th International Conference on*. IEEE, 2007, pp. 631–642.

[54] T. Nef and R. Riener, "Armin-design of a novel arm rehabilitation robot," in *Rehabilitation Robotics, 2005. ICORR 2005. 9th International Conference on*. IEEE, pp. 57–60.

[55] T. Nef, M. Mihelj, G. Colombo, and R. Riener, "Armin-robot for rehabilitation of the upper extremities," in *Robotics and Automation, 2006. ICRA 2006. Proceedings 2006 IEEE International Conference on*. IEEE, 2006, pp. 3152–3157.

[56] M. Mihelj, T. Nef, and R. Riener, "Armin ii-7 dof rehabilitation robot: mechanics and kinematics," in *Robotics and Automation, 2007 IEEE International Conference on*. IEEE, 2007, pp. 4120–4125.

[57] A. Ruiz, A. Forner-Cordero, E. Rocon, and J. Pons, "Exoskeletons for rehabilitation and motor control," in *Biomedical Robotics and Biomechatronics, 2006. BioRob 2006. The First IEEE/RAS-EMBS International Conference on*. IEEE, 2006, pp. 601–606.

[58] G. Johnson, D. Carus, G. Parrini, S. Marchese, and R. Valeggi, "The design of a five-degree-of-freedom powered orthosis for the upper limb," *Proceedings of the Institution of Mechanical Engineers, Part H: Journal of Engineering in Medicine*, vol. 215, no. 3, pp. 275–284, 2001.

[59] I. Sarakoglou, N. G. Tsagarakis, and D. G. Caldwell, "Occupational and physical therapy using a hand exoskeleton based exerciser," in *Intelligent Robots and Systems, 2004.(IROS 2004). Proceedings. 2004 IEEE/RSJ International Conference on*, vol. 3. IEEE, pp. 2973–2978.

[60] A. Wege and G. Hommel, "Development and control of a hand exoskeleton for rehabilitation of hand injuries," in *Intelligent Robots and Systems, 2005.(IROS 2005). 2005 IEEE/RSJ International Conference on*. IEEE, 2005, pp. 3046–3051.

[61] C. Carignan and M. Liszka, "Design of an arm exoskeleton with scapula motion for shoulder rehabilitation," in *Advanced Robotics, 2005. ICAR'05. Proceedings., 12th International Conference on*. IEEE, 2005, pp. 524–531.

[62] S. J. Ball, I. E. Brown, and S. H. Scott, "A planar 3dof robotic exoskeleton for rehabilitation and assessment," in *Engineering in Medicine and Biology Society, 2007. EMBS 2007. 29th Annual International Conference of the IEEE*. IEEE, 2007, pp. 4024–4027.

[63] ——, "Medarm: a rehabilitation robot with 5dof at the shoulder complex," in *Advanced intelligent mechatronics, 2007 IEEE/ASME international conference on*. IEEE, 2007, pp. 1–6.

[64] W. Chou, T. Wang, and J. Xiao, "Haptic interaction with virtual environment using an arm type exoskeleton device," in *Robotics and Automation, 2004. Proceedings. ICRA'04. 2004 IEEE International Conference on*, vol. 2. IEEE, 2004, pp. 1992–1997.

[65] L. Lucas, M. DiCicco, and Y. Matsuoka, "An emg-controlled hand exoskeleton for natural pinching," *Journal of Robotics and Mechatronics*, vol. 16, pp. 482–488, 2004.

[66] D. Sasaki, T. Noritsugu, and M. Takaiwa, "Development of active support splint driven by pneumatic soft actuator (assist)," in *Robotics and Automation, 2005. ICRA 2005. Proceedings of the 2005 IEEE International Conference on*. IEEE, 2005, pp. 520–525.

[67] T. Noritsugu, H. Yamamoto, D. Sasakil, and M. Takaiwa, "Wearable power assist device for hand grasping using pneumatic artificial rubber muscle," in *SICE 2004 Annual Conference*, vol. 1. IEEE, 2004, pp. 420–425.

[68] N. G. Tsagarakis and D. G. Caldwell, "Development and control of a 'soft-actuated'exoskeleton for use in physiotherapy and training," *Autonomous Robots*, vol. 15, no. 1, pp. 21–33, 2003.

[69] S. Lee, S. Park, M. Kim, and C.-W. Lee, "Design of a force reflecting master arm and master hand using pneumatic actuators," in *Robotics and Automation, 1998. Proceedings. 1998 IEEE International Conference on*, vol. 3. IEEE, 1998, pp. 2574–2579.

[70] C. D. Takahashi, L. Der-Yeghiaian, V. Le, R. R. Motiwala, and S. C. Cramer, "Robot-based hand motor therapy after stroke," *Brain*, vol. 131, no. 2, pp. 425–437, 2007.

[71] T. G. Sugar, J. He, E. J. Koeneman, J. B. Koeneman, R. Herman, H. Huang, R. S. Schultz, D. Herring, J. Wanberg, S. Balasubramanian *et al.*, "Design and control of rupert: a device for robotic upper extremity repetitive therapy," *IEEE transactions on neural systems and rehabilitation engineering*, vol. 15, no. 3, pp. 336–346, 2007.

[72] H. Kobayashi and K. Hiramatsu, "Development of muscle suit for upper limb," in *Robotics and Automation, 2004. Proceedings. ICRA'04. 2004 IEEE International Conference on*, vol. 3. IEEE, pp. 2480–2485.

[73] P. Polygerinos, Z. Wang, K. C. Galloway, R. J. Wood, and C. J. Walsh, "Soft robotic glove for combined assistance and at-home rehabilitation," *Robotics and Autonomous Systems*, vol. 73, pp. 135–143, 2015.

[74] H. K. Yap, B. W. K. Ang, J. H. Lim, J. C. H. Goh, and C. H. Yeow, "A fabric-regulated soft robotic glove with user intent detection using emg and rfid for hand assistive application," in *2016 IEEE International Conference on Robotics and Automation (ICRA)*, May 2016, pp. 3537–3542.

[75] M. Mistry, P. Mohajerian, and S. Schaal, "An exoskeleton robot for human arm movement study," in *Intelligent Robots and Systems, 2005.(IROS 2005). 2005 IEEE/RSJ International Conference on*. IEEE, 2005, pp. 4071–4076.

[76] T. Lenzi, S. De Rossi, N. Vitiello, A. Chiri, S. Roccella, F. Giovacchini, F. Vecchi, and M. C. Carrozza, "The neuro-robotics paradigm: Neurarm, neuroexos, handexos," in *Engineering in Medicine and Biology Society, 2009. EMBC 2009. Annual International Conference of the IEEE*. IEEE, 2009, pp. 2430–2433.

[77] C. Pylatiuk, A. Kargov, I. Gaiser, T. Werner, S. Schulz, and G. Bretthauer, "Design of a flexible fluidic actuation system for a hybrid elbow orthosis," in *Rehabilitation Robotics, 2009. ICORR 2009. IEEE International Conference on*. IEEE, 2009, pp. 167–171.

[78] K. Ohnishi, Y. Saito, T. Oshima, and T. Higashihara, "Powered orthosis and attachable power-assist device with hydraulic bilateral servo system," in *Engineering in Medicine and Biology Society (EMBC), 2013 35th Annual International Conference of the IEEE*. IEEE, 2013, pp. 2850–2853.

[79] Y. Mao and S. K. Agrawal, "Design of a cable-driven arm exoskeleton (carex) for neural rehabilitation," *IEEE Transactions on Robotics*, vol. 28, no. 4, pp. 922–931, 2012.

[80] T. Nef, M. Guidali, and R. Riener, "Armin iii–arm therapy exoskeleton with an ergonomic shoulder actuation," *Applied Bionics and Biomechanics*, vol. 6, no. 2, pp. 127–142, 2009.

[81] C. D. Takahashi, L. Der-Yeghiaian, V. Le, and S. C. Cramer, "A robotic device for hand motor therapy after stroke," in *Rehabilitation Robotics, 2005. ICORR 2005. 9th International Conference on*. IEEE, pp. 17–20.

[82] K. Kong and M. Tomizuka, "Control of exoskeletons inspired by fictitious gain in human model," *IEEE/ASME Transactions on Mechatronics*, vol. 14, no. 6, pp. 689–698, 2009.

[83] J. Pons, R. Ceres, and L. Calderon, "Introduction to wearable robotics," *Wearable Robots: Biomechatronic Exoskeletons*, pp. 1–2, 2008.

[84] T. Hayashi, H. Kawamoto, and Y. Sankai, "Control method of robot suit hal working as operator's muscle using biological and dynamical information," in *Intelligent Robots and Systems, 2005.(IROS 2005). 2005 IEEE/RSJ International Conference on*. IEEE, 2005, pp. 3063–3068.

[85] O. Bida, D. Rancourt, and E. Clancy, "Electromyogram (emg) amplitude estimation and joint torque model performance," in *Bioengineering Conference, 2005. Proceedings of the IEEE 31st Annual Northeast.* IEEE, 2005, pp. 229–230.

[86] O. F. Manette and M. A. Maier, "Temporal processing in primate motor control: relation between cortical and emg activity," *IEEE Transactions on Neural Networks*, vol. 15, no. 5, pp. 1260–1267, 2004.

[87] R. A. R. C. Gopura, K. Kiguchi, and Y. Li, "Sueful-7: A 7dof upper-limb exoskeleton robot with muscle-model-oriented emg-based control," in *Intelligent Robots and Systems, 2009. IROS 2009. IEEE/RSJ International Conference on.* IEEE, 2009, pp. 1126–1131.

[88] K. Kong and D. Jeon, "Design and control of an exoskeleton for the elderly and patients," *IEEE/ASME Transactions on mechatronics*, vol. 11, no. 4, pp. 428–432, 2006.

[89] K. Yamamoto, M. Ishii, H. Noborisaka, and K. Hyodo, "Stand alone wearable power assisting suit-sensing and control systems," in *Robot and Human Interactive Communication, 2004. ROMAN 2004. 13th IEEE International Workshop on.* IEEE, 2004, pp. 661–666.

[90] N. Karavas, A. Ajoudani, N. Tsagarakis, J. Saglia, A. Bicchi, and D. Caldwell, "Tele-impedance based assistive control for a compliant knee exoskeleton," *Robotics and Autonomous Systems*, vol. 73, pp. 78–90, 2015.

[91] G. Aguirre-Ollinger, J. E. Colgate, M. A. Peshkin, and A. Goswami, "Active-impedance control of a lower-limb assistive exoskeleton," in *Rehabilitation Robotics, 2007. ICORR 2007. IEEE 10th International Conference on.* IEEE, 2007, pp. 188–195.

[92] E. T. Wolbrecht, V. Chan, D. J. Reinkensmeyer, and J. E. Bobrow, "Optimizing compliant, model-based robotic assistance to promote neurorehabilitation," *IEEE Transactions on Neural Systems and Rehabilitation Engineering*, vol. 16, no. 3, pp. 286–297, 2008.

[93] M. G. Carmichael and D. Liu, "Experimental evaluation of a model-based assistance-as-needed paradigm using an assistive robot," in *Engineering in Medicine and Biology Society (EMBC), 2013 35th Annual International Conference of the IEEE.* IEEE, 2013, pp. 866–869.

[94] B. K. Dinh, M. Xiloyannis, L. Cappello, C. W. Antuvan, S.-C. Yen, and L. Masia, "Adaptive backlash compensation in upper limb soft wearable

exoskeletons," *Robotics and Autonomous Systems*, vol. 92, pp. 173 – 186, 2017. [Online]. Available: http://www.sciencedirect.com/science/article/pii/S0921889016303591

[95] M. Xiloyannis, L. Cappello, B. Khanh Dinh, C. W. Antuvan, and L. Masia, *Design and Preliminary Testing of a Soft Exosuit for Assisting Elbow Movements and Hand Grasping*. Cham: Springer International Publishing, 2017, pp. 557–561. [Online]. Available: https://doi.org/10.1007/978-3-319-46669-9_92

[96] I. A. Murray and G. R. Johnson, "A study of the external forces and moments at the shoulder and elbow while performing every day tasks," *Clinical biomechanics*, vol. 19, no. 6, pp. 586–594, 2004.

[97] M. Buckley, A. Yardley, G. Johnson, and D. Cams, "Dynamics of the upper limb during performance of the tasks of everyday living—a review of the current knowledge base," *Proceedings of the Institution of Mechanical Engineers, Part H: Journal of Engineering in Medicine*, vol. 210, no. 4, pp. 241–247, 1996.

[98] D. Magermans, E. Chadwick, H. Veeger, and F. Van Der Helm, "Requirements for upper extremity motions during activities of daily living," *Clinical Biomechanics*, vol. 20, no. 6, pp. 591–599, 2005.

[99] M. C. Hume, H. Gellman, H. McKellop, and R. H. Brumfield, "Functional range of motion of the joints of the hand," *The Journal of hand surgery*, vol. 15, no. 2, pp. 240–243, 1990.

[100] L. Cappello, D. K. Binh, S.-C. Yen, and L. Masia, "Design and preliminary characterization of a soft wearable exoskeleton for upper limb," in *6th IEEE International Conference on Biomedical Robotics and Biomechatronics (BioRob)*, June 2016, pp. 623–630.

[101] M. Xiloyannis, L. Cappello, K. D. Binh, C. W. Antuvan, and L. Masia, "Preliminary design and control of a soft exosuit for assisting elbow movements and hand grasping in activities of daily living," *Journal of Rehabilitation and Assistive Technologies Engineering*, vol. 4, 2017. [Online]. Available: http://dx.doi.org/10.1177/2055668316680315

[102] R. M. Murray, S. S. Sastry, and L. Zexiang, *A Mathematical Introduction to Robotic Manipulation*, 1st ed. Boca Raton, FL, USA: CRC Press, Inc., 1994.

[103] J. T. McConville, C. E. Clauser, T. D. Churchill, J. Cuzzi, and I. Kaleps, "Anthropometric relationships of body and body segment moments of inertia," Anthropology Research Project Inc Yellow Springs Oh, Tech. Rep., 1980.

[104] H. In, H. Lee, U. Jeong, B. Kang, and K.-J. Cho, "Feasibility study of a slack enabling actuator for actuating tendon-driven soft wearable robot without pretension," in *IEEE International Conference on Robotics and Automation (ICRA)*, May 2015, pp. 1229–1234.

[105] H. In, U. Jeong, H. Lee, and K. J. Cho, "A novel slack-enabling tendon drive that improves efficiency, size, and safety in soft wearable robots," *IEEE/ASME Transactions on Mechatronics*, vol. 22, no. 1, pp. 59–70, Feb 2017.

[106] B. K. Dinh, M. Xiloyannis, C. W. Antuvan, L. Cappello, and L. Masia, "Hierarchical cascade controller for assistance modulation in a soft wearable arm exoskeleton," *IEEE Robotics and Automation Letters*, vol. 2, no. 3, pp. 1786–1793, July 2017.

[107] N. Hogan, "Impedance control: An approach to manipulation," in *1984 American Control Conference*, June 1984, pp. 304–313.

[108] G. Aguirre-Ollinger, J. E. Colgate, M. A. Peshkin, and A. Goswami, "Active-impedance control of a lower-limb assistive exoskeleton," in *IEEE 10th International Conference on Rehabilitation Robotics*, June 2007, pp. 188–195.

[109] ——, "Design of an active one-degree-of-freedom lower-limb exoskeleton with inertia compensation," *The International Journal of Robotics Research*, vol. 30, no. 4, pp. 486–499, 2011. [Online]. Available: http://dx.doi.org/10.1177/0278364910385730

[110] G. Aguirre-Ollinger, A. Goswami, J. Colgate, and M. Peshkin, "Controller for an assistive exoskeleton based on active impedance," June 2010, uS Patent 7,731,670. [Online]. Available: https://www.google.com/patents/US7731670

[111] G. Saggio, F. Riillo, L. Sbernini, and L. R. Quitadamo, "Resistive flex sensors: a survey," *Smart Materials and Structures*, vol. 25, no. 1, p. 013001, 2015.

[112] R. M. Murray, Z. Li, S. S. Sastry, and S. S. Sastry, "A mathematical introduction to robotic manipulation," pp. 293–296, 1994.

[113] K. Kong and M. Tomizuka, "Control of exoskeletons inspired by fictitious gain in human model," *IEEE/ASME Transactions on Mechatronics*, vol. 14, no. 6, pp. 689–698, Dec 2009.

[114] M. B. Weinger, M. E. Wiklund, and D. J. Gardner-Bonneau, *Handbook of Human Factors in Medical Device Design*, 2010.

[115] R. Ronsse, N. Vitiello, T. Lenzi, J. van den Kieboom, M. C. Carrozza, and A. J. Ijspeert, "Human-robot synchrony: Flexible assistance using adaptive oscillators," *IEEE Transactions on Biomedical Engineering*, vol. 58, no. 4, pp. 1001–1012, April 2011.

[116] W. Huo, S. Mohammed, Y. Amirat, and K. Kong, "Active impedance control of a lower limb exoskeleton to assist sit-to-stand movement," in *2016 IEEE International Conference on Robotics and Automation (ICRA)*, May 2016, pp. 3530–3536.

[117] L. E. Kahn, P. S. Lum, W. Z. Rymer, and D. J. Reinkensmeyer, "Robot-assisted movement training for the stroke-impaired arm: Does it matter what the robot does?" *Journal of rehabilitation research and development*, vol. 43, no. 5, pp. 619–630, 2006.

[118] B. K. Dinh, L. Cappello, M. Xiloyannis, and L. Masia, "Position control using adaptive backlash compensation for bowden cable transmission in soft wearable exoskeleton," in *2016 IEEE/RSJ International Conference on Intelligent Robots and Systems (IROS)*, Oct 2016, pp. 5670–5676.

[119] S. B. Kesner and R. D. Howe, "Position control of motion compensation cardiac catheters," *IEEE Transactions on Robotics*, vol. 27, no. 6, pp. 1045–1055, 2011.

[120] T. Fuxiang and W. Xingsong, "The design of a tendon-sheath-driven robot," in *15th International Conference on Mechatronics and Machine Vision in Practice*. IEEE, 2008, pp. 280–284.

[121] Q. Wu, X. Wang, F. Du, and X. Zhang, "Design and control of a powered hip exoskeleton for walking assistance," *International Journal of Advanced Robotic Systems*, vol. 12, 2015.

[122] R. Zglimbea, V. Finca, E. Greaban, and M. Constantin, "Identification of systems with friction via distributions using the modified friction lugre model," in *Proceedings of the 13th WSEAS International Conference on Systems", Athens*, 2009, pp. 579–584.

[123] F. Ikhouane and J. Rodellar, *Systems with hysteresis: Analysis, identification and control using the Bouc-Wen model*. John Wiley & Sons, 2007.

[124] X. Zhu and X. Lu, "Parametric identification of bouc-wen model and its application in mild steel damper modeling," *Procedia Engineering*, vol. 14, pp. 318–324, 2011.

[125] T. N. Do, T. Tjahjowidodo, M. W. S. Lau, and S. J. Phee, "Position control of asymmetric nonlinearities for a cable-conduit mechanism," *IEEE Transactions on Automation Science and Engineering*, vol. PP, no. 99, pp. 1–9, 2015, doi: 10.1109/TASE.2015.2438319.

[126] G. Tao and P. V. Kokotovic, "Adaptive control of systems with backlash," *Automatica*, vol. 29, no. 2, pp. 323–335, 1993.

[127] F. Ikhouane, J. E. Hurtado, and J. Rodellar, "Variation of the hysteresis loop with the bouc–wen model parameters," *Nonlinear Dynamics*, vol. 48, no. 4, pp. 361–380, 2007.

[128] J.-J. E. Slotine and W. Li, *Applied nonlinear control*. Prentice-hall Englewood Cliffs, NJ, 1991, vol. 199, no. 1.

[129] J. Wang, S. Ge, and T. Lee, "Adaptive friction compensation for servo mechanisms," in *Adaptive control of nonsmooth dynamic systems*. Springer, 2001, pp. 211–248.

[130] M. M. Polycarpou, P. Ioannou *et al.*, "A robust adaptive nonlinear control design," in *American Control Conference*. IEEE, 1993, pp. 1365–1369.

[131] P. A. Ioannou and J. Sun, *Robust Adaptive Control*. Upper Saddle River, NJ, USA: Prentice-Hall, Inc., 1995.

[132] H. Olsson, K. Åström, C. C. de Wit, M. Gäfvert, and P. Lischinsky, "Friction models and friction compensation," *European Journal of Control*, vol. 4, no. 3, pp. 176 – 195, 1998.

[133] V. Van Geffen, "A study of friction models and friction compensation."

[134] T. N. Do, T. Tjahjowidodo, M. W. S. Lau, and S. J. Phee, "Nonlinear friction modelling and compensation control of hysteresis phenomena for a pair of tendon-sheath actuated surgical robots," *Mechanical Systems and Signal Processing*, vol. 60–61, pp. 770 – 784, 2015.

[135] ——, "A new approach of friction model for tendon-sheath actuated surgical systems: Nonlinear modelling and parameter identification," *Mechanism and Machine Theory*, vol. 85, pp. 14–24, 2015.

[136] P. R. Dahl, "A solid friction model," DTIC Document, Tech. Rep., 1968.

[137] C. C. De Wit, H. Olsson, K. J. Astrom, and P. Lischinsky, "A new model for control of systems with friction," *IEEE Transactions on automatic control*, vol. 40, no. 3, pp. 419–425, 1995.

[138] K. Johanastrom and C. Canudas-de Wit, "Revisiting the lugre friction model," *IEEE control Systems*, vol. 28, no. 6, pp. 101–114, 2008.

[139] J. Bae, K. Kong, and M. Tomizuka, "Cable friction compensation and rehabilitation algorithms for a cable-driven human assistive system," in *ASME 2010 Dynamic Systems and Control Conference*. American Society of Mechanical Engineers, pp. 777–783.

[140] U. Jeong and K. J. Cho, "Feedforward friction compensation of bowden-cable transmission via loop routing," in *Intelligent Robots and Systems (IROS), 2015 IEEE/RSJ International Conference on*, Sept 2015, pp. 5948–5953.

[141] H. K. Khalil and J. Grizzle, *Nonlinear systems*. Prentice hall New Jersey, 1996, vol. 3.

[142] P. Ioannou and A. Datta, "Robust adaptive control: a unified approach," *Proceedings of the IEEE*, vol. 79, no. 12, pp. 1736–1768, Dec 1991.

[143] E. J. Rouse, L. M. Mooney, and H. M. Herr, "Clutchable series-elastic actuator: Implications for prosthetic knee design," *The International Journal of Robotics Research*, vol. 33, no. 13, pp. 1611–1625, 2014.